AD NUMBER

AD821877

LIMITATION CHANGES

TO:

Approved for public release; distribution is unlimited.

FROM:

Distribution authorized to U.S. Gov't. agencies and their contractors; Critical Technology; MAR 1967. Other requests shall be referred to Air Force Space and Missile Systems Organization, Attn: SMSDM-1, Norton AFB, CA 92409. This document contains export-controlled technical data.

AUTHORITY

samso usaf ltr, 28 feb 1972

"MEAN FLOW MEASUREMENTS IN AN AXISYMMETRIC COMPRESSIBLE TURBULENT WAKE"

Publication No. U-3978

TECHNICAL REPORT

MEAN FLOW MEASUREMENTS IN AN AXISYMMETRIC COMPRESSIBLE TURBULENT WAKE

Monitored By: Ballistic Systems Division
Air Force Systems Command
Norton Air Force Base, California

Under Contract: AF 04(694)-994

Sponsored By: Advanced Research Projects Agency
Department of Defense
ARPA Order No. 888, Amendment No. 1

Prepared By: Dr. A. Demetriades

1 March 1967

PHILCO-FORD CORPORATION
Space and Re-entry Systems
Newport Beach, California

NOMENCLATURE

A	Wake area
C_D	Wake drag coefficient
C_p	Specific heat at constant pressure
D	Model diameter
d	Hot-wire diameter
h	Enthalpy
I	Hot-wire current
k	Air thermal conductivity at stagnation conditions
L	Transverse velocity scale
ℓ	Hot-wire length
M	Mach number
Nu_o	Hot-wire Nusselt number at zero current and at stagnation thermal conductivity
p	Static pressure
p_o	Tunnel stagnation pressure
p_t	Pitot (impact) pressure
q	Heat flux into (out of) hot-wire
r	Radius

NOMENCLATURE (Continued)

$\bar{r}$	Howarth-Dorodnitzyn radius (Equation (27))
r^*, $r_{1/2}$	Wake radius at which $\tilde{u} = 0.5$
R	Hot-wire resistance
R'	Reference hot-wire resistance
R_T	Turbulent Reynolds number
Re_o	Hot-wire Reynolds number at stagnation viscosity
R_{aw}	Hot-wire resistance at T_{aw}
R_{e_w}	Wake Reynolds number (Equation (32))
T	Temperature
T'	Temperature of hot-wire corresponding to R'
$\tilde{T}$	Nondimensional temperature
T_w	Hot-wire temperature
T_{aw}	T_w at I = 0
T_o	Total temperature (local or tunnel)
u	Flow axial velocity
$\tilde{u}$	Nondimensional axial velocity
U	Characteristic velocity = $u_\infty - u(0)$
w	Velocity defect (Equation (4))
WEA	Wake Experiment A (Y traverses)
WEB	Wake Experiment B (Z traverses)
WEC	Wake Experiment C (X traverses)
x	Axial coordinate
x_o	Axial location of virtual origin

NOMENCLATURE (Continued)

$\bar{x}$	Nondimensional axial coordinate (Equation (13))
y	Radial coordinate (up-down)
z	Radial coordinate (left-right)
α	Temperature coefficient of resistance
γ	Ratio of specific heats
η	Nondimensional radius
η	Recovery factor of hot-wire
θ	Temperature defect (Equation (10))
Ⓗ	Characteristic temperature = $T(0) - T_\infty$
μ_o	Stagnation viscosity
ν	Laminar kinematic viscosity
ν_T	Incompressible turbulent kinematic viscosity
$\bar{\nu}_T$	Compressible turbulent kinematic viscosity
ρ	Air density
σ_T	Apparent turbulent Prandtl number
(0)	Refers to axis properties
∞	Refers to properties outside wake

ABSTRACT

The mean flow field of the axisymmetric turbulent wake shed by a very slender body at Mach 3 has been mapped with the aid of the pitot and static pressure probes and the hot-wire anemometer. The experimental geometry was chosen so that no inviscid wake existed, and the measurements were carried out to about 100 diameters downstream of the base. The axial variation of the velocity and temperature defects appears to obey classical decay laws following a relaxation distance of at least 40 diameters from the transition region. By contrast, the radial profiles of these properties relax quickly to a self-preserving form; both the temperature and the velocity radial variations fit single-parameter Gaussian distributions quite well. The proper radial similarity variable is the radius divided by the transverse wake scale; equally good agreement obtains for a Howarth-Dorodnitzyn-transformed radius, although this issue is still unsettled because of the low Mach number used. The turbulent Reynolds and Prandtl numbers computed indirectly from the data agree well with similar results from low-speed turbulent flows.

PREFACE

The practical need for understanding the characteristics of hypersonic turbulent wakes led Aeronutronic Division of Philco-Ford Corporation to initiate, in 1964, a comprehensive research program whose eventual aim is the prediction of electron density fluctuation characteristics in hydrodynamically turbulent plasmas. This research includes a broad scope of activity ranging from the construction of suitable facilities and the development of techniques to the detailed diagnosis of several free compressible turbulent flow configurations.

The present report describes the equipment and techniques used at Aeronutronic for wake research and the results obtained on the mean properties of the axisymmetric compressible turbulent wake, as observed by probes stationary with respect to the model. The stationary-random aspect of the wake and its turbulent transport properties will be presented shortly in Part II: Intermittency and the Stationary-Random Aspect of the Axisymmetric Compressible Wake, to be followed by Part III: Modal and Spectral Analysis of the Turbulent Axisymmetric Compressible Wake. Further reports will deal with corresponding problems of two-dimensional wakes (Parts IV through VI) and certain topics in the mean and fluctuation characteristics of turbulent plasmas.

CONTENTS

CONTENTS (Continued)

SECTION 1

INTRODUCTION

Within the last few years the wakes of vehicles entering the Earth's atmosphere at hypersonic speeds have become the subject of intense interest and study. Literally hundreds of publications have appeared on the various aerodynamic and physicochemical aspects of this problem.* Some such aspects deal with fundamental phenomena in fluid mechanics and chemistry about which little was known at the time the wake problem became popular; such are, for example, the structure of the mean and turbulent wake flow field, the relevant chemical kinetics and the like. Much of this information can be supplied only by experiment, and it has been expedient to adapt older, low-speed experimental findings for use in predicting hypersonic wake characteristics. The legacy of this often unwarranted practice is a patchwork of hypotheses and approximations based on tenuous analogies between two formally different fluid-mechanical regimes. By contrast, there have been only a handful of basic experiments done under more relevant conditions in a way bridging the gap between the low-speed work and the application to hypersonic flight. This report covers the initial phase of a systematic experimental exploration of the fluid-mechanic features of the compressible turbulent wake.

Turbulent wakes have been studied at length by Townsend[4] and others, at low speeds, that is, under circumstances where the only fluctuating quantity of significance was the velocity. The hypersonic wake, however, is characterized by large density and temperature fluctuations as well, and it is therefore necessary to extend the earlier work[4] into high-speed regimes where

*Of the numerous papers written on wakes in recent years, those of Feldman[1] and Lees[2] are historically significant. For a recent review of the current state of the art to about 1966, one should read the survey paper of Lykoudis.[3]

compressibility effects are dominant. In such studies it is necessary to understand, at first, the so-called mean flow field; that is, the distribution of the time-averaged (or, in a restricted spatial sense, the space-averaged) properties such as the velocity, density, pressure, and temperature. It is especially important to find the self-preserving or similar form of these distributions and the proper axial and radial coordinates by which these distributions can be expressed. From these results one can then obtain turbulent transport properties cast in the form of turbulent Reynolds and Prandtl numbers; such nondimensional presentation is equally important for the dependent and independent variables of the flow so that the body geometry will appear only implicitly in integrals of the fluid motion in order to enhance the generality of the results.

The first and only attempt to settle these matters was made by Lees and his co-workers[5,6,7] who concentrated on two-dimensional blunt-body wakes at Mach 6. Axisymmetric wake experiments are equally scarce, available data existing only from the work of Zakkay,[8] and Ragsdale and Darling.[9] The former experiment yielded information to several hundred diameters behind the body, although the data are not abundant to the point where correlations could be drawn. In the latter work a larger volume of more careful measurements were obtained; however, no data are available beyond 14 diameters from the base and it is doubtful that self-preservation could set in so close to the model. Further, in neither of the above experiments was an attempt made to separate the inviscid from the viscous wake structure or to indicate the similarity parameters and profiles.

The present work is aimed at studying the self-preserving axisymmetric compressible turbulent wake. In what follows, we are distinctly concerned with the "far-wake," that is, with the region considerably downstream of the reattachment point which provides the terminus of the "base-flow" region. In choosing to begin with the axisymmetric geometry, it was decided to avoid model support methods which could conceivably interfere with the wake flow. Wires and struts were thus ruled out. The cantilevered-rod scheme explained in detail below was chosen because it seemed to provide the "cleanest" axisymmetric configuration. As events proved, a second advantage enjoyed by this scheme was the almost complete absence of an inviscid wake, so that the behavior of the viscous core could be studied without difficulty. In order to study the self-preserving wake an attempt was made to take a large volume of data for as large a wake length as possible. The latter was of the order of 100 diameters, shorter than would be desirable by comparison with Townsend's work[4] but, as events proved, adequate to indicate the most probable self-preserving form of the wake. A preliminary report of the present work forms part of Reference 10.

SECTION 2

FACILITIES AND APPARATUS

2.1 WIND TUNNEL

The experiment was performed at the Mach 3 continuous supersonic wind tunnel at the Aeronutronic Division of Philco-Ford. It is described in detail in Reference 11. The stagnation pressure chosen was 508 mm Hg abs, and the total temperature was 27°C, for which the Reynolds number in the test section was 50,000 per cm. A view of the facility is shown in Figure 1.

2.2 MODEL

The desire to produce a long (in terms of diameters) wake free of inviscid gradients generated the requirement that a small slender body should be placed at the upstream end of the test rhombus. The use of support wires and magnetic balancing in order to accomplish this purpose has been reported elsewhere. The advantages and disadvantages of such techniques [12,13] are still a matter of some controversy which can be settled only as a larger group of experiments and facilities are brought into play. Briefly, the following conclusions can be drawn from the literature:

(1) Structurally adequate support wires produce flow interference, the exact amount of which is impossible to determine from the scant literature on the subject. Behrens, however, reports that the inviscid wake of a circular wire is easily detectable at Mach 6, at 1000 diameters downstream.

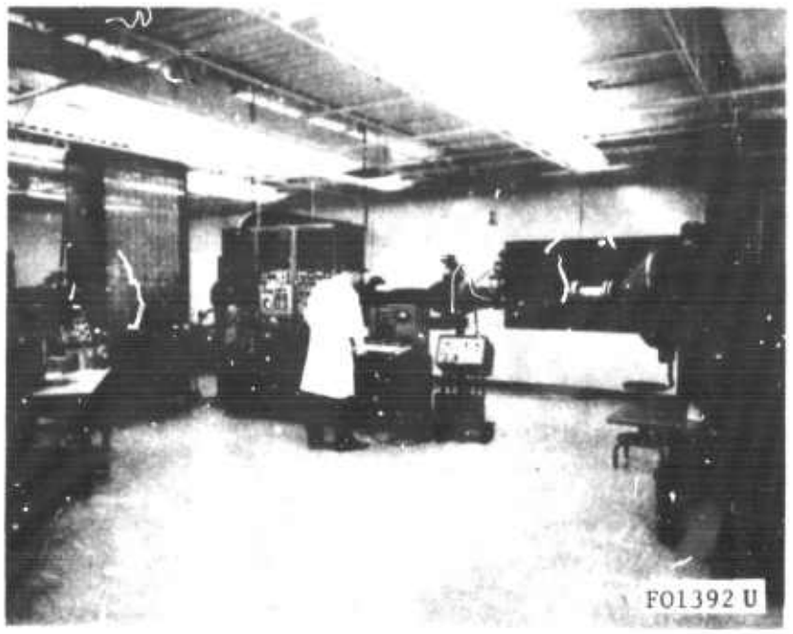

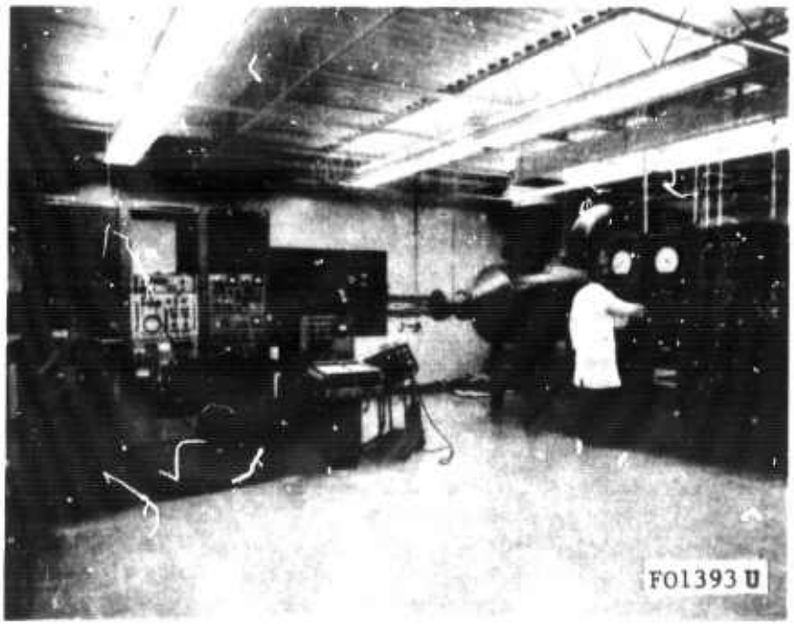

Figure 5. View of the supersonic wind-tunnel experimental area. Top: Operator adjusts the tunnel flow conditions from console at right. Bottom: Operator is at console on left which contains experiment electronic apparatus. Test-section is at center.

(2) Angle of attack effects are very pronounced for slender bodies, especially at increasing Mach numbers. Such effects can occur because of uneven wire supports and, quite often, because the angle of attack cannot be predicted or controlled accurately.

(3) Magnetic balance systems are expensive and cumbersome to construct and perfect. Besides, no far-wake tests with slender bodies so suspended have been reported.*

The model-support system decided upon consisted of a long circular rod supported upstream of the throat and cantilevered into the test section through the throat, as shown on Figure 2. The axis of the rod coincided with that of the tunnel, and its (uniform) diameter was 0.156 inch. The wake was produced by the boundary-layer of the rod shed into the test section; a wake length of an order of 10 inches was thus available. It is noteworthy that this method of producing an axisymmetric flow is by no means new, having been employed by Richmond,[16] Badrinarayanan,[17] and Zakkay,[8] and presumably, others as well. This scheme is, for obvious reasons, limited to low-supersonic wind tunnels.

The cantilevered rod showed a tendency to vibrate during the run. This vibration was eliminated by substituting a hollow rod in place of a solid one. A problem initially thought more serious concerned the effect of the presence of the rod on the free stream flow. Measurements quickly showed that this effect was negligible. Specifically, Figure 3 shows a pitot-tube trace taken vertically across the tunnel with and without the rod in place. The very near correspondence of these two traces shows that neither spatial flow nonuniformities nor a level shift, other than those due to the wake flow, occurred.

The model was neither heated nor cooled in any fashion. Because of its large fineness ratio (of order 100) it could thus be considered adiabatic with respect to the tunnel total temperature.

For further details regarding the flow about the model the reader is referred to Section 3.1.

---

*Experiments in the near wake of a magnetically suspended cone are currently underway by Bogdonoff[15] and his co-workers at Princeton.

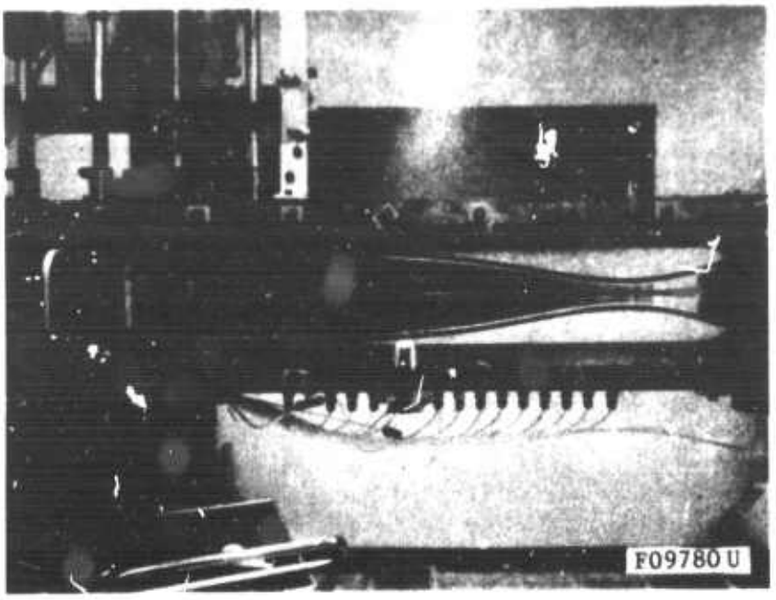

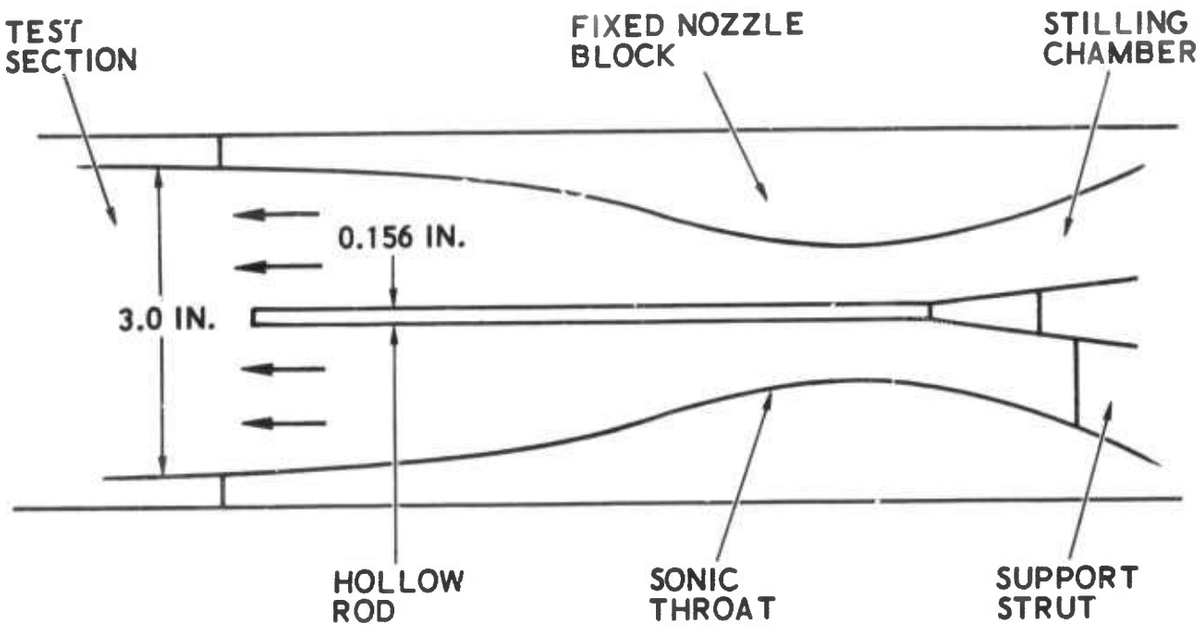

F09781 U

FIGURE 2. TOP: PHOTOGRAPH OF TEST SECTION SHOWING AXISYMMETRIC MODEL AT LEFT, PROBE AT LEFT AND PROBE ACTUATOR (TOP LEFT). BOTTOM: DETAILS OF THE AXISYMMETRIC MODEL.

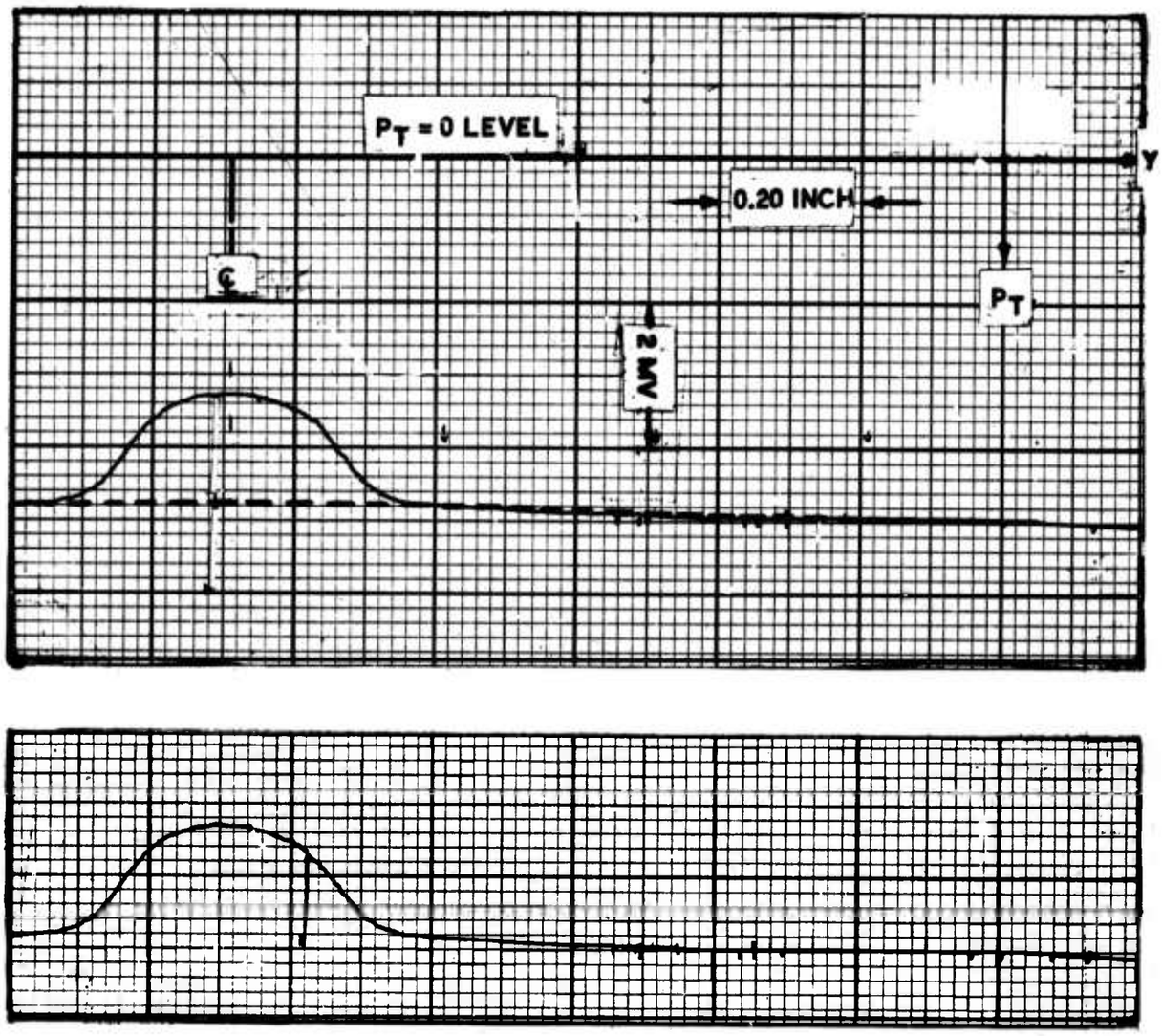

FIGURE 3. PITOT-PRESSURE TRACE TAKEN WITH (SOLID LINE) AND WITHOUT (DASHED LINE) THE AXISYMMETRIC MODEL IN THE TUNNEL. P_o = 508 MM HG ABS.

F09782U

2.3 INSTRUMENTATION

2.3.1 GENERAL CONSIDERATIONS

For supersonic flows of the type employed in this experiment and for known flow direction,** the flow field can be described completely by means of a minimum of three measurements. The instruments used in the present work consisted of the pitot probe for impact pressure, the static pressure probe for the static pressure, and the hot-wire probe for simultaneously measuring the total temperature and the mass flow flux. Compared with the required three, these four measurements allowed one redundancy to be used as a cross-check of the experimental results. In a recent study Bauer[18] concluded that for the conditions of the present work the group of three measurements resulting in greatest precision is the (p_T, p, T_o) group; that is, the impact (pitot) pressure, static pressure and total temperature, a fortunate fact since these measurements are usually also the most accurate. The mass-flow-flux measurement was thus used as a redundancy check.

Because p_T and T_o are effectively "integrals of motion" a question arises regarding possible errors in their measurement due to excessive turbulence, such as reported originally by Goldstein.[19] Lack of time has thus far prevented a much-needed systematic study of this effect. As pointed out in Reference 10, however, there are indications that these two properties fluctuated but little, partly because, as in the case of T_o, the flow velocity and temperature fluctuations in the wake were anticorrelated. The same reason would cause the mass-flux fluctuation to be rather large. An <u>a posteriori</u> justification exists, therefore, in the choice of the (p_T, p, T_o) group so far as the turbulent is concerned.

Because of the small diameter of the wake, spatial resolution was a problem. The major offender here was the static probe, whose diameter was 0.042 inch, or about four times smaller than the body diameter. As expected, however, the static pressure gradients in the wake were so slight that ample spatial resolution could be achieved with the static pressure probe as well.

2.3.2 PITOT PROBE

The pitot measurements were made with the probe shown on Figure 4. This probe consists essentially of two parts: a miniature pressure transducer positioned in a brass holder, and a bullet-shaped head terminating in a thin tube projecting forward. When the head is attached on the brass holder, one has a pitot tube of small dimensions and unusually high frequency response (of order 1 second), obtained because the internal volume between the tube tip and the transducer diaphragm is very small. With this arrangement it was possible to get an analog output of pitot pressure versus

---

** Because of the near-parallel nature of far-wake flows, the flow direction could safely be assumed to lie parallel to the tunnel walls.

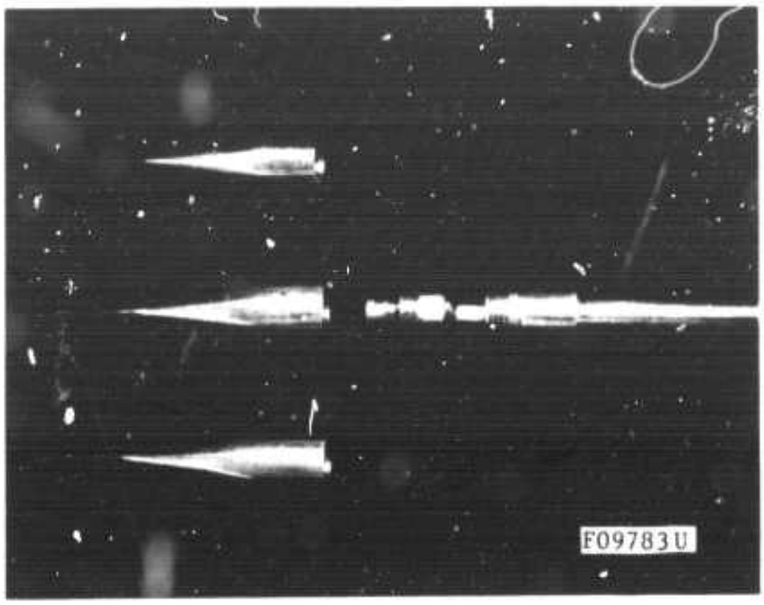

FIGURE 4. THE PITOT PROBE IN DISASSEMBLED FORM SHOWING TRANSDUCER (CENTER) TRANSDUCER SOCKET (RIGHT) AND THREE INTERCHANGEABLE PITOT "HEADS" (LEFT) OF THE TYPE USED.

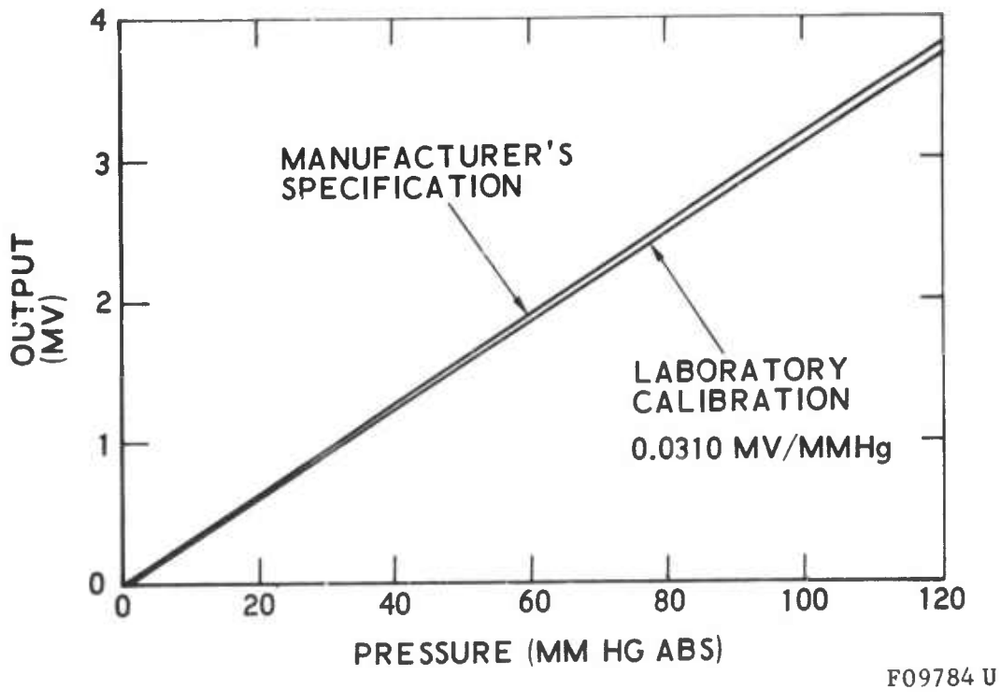

FIGURE 5. CALIBRATION OF PA 222 PRESSURE TRANSDUCER.

position in the flow by continuously traversing the probe in the tunnel at slow to moderate speed. A second advantage was gained by constructing several detachable heads of different geometry so that rapid interchanging greatly expedited the experimental work.

The miniature transducer employed was a Statham model PA 222 (0 to 10 psia) whose diameter is 0.25 inch, and was normally excited by 4 volts dc. The manufacturer's calibration was checked frequently against a 0 to 100 mm and a 0 to 400 mm Wallace-Tiernan diaphragm gage, which had a precision of 0.2 percent. Because of slight shifts, calibrations were always performed just prior to each series of measurements. Typical data are shown on Figure 5.

In order to assess the effect of probe tip interference with the flow in regions of large gradients, a number of heads with different diameter tubes were constructed. A test was conducted by attaching five different heads on the probe and taking pitot profiles of the wake with each. The results are shown in Figure 6. Interference is noted for tube tip greater than 0.008 inch, OD, and the latter size (with an ID of 0.004 inch) was chosen for the measurements. During the same test it was attempted to gage the effect of the turbulence on the pitot reading. If this effect was significant, it was expected to vary with large variations in the tip opening because of the finite spatial correlation of the fluctuations. In Figure 6 it is shown that the pitot reading on the axis does not vary as the tip size is changed from 0.006 inch to 0.125 inch, the latter being 0.8 of the body diameter. Although the subject is far from settled, this was interpreted as showing a negligible effect of turbulence on the pitot reading.

Finally, the effects of low density were estimated. The unit Reynolds number was at its worst of order 25,000 per cm and therefore the Reynolds number was of order 600, much larger than that for which low Reynolds number effects are discernible.[20]

2.3.3 STATIC PRESSURE PROBE

Static pressures could in principle be used with the arrangement described in the previous section through the use of a static tube head. Repeated and unresolved inconsistencies in such data forced the use of the alternate arrangement described below.

A separate static pressure probe, shown in Figure 7, was built, the sensitive element of which consisted of a 0.042 inch diameter steel tube capped by a circular cone of about 15 degrees half-angle. Three 0.015 inch diameter holes are drilled at 120 degree intervals around the tube about 0.5 inch behind the cone shoulder to ensure against slight chance misalignments and thus alleviate angle of attack effects. The pressure signal was led outside the tunnel to a Statham PA 731 0-5 psia transducer, which was also

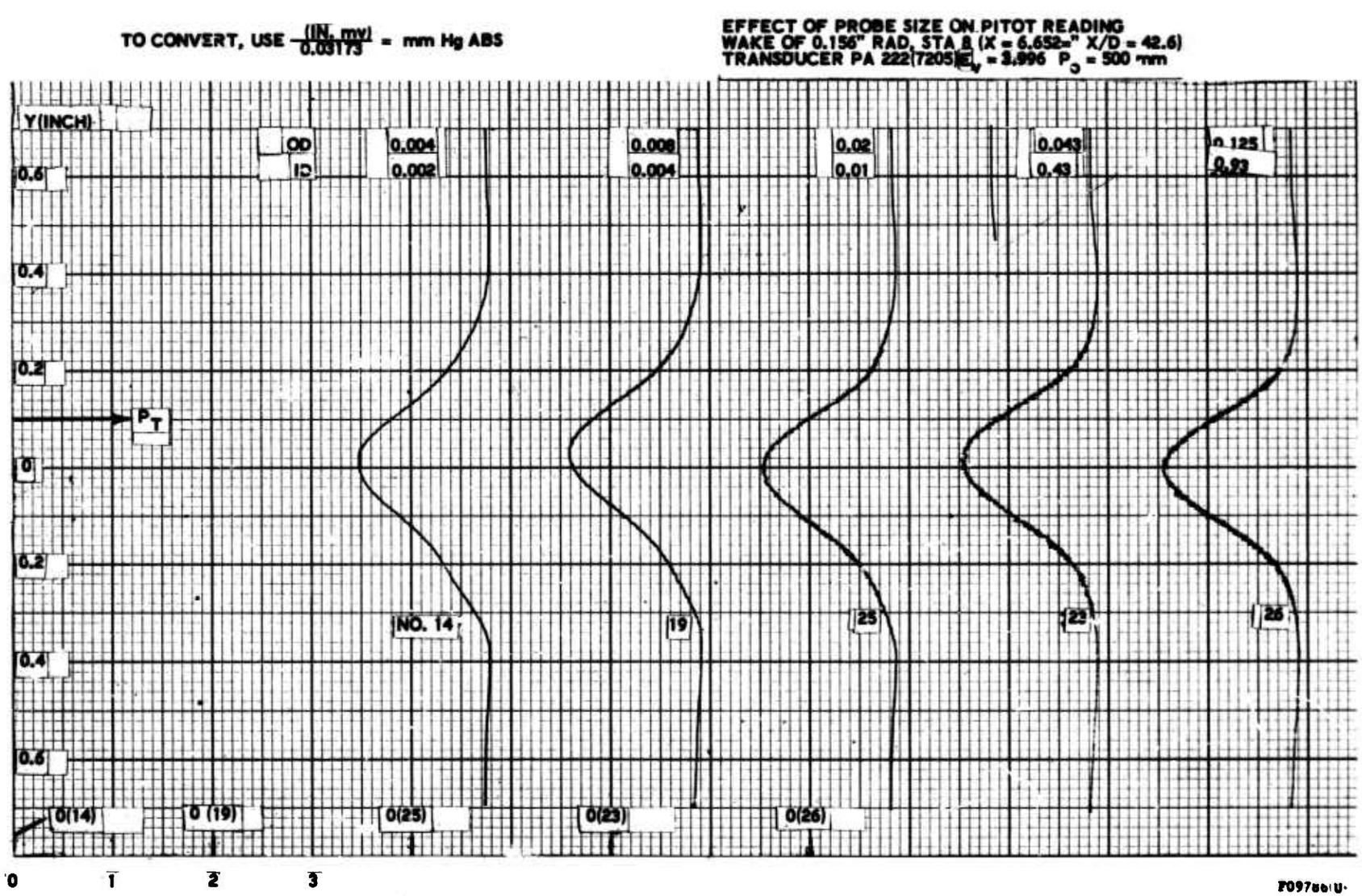

FIGURE 6. PITOT PRESSURE DISTRIBUTIONS WITH RADIUS SHOWING WAKE PROFILE DISTORTION WITH INCREASING PROBE DIAMETER.

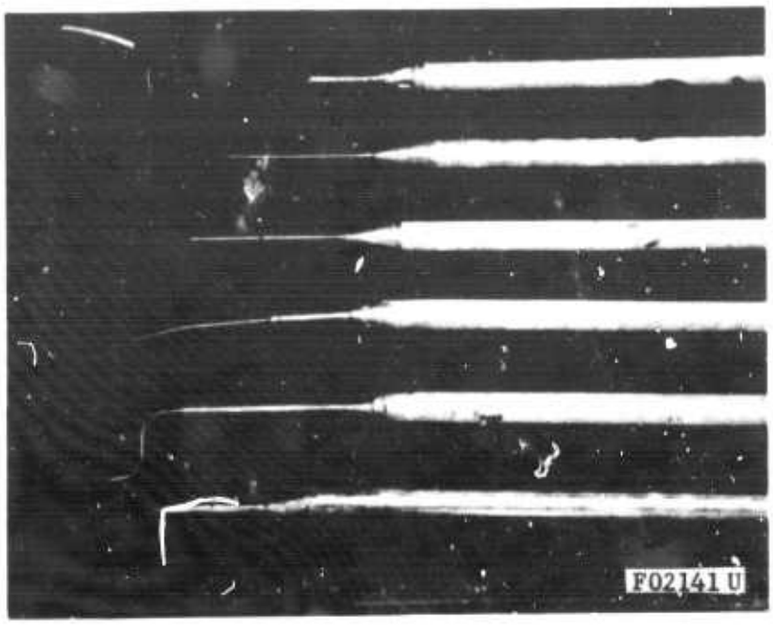

FIGURE 7. VARIOUS PRESSURE PROBES USED IN THIS WORK SHOWING THE STATIC PRESSURE PROBE (THIRD FROM TOP).

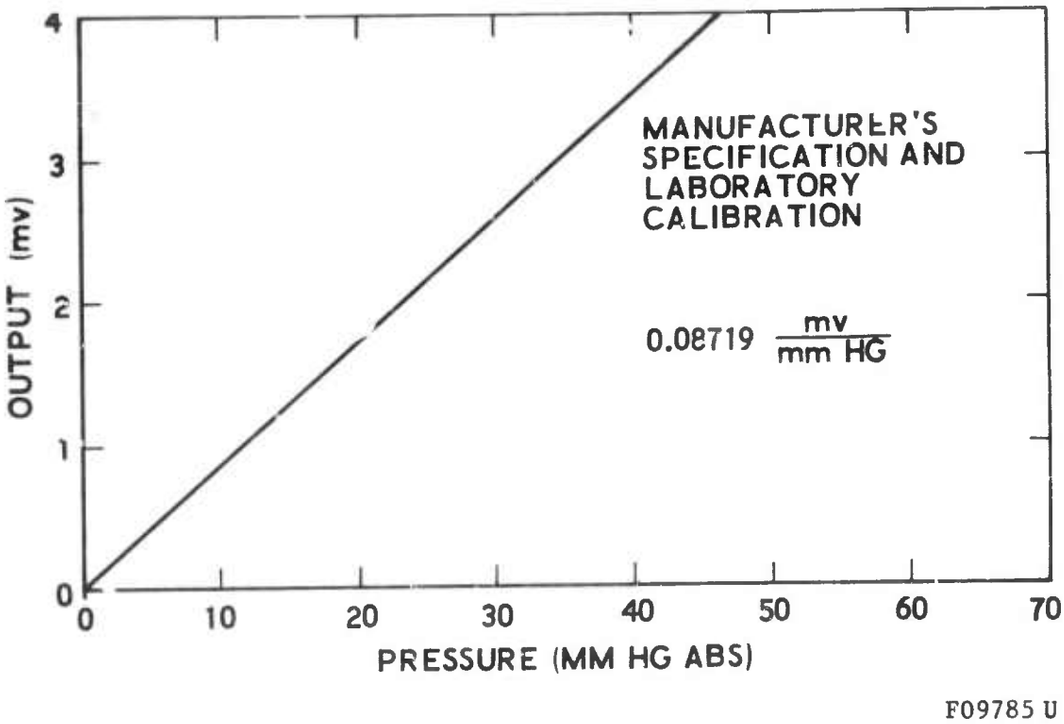

FIGURE 8. CALIBRATION OF PA 731 TRANSDUCER USED FOR THE STATIC PRESSURE MEASUREMENTS.

calibrated previous to every measurement with the aid of a 0 to 100 mm Hg Wallace-Tiernan gage; typical calibration data are shown in Figure 8. This scheme had much slower response than that described in Paragraph 2.3.2 and thus this probe was traversed at the slowest possible speeds of the probe actuator (of order 0.0005 inch per second). This, coupled with the very small static pressure gradients encountered, ensured the accuracy of the static pressure measurement.

As mentioned previously, the static probe was always used in supersonic flow where the direction of flow was well known, so that angle of attack effects were unimportant. The effect of the finite probe length on the measurement was more significant because of the known importance of the probe tip inviscid effect and that of the probe boundary layer. These corrections have been considered by the various authors, including Behrens[21] who discussed a probe geometry identical to the one employed herein. Again, the Mach numbers encountered were too low, and the Reynolds numbers too high, to cause any significant interactions. For example, the hypersonic interaction parameter χ was typically 0.1 for a correction of order 0.5 percent.

2.3.4 HOT-WIRE ANEMOMETER

The anemometer probe, pictured in Figure 9, consisted of two sharp-pointed needles across the tips of which a Pt 10 percent Rh wire was held by soft solder. For the WEA experiment (see below) the wire was 0.0001 inch in diameter; all subsequent experiments utilized 0.00005 inch diameter wires. The aspect ratios were of order 200 in all cases.

The correct use of the hot-wire anemometer as an integral part of a diagnostic system in compressible low density flows was first applied by Dewey[22] and was preceded by extensive investigations of the heat-loss laws at high speed and the solution of the crucial end-effect problems.[22] In its present form, and notwithstanding improvements incorporated in this work, the hot-wire technique remains an exacting and cumbersome process requiring computer programs for data reduction. Dewey and subsequently Herzog[23] formalized the hot-wire procedure on the basis of (a) a "universal" heat transfer law and (b) a procedure for correcting for end losses by which a hot wire could be used without need for calibration in a known flow. In the present experiment, however, the anemometer was used concurrently for turbulence measurements which further restricted the geometry of the wire approximately to a semicircular shape and there were doubts whether Dewey's procedure could be applied to such a wire because of its complex end-loss characteristics. To overcome this defect, the wires were calibrated individually in a known flow. As discussed in Appendix A, this

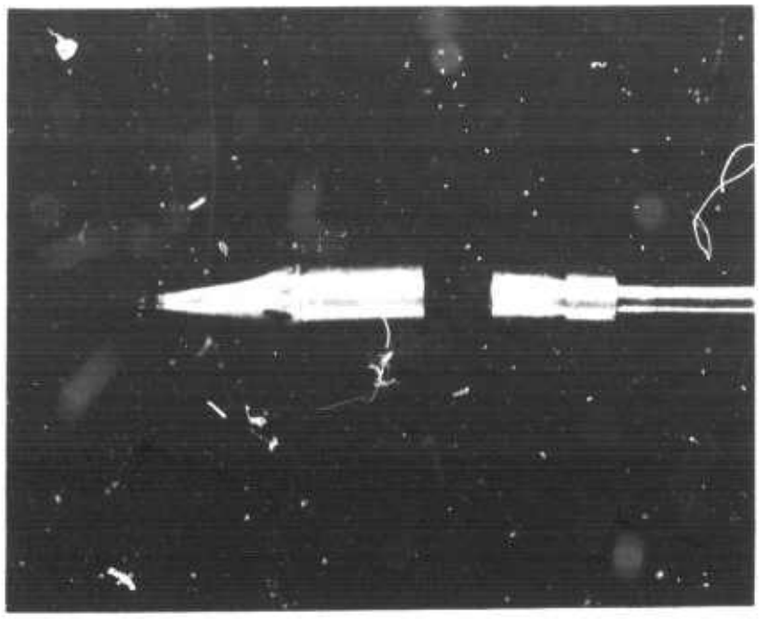

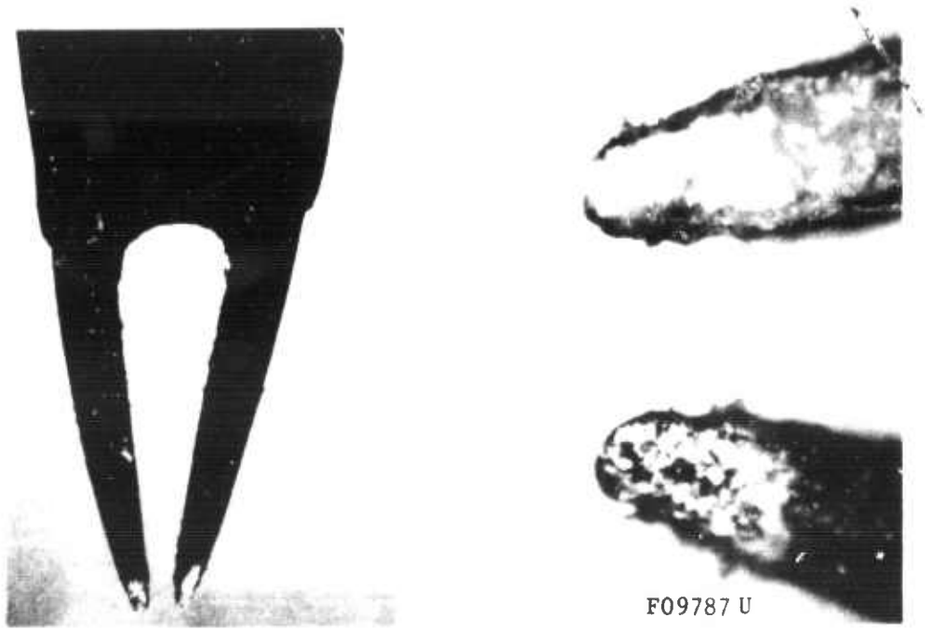

FIGURE 9. HOT-WIRE ANEMONETER PROBE SHOWN AT NEARLY FULL-SCALE AND ABOUT 100 X MAGNIFICATION (BELOW, RIGHT).

procedure alleviated the need for end-loss corrections. The preparation of the wire was as follows:

(1) Mounting and Annealing. Wires were mounted with sufficient slack; the approximate initial resistance desired was in the range 36 to 38 ohms for a 0.00005 inch diameter wire which ensures an aspect ratio of about 200. The wire was then annealed to a dull glow at slightly over 12 ma for a few minutes.

(2) Tunnel Endurance Test. The wire was inserted in the wind tunnel and subjected to supersonic flow to allow permanent structural changes to occur.

(3) First Oven Calibration. The temperature resistance behavior of the wire was measured in the range 0 to 100°C in a controlled oven. Five temperatures in this range were chosen and at each, the wire resistance R was read for the following currents, I: 0.430, 0.7, 1.0, 1.1, 1.2, 1.3, 1.4, and 1.5 ma. The heating due to these currents is very small and thus R was a linear function of I^2. The resistance $R(I = 0)$ was next obtained by extrapolation and, after subtracting the line resistance $R_L = 0.95$ ohm, the curve R versus T (the temperature) was obtained. With the aid of the resistivity formula

$$R = R' \left[1 + \alpha(T - T')\right] \tag{1}$$

where $T' = 0°C$, the values of $\alpha(0°C)$ and $R'(0°C)$ was obtained.* Typical values of α thus found were in the range 1.45 to 1.65 x 10^{-3} ohm/°C, with the majority being somewhat below the value 1.6 x 10^{-3} recommended by Morkovin.[25] This difference might be due to end-effects arising from the modest aspect ratios used. Table I gives typical values of α and the resistance-temperature slope αR.

(4) First Flow Calibration. The objective of this step was to obtain the variation of the Nusselt number at zero overheat Nu_o and of the wire recovery factor η with Reynolds number Re_o for each wire. The subscripts here refer to stagnation conditions, that is,

$$Nu_o = \left[\frac{qd}{T_w - T_{aw}} \frac{1}{k_o}\right]_{I=0} \tag{2}$$

$$Re_o = \rho \frac{ud}{\mu_o} \tag{3}$$

*Note that Spangenberg[24] observed that the second coefficient of resistivity was zero for 0.00005 inch Pt 10 percent Rh wires.

TABLE I

HOT-WIRE CHARACTERISTICS (0.00005 INCH WIRES ONLY)

Wire No.	R(0°C) (ohms)	αR(0°C) ohm/°C	Aspect Ratio	(α per °C)
2-4/2	34.27	0.0508	191	1.482×10^{-3}
3-4/2	34.70	0.0495	193	1.427
3-11/2	34.05	0.0574	190	1.686
6-1/1	38.48	0.0589	214	1.53
6-9/1	35.82	0.0606	202	1.692
6-15/2	34.85	0.0555	195	1.593
9-9/?	34.20	0.0502	191	1.468
9-29/1	35.05	0.0534	196	1.524
10-3/1	34.48	0.0547	193	1.586
10-4/1	34.48	0.0547	193	1.586
10-15/1	35.84	0.0554	200	1.546
12-7/1	35.00	0.0532	196	1.520
12-9/2	36.74	0.0622	206	1.693
12-9/1	33.27	0.0501	186	1.501
12-12/2	37.09	0.0560	207	1.510
12-14/2	36.36	0.0557	204	1.532
12-16/1	35.80	0.0547	200	1.528
12-20/2	35.87	0.0538	200	1.500
12-21/2	35.68	0.0549	199	1.539
1-4/2	37.25	0.0568	208	1.525
1-10/2	36.95	0.0559	206	1.507
Averages:		0.0550	199	1.546×10^{-3}

and also

$$\eta = \frac{T_{aw}}{T_o} \tag{4}$$

where T_{aw} is the adiabatic wire temperature (at zero current I). The main advantage of these correlations is their insensitivity to Mach number M for $M \geq 2$ and their very small variation in the interval $1.5 < M < 2$, and the fact that the Mach numbers is the position of wake surveyed did not lie below about 1.5.

Because conditions external to the wake were almost at free stream level, a calibration point was chosen at x = 4.152 inch behind the body base with transverse coordinates y = 0, z = 0.400 inch. Since the latter two coordinates are measured from the wake axis, the latter was always found first prior to each flow calibration (see Paragraph 3.5 below). Conditions at the calibration point are shown in Table II. Note that the actual local stagnation pressure P_{oeff} is somewhat below the tunnel total pressure P_o, probably due to entropy losses in the weak compression fans downstream of the base.

In the flow calibration process the derivative $\partial R/\partial I^2$ was formed by reading R at values of current I = 0.5, 1.5, 2.1, 2.6, and 2.9 ma. The Nusselt number Nu_o at zero overheat is then given by

$$Nu_o = \frac{\alpha_r R_r}{\pi \ell k_o} \frac{R_{aw}}{\partial R/\partial I^2} \tag{5}$$

where α_r R_r and ℓ were obtained from the oven calibration (Equation (1)), R_{aw} is the adiabatic (zero current) resistance at the calibration point and k the air thermal conductivity computed at the known total temperature.[26] By the same token, the density ρ and velocity u were known at the calibration point, while the viscosity μ_o at stagnation temperature T_o was computed by Sutherland's formula.[27] The recovery factor was computed by using R_{aw} to obtain T_{aw} from Equation (1), and T_o.

Typical flow calibration curves are shown in Figures 10 and 11. The "universal" heat transfer law for infinite wires as correlated by Dewey[22] is also shown. As expected, the Nu_o - Re_o curve for aspect ratio 200 lies considerably higher then Dewey's curve. In fact points from the present results, correlated for the end effects, were found to lie on the universal calibration.

TABLE II

CONDITIONS AT THE CALIBRATION POINT

1. Coordinate x: 4.152 inches behind body
2. Coordinate y: 0 inch off axis
3. Coordinate z: 0.400 inch off axis

P_o (tunnel) mm Hg abs	P_{oeff} mm Hg abs
382	337
400	360
450	415
500	465
550	419
600	569
650	624

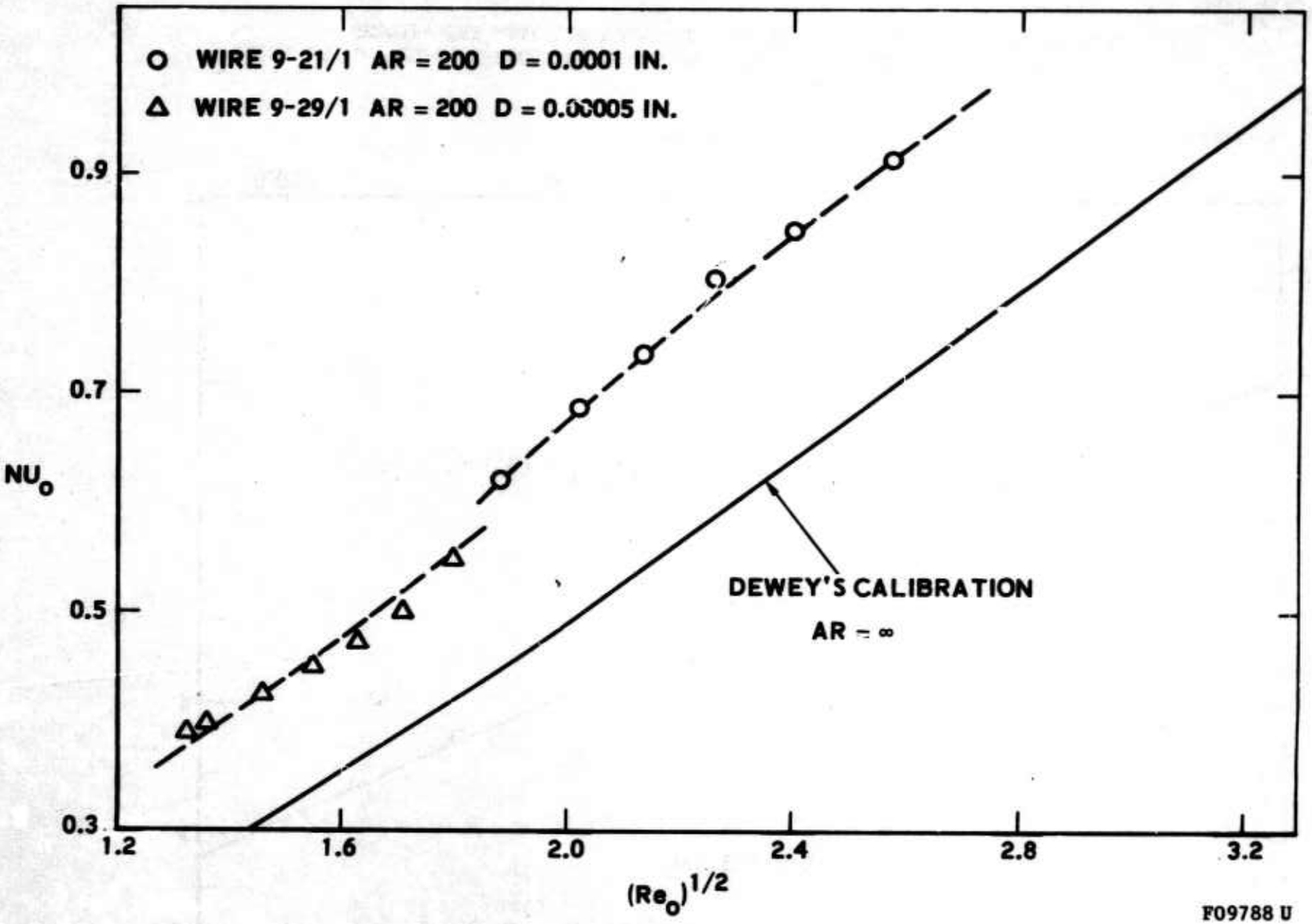

FIGURE 10. HEAT-TRANSFER CHARACTERISTICS OF TYPICAL HOT-WIRE PROBES; OFFSET FROM DEWEY'S CORRELATION IS DUE TO ASPECT RATIO A.R.

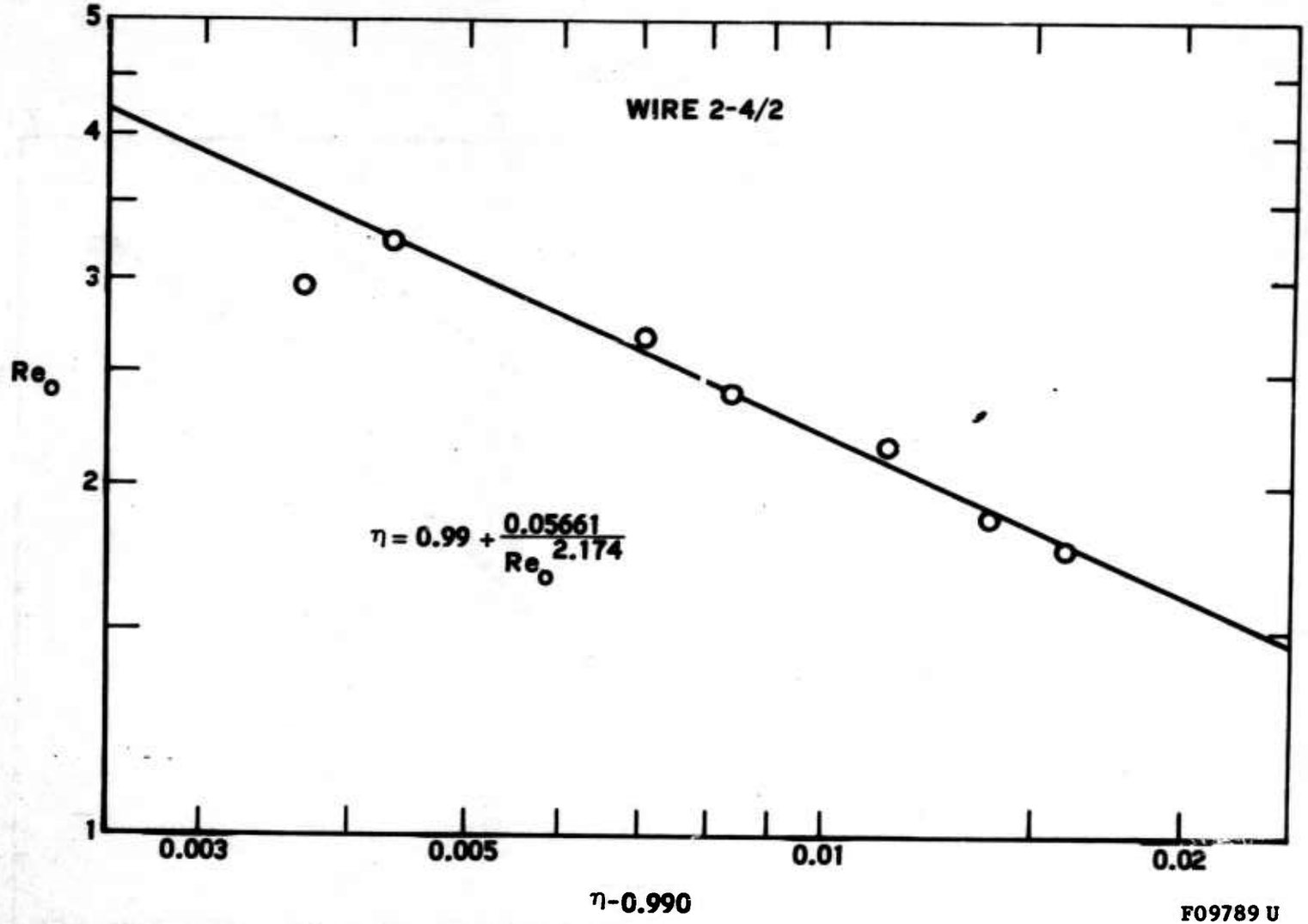

FIGURE 11. TEMPERATURE-RECOVERY CHARACTERISTIC OF TYPICAL HOT-WIRE PROBE SHOWING THE ANALYTIC FORM USED FOR INPUT TO THE COMPUTER PROGRAM.

The calibration curves obtained were put into analytical form for use in the computer program. Generally the form of these equations is

$$Nu_o = ARe_o + B\sqrt{Re_o} + C \tag{6}$$

$$\eta = D + ERe_o^F \tag{7}$$

with the constants A, B, etc., given in Table III.

TABLE III

CHARACTERISTICS OF WIRES USED FOR MEASUREMENTS

Material:	Pt 10% Rh
Diameter:	0.00010 inch (WEA) 0.00005 inch (WEB)
Length:	0.02 inch (WEA) 0.01 inch (WEB)

Heat Loss Characteristic:

$$Nu_o = 0.04186\ Re_o + 0.1803\ \sqrt{Re_o} + 0.1078$$

Recovery Factor Characteristic:

$$\eta = 0.9900 + \frac{0.05661}{Re_o\ 2.174}$$

(5) Subsequent Oven and Flow Calibration. After use it was desirable to subject the wire to further calibrations to ensure that its characteristics remained unchanged during the measurements. Figure 12 shows a second oven calibration of wire 10-4/1 which indicates that no significant changes occurred to the wire after prolonged use in the tunnel. Generally, subjecting the wires to repeated calibrations was not possible since the wires often broke after a series of measurements. As a rule, therefore, other indicators had to be used, such as the day-to-day change of wire resistance in still air or its resistance at certain preselected conditions in the flow. Resistance changes of more than 1 percent forced the rejection of accumulated data.

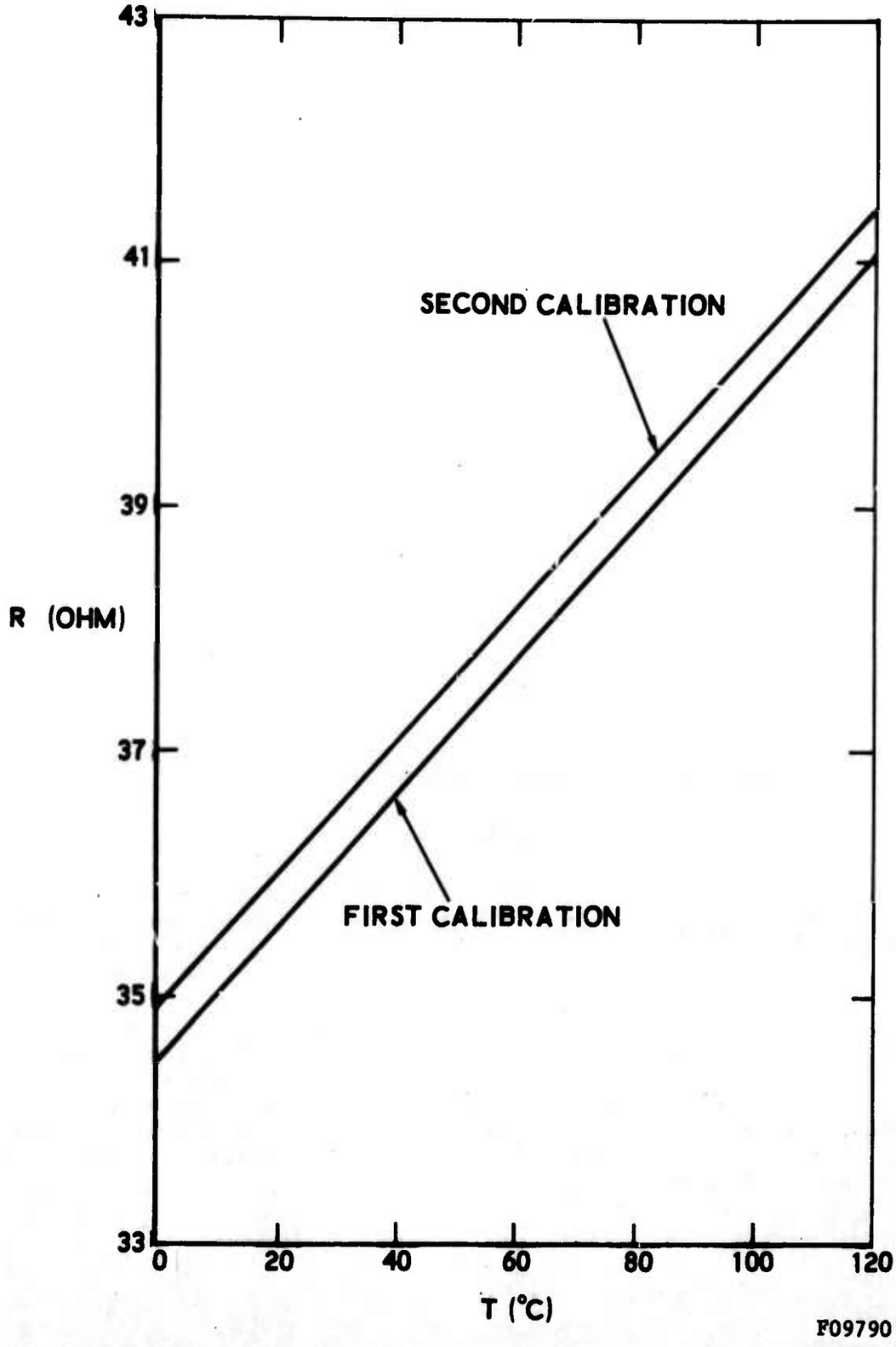

FIGURE 12. TYPICAL OVEN CALIBRATION OF 0.00005 INCH - DIAMETER WIRE. CALIBRATION SHIFT, OBSERVED AFTER PROLONGED USE, DOES NOT AFFECT THE TEMPERATURE - RESISTANCE SLOPE.

A systematic study of such changes of wire properties was conducted in order to confirm the observations of other workers regarding the effect of creep and deformation. Deformation due to the mechanical loads routine to these measurements was found insignificant; for example, no resistance shifts were found after consecutive starts and stops of the flow. The effect of creep manifested itself in the form of "aging" whereby daily resistance changes of order of 0.1 ohm per day were noted. Whenever possible, therefore, measurements were made immediately after calibration. The characteristics of wires used in this experiment are shown on Table I.

2.3.5 SCHLIEREN SYSTEM

A 60-inch focal length single-pass schlieren system was available for the measurements. Although this system was very sensitive by schlieren standards, it was not adequate for photographing the axisymmetric wake flow to any detail. Useful observations were made, however, on parts of the flow field (e.g., the nozzle wall boundary layer) where two-dimensionality enhanced the image.

SECTION 3

PRELIMINARY OBSERVATIONS

3.1 EXTERNAL FLOW FIELD

Surveys of the external flow field without the rod were conducted and are shown on Figures 17 through 21 of Reference 11. With the rod in place the external flow can be studied in the results to be quoted below. In either case the flow was found to be uniform, steady and repeatable.

3.2 TRANSITION TO TURBULENCE

Schlieren photography, pitot probe and preliminary hot-wire measurements disclosed that, as expected, the sidewall boundary layer was laminar at the lower tunnel stagnation pressures p_o and wholly turbulent at the higher pressures. The approximate location of the transition zone with p_o is shown in Figure 23 of Reference 11 as a function of distance from the throat. The circular rod, also being effectively another tunnel "wall," showed the same transition characteristics. Below about p_o = 480 mm Hg the wake shed off the rod was laminar, and transition in the wake moved downstream as the pressure was decreased further. It was therefore necessary to choose a p_o for these experiments so that the layer on the rod was laminar (i.e., the wake would not be too thick initially), and that it would become turbulent as early downstream of the base as possible. The pressure p_o = 508 mm was chosen on that account, and transition in this case was found to lie between x/D = 10 and 15, where x is the streamwise distance from the base and D the rod diameter (D = 0.156 inch).

Although turbulence is considered retentive of only the integral properties of the flow which generated it, a survey of the rod boundary layer at the plane of the base was made. The resulting pitot pressure profile is shown on Figure 13. It displays the form typical of a laminar boundary layer.

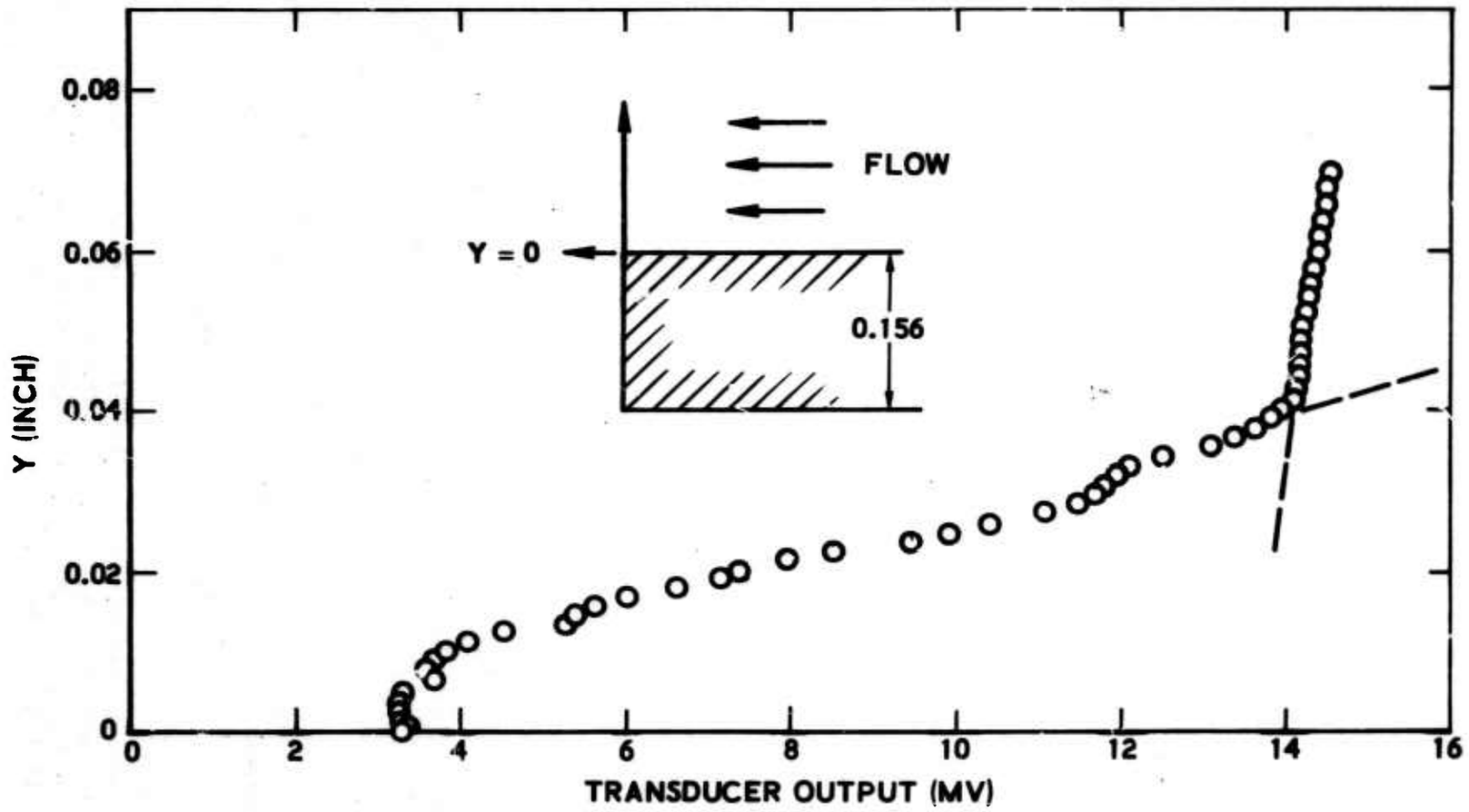

FIGURE 13. PITOT-PRESSURE PROFILE OF THE ROD BOUNDARY-LAYER IN THE PLANE OF ITS BASE. P_o = 508 MM HG.

3.3 FREE STREAM TURBULENCE

The turbulence level in the free-stream has been measured at low (420 mm) and high (735 mm) total pressures. The energy spectrum of the turbulence level was taken at these pressures primarily to ensure that the frequency response of the electronics was adequate and to infer the scale of the disturbances. The fluctuations for low and high pressures were, respectively: mass-flow fluctuations, 1.47 and 0.82 percent; total temperature fluctuations, 0.42 and 0.23 percent; and the correlation coefficient, +0.87 and +0.5. Although these figures are a factor of two to three higher than desired, it has already been found that they represent a stream turbulence level considerably lower than that generated by the wake itself and, moreover, uniform within the test flow area. There is therefore no danger of obscuring the wake itself, although efforts to verify and reduce this free-stream level are planned for the sake of completeness.

3.4 MODEL ALIGNMENT AND FLOW SYMMETRY

The flow about slender bodies at supersonic and hypersonic speeds is very sensitive to the angle of attack. This problem is serious for axisymmetric geometries and is further compounded by the fact that the flow direction in any wind tunnel is known only approximately. Special care was therefore taken to ensure that the flow in the wake was symmetric.

Referring to Figure 14, the basic precept is that the angle of attack is zero (1) when the flow proprties are mirror-symmetric about the axis in the XY and XZ plane and (2) when at each X station the XY and XZ property profiles are identical. During the wake Experiment A (WEA) traverses only in the Y (up-down) direction were made; the model was realigned until these profiles were symmetric. To ensure that the traverse crossed the axis, the probe then was adjusted repeatedly in the Z-direction until the pitot pressure was the lowest obtainable at its minimum point. For the wake Experiment B (WEB) the Z-motion component of the probe actuator became available (see Reference 11, Paragraph 2.5.19) and the model alignment was performed more properly. The wake axis was first established by alternating Y- and Z-traverses. The model was then tilted slightly either by adjustment of its strut upstream of the throat or by slightly bending the rod at the throat. Radial, i.e., mirror-symmetry about the axis could easily be established. Peripheral symmetry (i.e., identical Y- and Z-profiles) was harder to get, although not far from ideal, as Figures 15 and 16 indicate. Realignment was necessary several times during each experiment as the model and probe were removed often to avail the tunnel to other purposes.

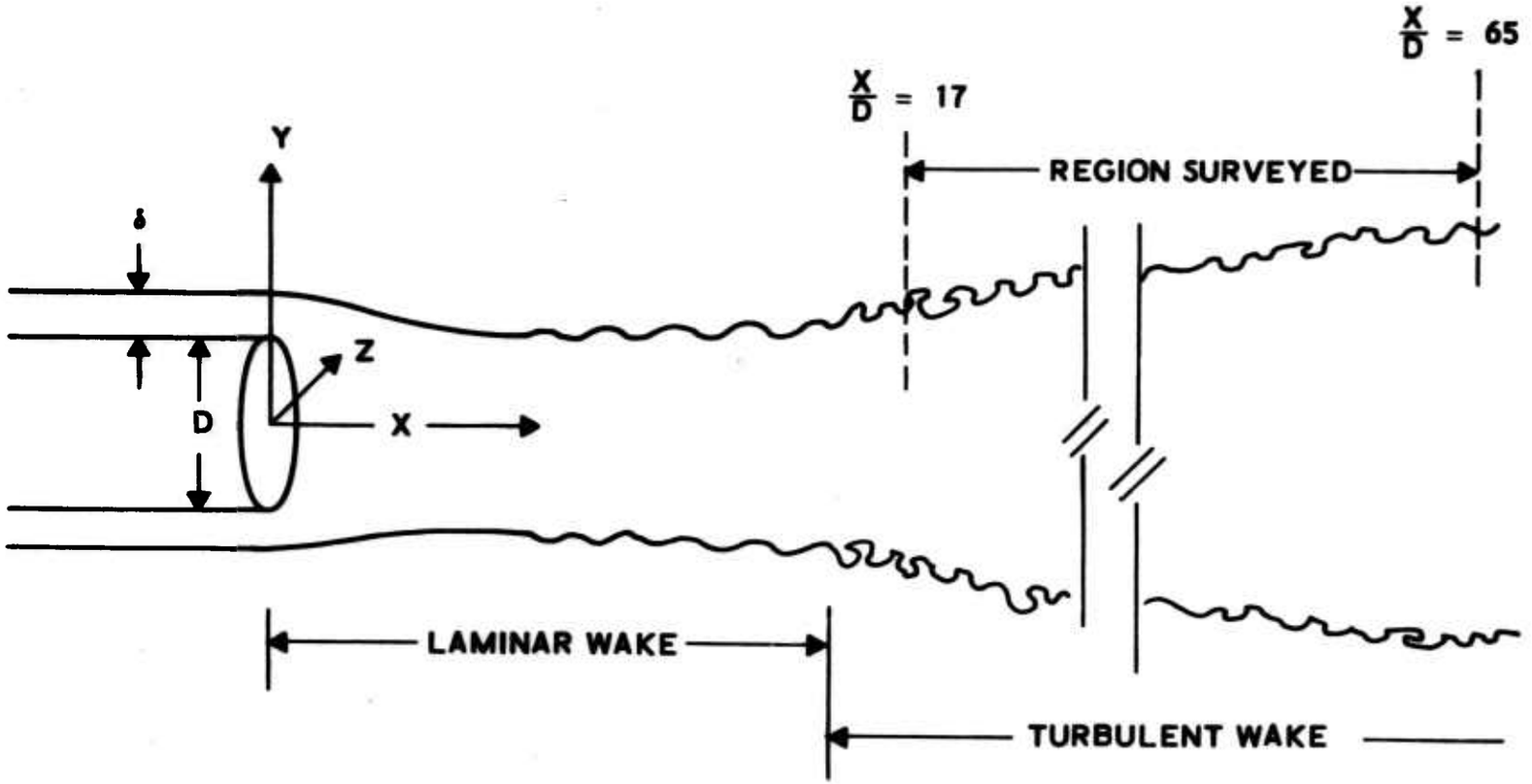

F09792 U

FIGURE 14. GEOMETRY AND NOMENCLATURE OF AXISYMMETRIC WAKE EXPERIMENT.

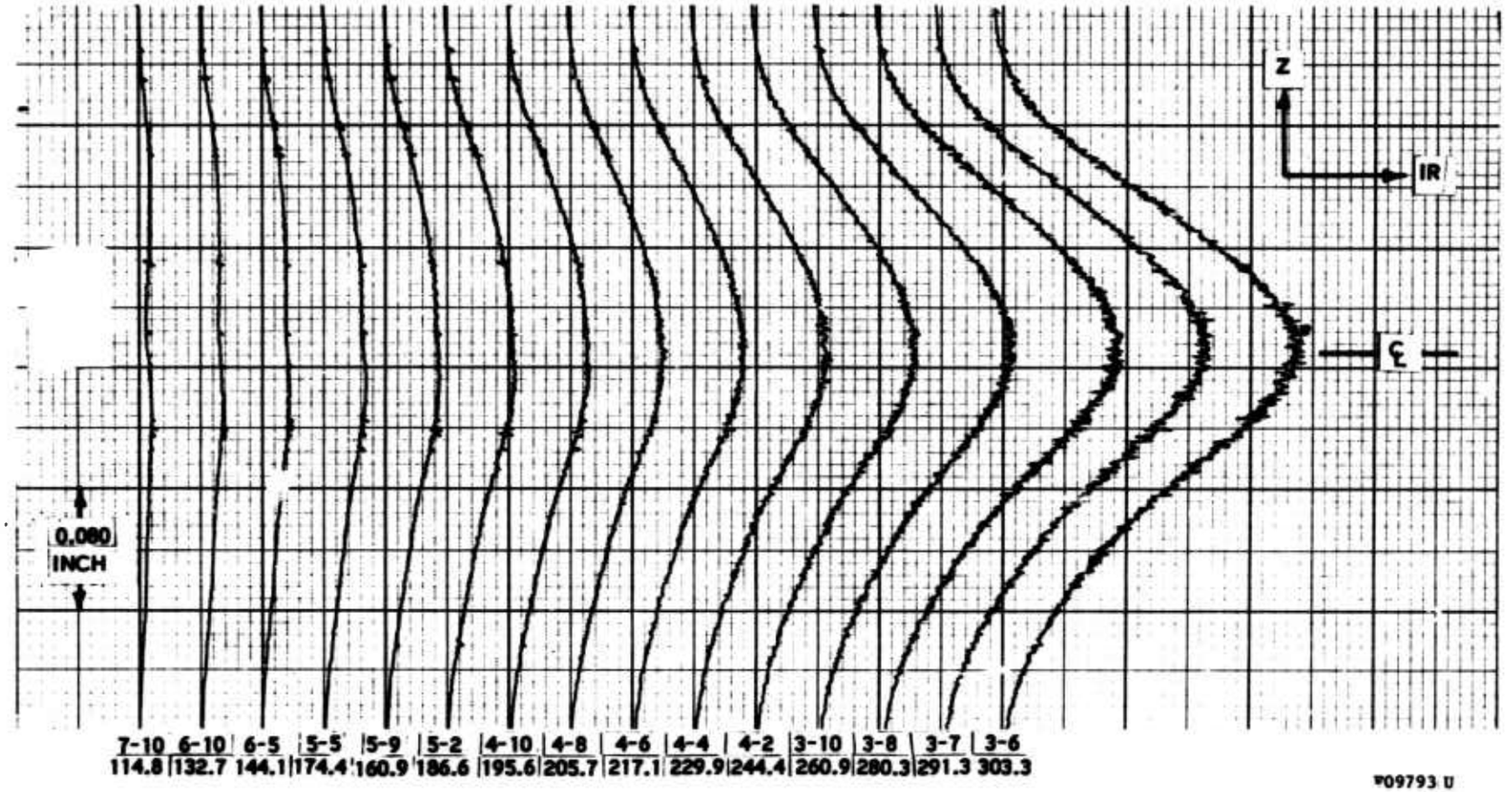

FIGURE 15. MEAN HOT-WIRE PROFILES (WIRE VOLTAGE VS. RADIUS) AT DIFFERENT CURRENTS REPRODUCED DIRECTLY FROM THE X-Y PLOTTER TO SHOW WAKE RADIAL SYMMETRY.

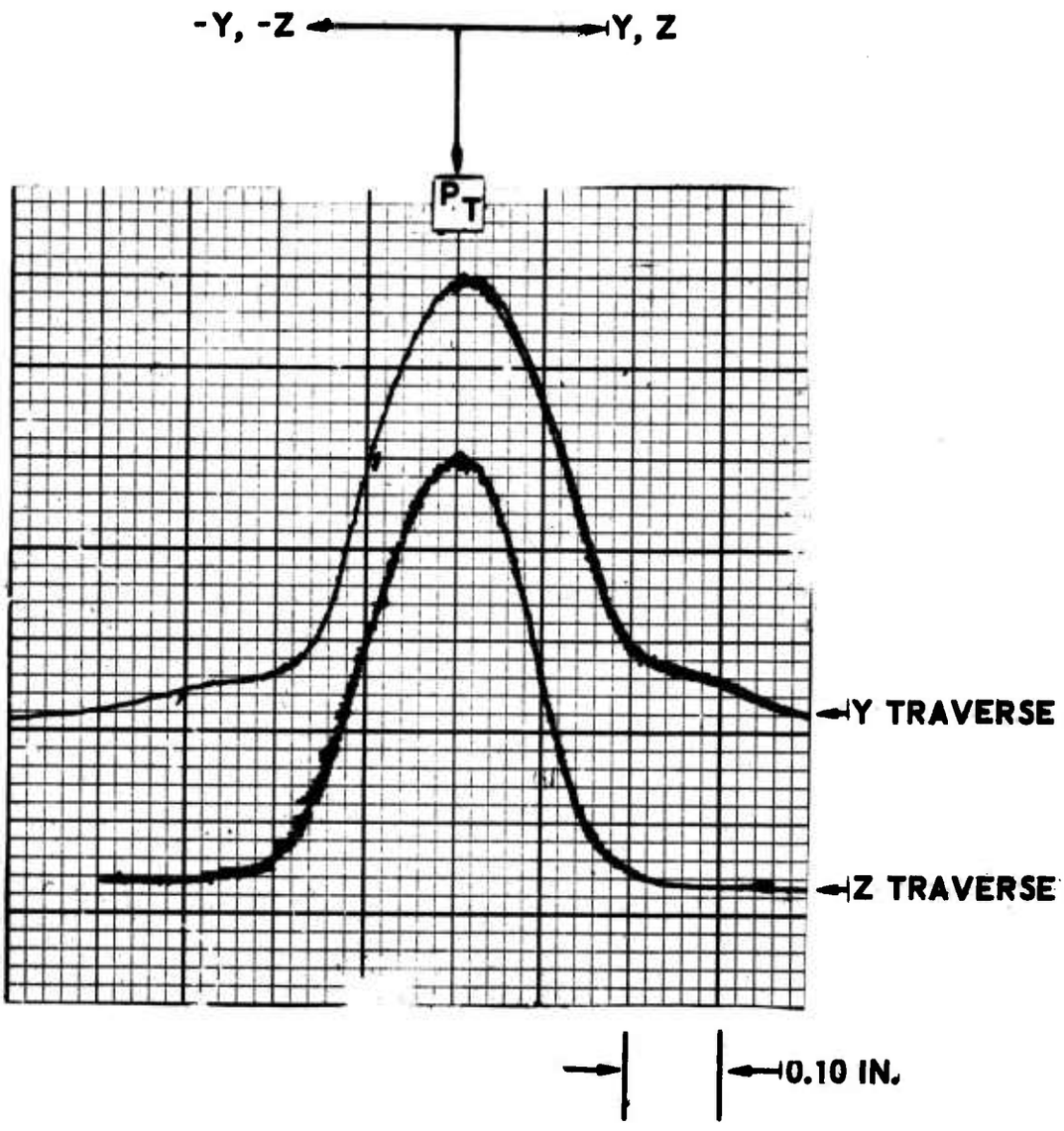

FIGURE 16. PERIPHERAL WAKE SYMMETRY AS SEEN BY Y (UP-DOWN) AND Z (RIGHT-LEFT) PITOT PRESSURE TRAVERSES.

SECTION 4

EXPERIMENTAL PROCEDURE

The axisymmetric wake was surveyed from a distance of x = 2.652 inches behind the base (corresponding to X/D = 17) to x = 10.652 inches. In experiments WEA and WEB this region was marked to 17 x-stations (called x station 0, 1, 2 . . .) spaced 0.50 inch apart. At each s tation the wake was surveyed radially - along Y in WEA, and along Z in the WEB. In wake Experiment C (WEC) the wake was traversed axially (along x) along the axis and also along a line parallel to the axis at y = 0, z = 0.400 inch. The intent of WEC was to provide a separate measurement of axial properties.

For all measurements the probes were first "centered" by alternating y- and z-traverses. At each x-station the probes were then traversed in the indicated direction and a continuous trace of pressure versus distance was obtained by an x-y plotter. Since the profiles were symmetrical, emphasis was placed in obtaining one-half of the complete traverse, especially for the hot-wire where fear of wire breakage accelerates the data-taking procedure. A continuous trace, besides being more accurate and much faster than a point-by-point measurement, provides one with an option as to how many individual points along the radius one wishes to process through the computer. In the hot-wire traces "index points" obtained with a digital voltmeter were marked at the extremities of the traces for purposes of cross-checking and calibration.

Since the local Nusselt number requires, at each point, the measurement of the slope $\partial R/\partial I^2$ (Equation (5)) five hot-wire traverses at each x station were taken at the following current settings: i = 1.00, 2.2, 2.7, 3.0, and 3.4 ma. The line resistance was 1.04 ohm.

SECTION 5

DATA REDUCTION

As indicated above, seven traverses were obtained at each x-station for experiments WEA and WEB (static, pitot pressure and five hot-wire traces) providing, in principle, an infinite number of radial points. For reasons of expediency 23 radial points were selected at each x-station, spaced 0.128 D apart, for analysis. The latter was programmed on the Philco 2000 digital computer; the relevant programs for the corresponding experiments are called WEA and WEB-I, and WEC. The data available from the WEC experiment consisted of seven x-traces and on seven off the wake axis. These were divided into x increments of 0.25 inch. The three programs are essentially the same and are described in Appendixes B and C.

Experiments WEA and WEB involved, as mentioned above, radial measurements at fourteen preselected axial locations (stations 0 through 13); data at stations 14 through 16 were taken during WEA, but they were of inferior quality because of poor flow at the diffuser entrance, and are not included in the data reduction process. These stations are displayed on Table IV. Furthermore, the WEA experiment was prejudged to be of somewhat inferior quality to that of WEB mainly because the probe centering procedures used during the former were not as foolproof.

As mentioned above, enough measurements were taken for WEC to utilize the WEA or WEB-I programs. During the data reduction process, however, it was noticed that the hot wire with which data for the WEC were taken and had undergone a sudden resistance change, apparently as the result of overnight creep. The hot-wire data were unusable; however, because of the rather slow T_o variation along the axis it was decided to reduce the pitot-static data with the assumption of a constant T_o. The WEC program was thus quite simple.

TABLE IV

AXIAL MEASURING STATIONS

Station	x (inch)	X/D
0	2.652	17.00
1	3.152	20.21
2	3.652	23.41
3	4.152	26.62
4	4.652	29.82
5	5.152	33.03
6	5.652	36.23
7	6.152	39.44
8	6.652	42.64
9	7.152	45.85
10	7.652	49.05
11	8.152	52.26
12	8.652	55.46
13	9.152	58.67
14	9.652	61.87
15	10.152	65.08
16	10.652	68.28

These three programs were designed to reduce the probe readings into flow variables (velocity, density, etc.) and to take a first step toward nondimensional representation, i.e., nondimensional variables versus nondimensional radii and axial distances. There are, however, a number of possible nondimensionalizations and their comparison is an objective of this work. Program WEB-V was set up to conduct such a comparison.

Originally, this program was also designed to deduce turbulent transport properties in the axisymmetric wake through a point-by-point evaluation of first- and second-flow derivatives. Because of the normal scatter of experimental points this scheme was unsuccessful and an improved procedure is now being used.

SECTION 6

RESULTS AND DISCUSSION

6.1 DIMENSIONAL FLOW PARAMETERS

The radial and axial distributions of flow axial velocity, pressure, temperature, and density have been obtained in the range X/D = 17 to 65 in this experiment. Typical results appear in Figures 17 through 19. The satisfactory agreement among the three different experiments performed should be noted.* On the surface, these results can be summarized briefly as follows:

(1) The static pressure is approximately constant both along and across the wake. Figures 18 and 19 show that the worst case (far downstream) the ratio of pressure and inertial force is of order

$$(dp/dx)/\rho u \frac{du}{dx} = 0.5 \qquad (8)$$

and is actually very much smaller nearer the body; this allows the pressure gradient to be neglected in further discussion.

*Strictly speaking, elements additional to periphery symmetry are involved in comparing the three experiments. Large time intervals (e.g., months) lapsed between experiments and different hot wires and other slight differences in instrumentation were used.

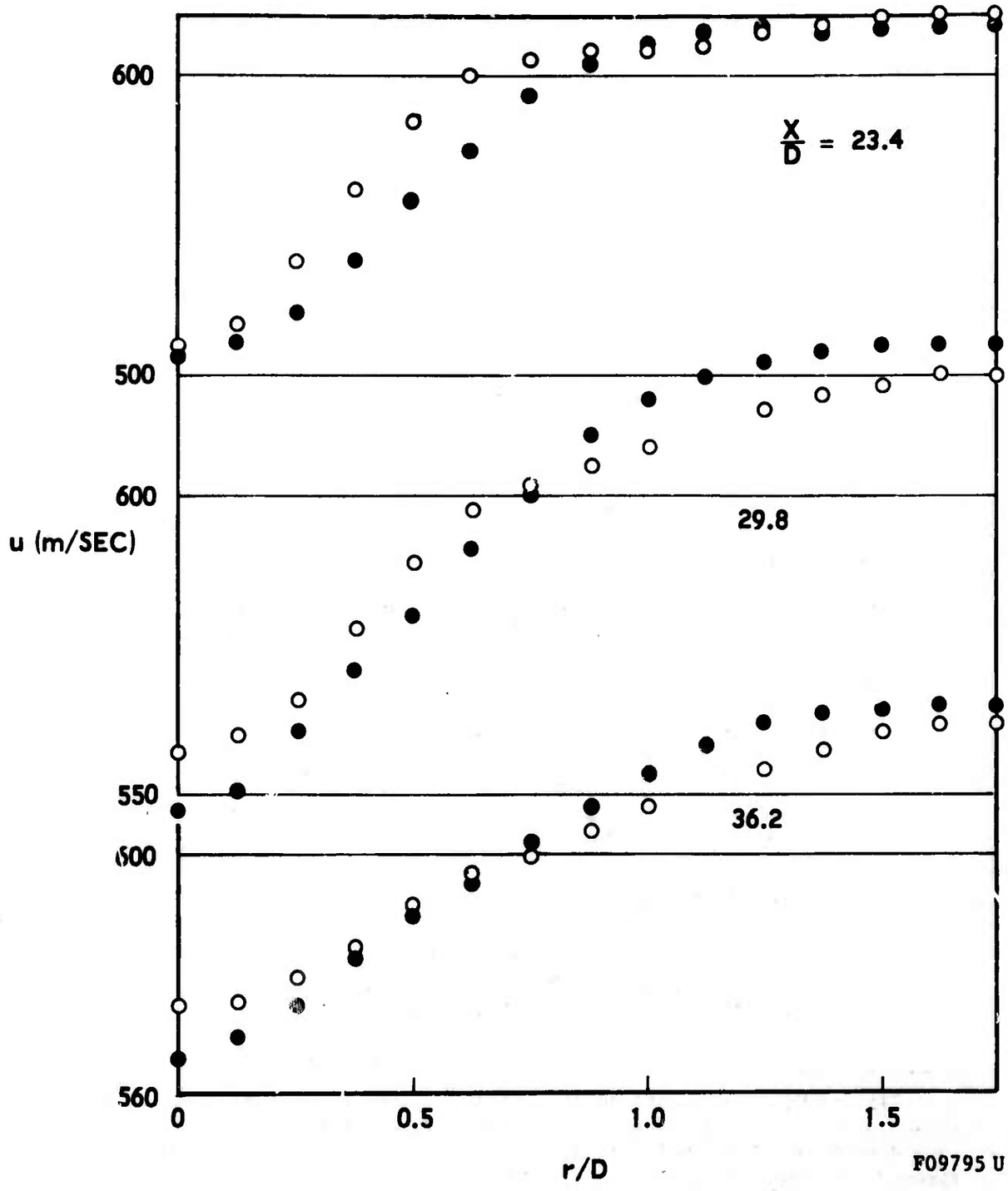

FIGURE 17. TYPICAL DISTRIBUTIONS OF AXIAL VELOCITY VERSUS RADIUS (BLACK CIRCLES: WEB, OPEN CIRCLES: WEA)

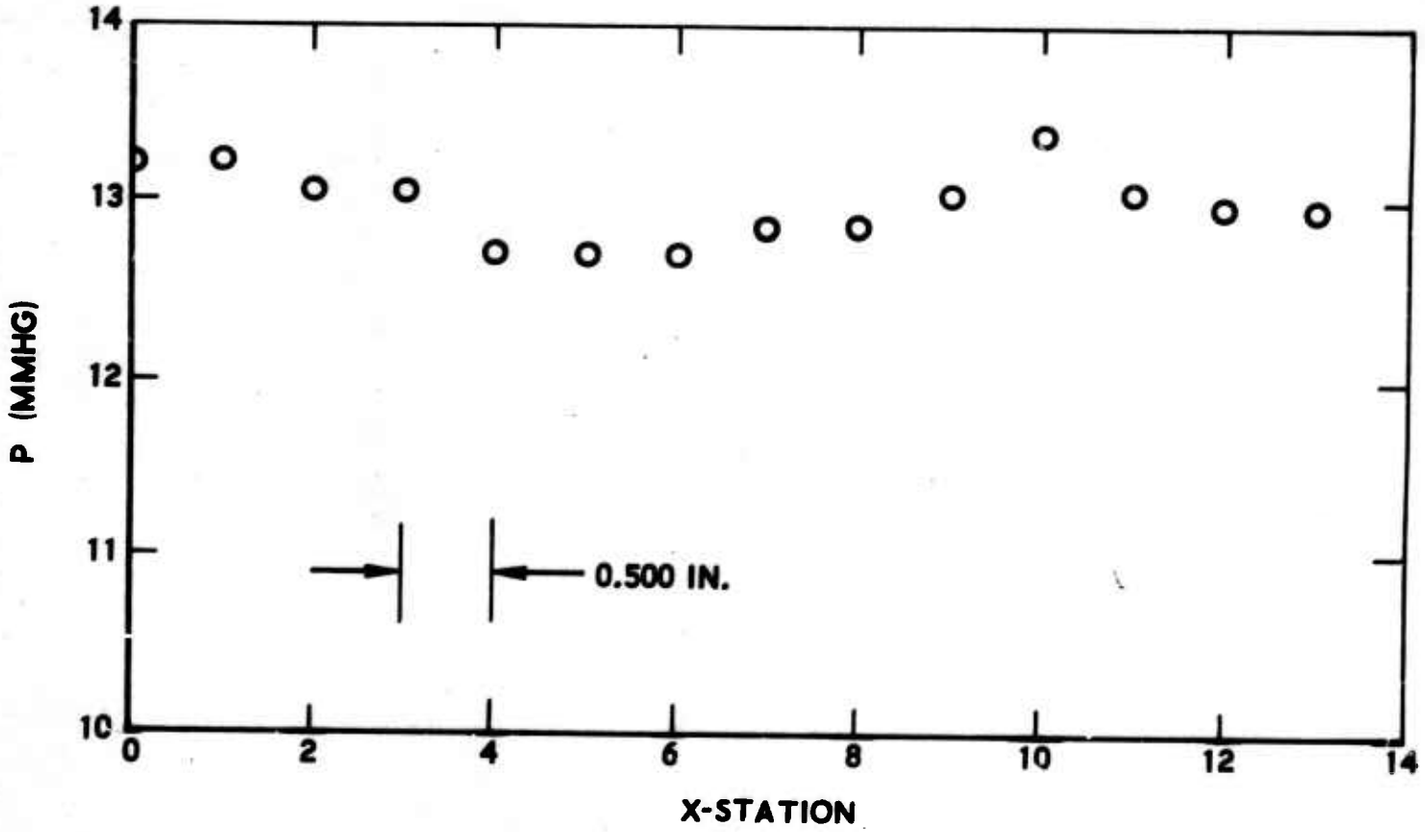

F09796 U

FIGURE 18. VARIATION OF AXIS STATIC PRESSURE IN THE REGION INVESTIGATED.

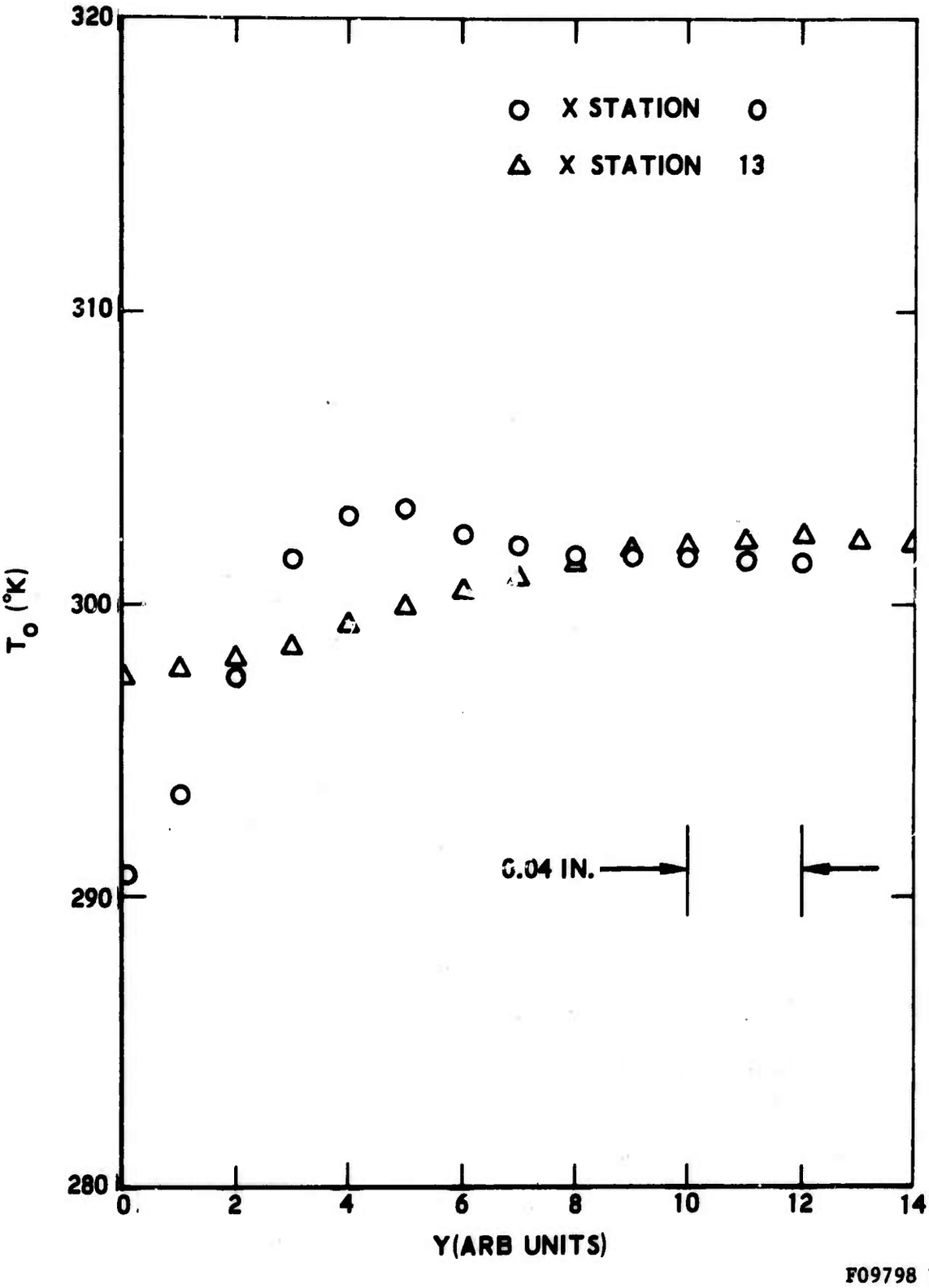

FIGURE 19. TYPICAL RADIAL VARIATION OF LOCAL TOTAL TEMPERATURE, T_o

(2) The flow in the wake during Experiment WEA was found d rted beyond Station 13 (corresponding t. $x/D = 58.7$). Although data from these stations are occasionally discussed below, no data at Stations 14 through 16 were obtained in WEB and WEC.

(3) The axial variation of the axis properties (velocity, density, and temperature) is smooth and normal to the farthest station investigated.

6.2 REDUNDANCY CHECK

As explained earlier, the Reynolds number, $Re_o = \rho ud/\mu_o$ (where ρ and u are local values, d is the wire diameter, and μ_o is the viscosity evaluated at the local stagnation temperature), was the fourth quantity measured at each point for purposes of redundancy. This check was performed by utilizing the data (from the WEA and WEB-T outputs) as inputs into the WEB-V program.* Figure 20 shows the results of this redundancy check; agreement with the (P_T, P, T_o) group of measurements was very satisfactory considering that the Re_o-measurement is inherently unsafe unless large variations in Reynolds number are involved and many I versus R points are used.

For a small number of x-stations in WEB, an unexplainably large shift in the level of Re_o, as supplied by the WEB-I output, was seen. Indications are that this discrepancy, almost a factor of 2, was the result of possible misreading of the wire current values. Once again, this occurrence accents the wisdom of not choosing Re_o as a primary sensing mechanism.

6.3 NONDIMENSIONAL REPRESENTATIONS AND SCALING LAWS

The ultimate purposes of this experiment are to provide an insight into the physical mechanism of turbulent transport and to arrange the data in a form useful for practical applications. In preparation for this, empirical ideas anticipating the experimental results will be presented in the following paragraphs.

6.3.1 VIRTUAL ORIGIN

Because transition occurs at some distance downstream of the base and the rate of wake growth is reasonably expected to change at transition, it is necessary to find the virtual origin of the wake. Origin implies the point on the axis where the fluid stagnates, i.e., where $u = 0$ and $T = T_o$. To accomplish this, the velocity and temperature "defects"

$$w \equiv \frac{u_\infty - u(o)}{u_\infty} \qquad (9)$$

*See Appendix D

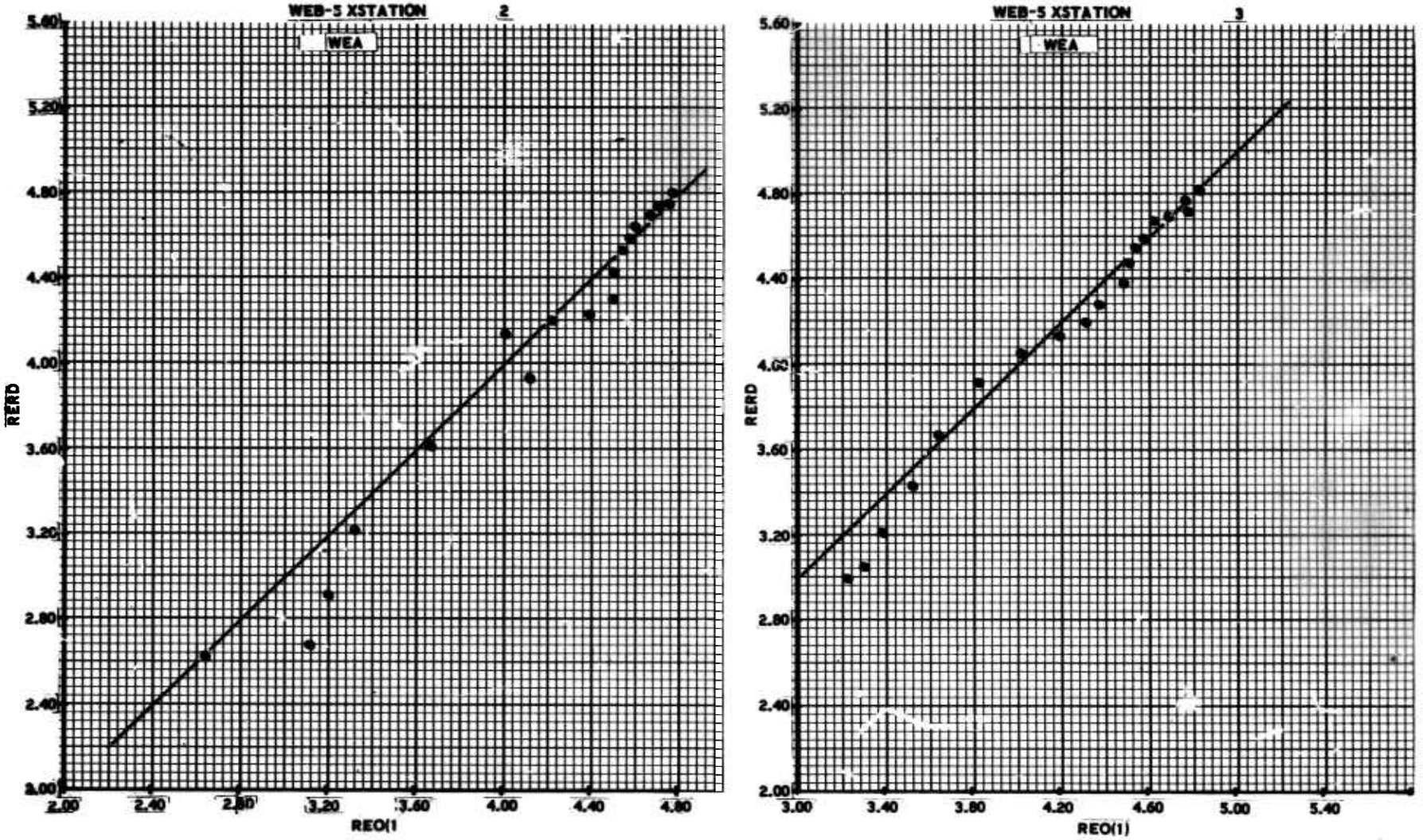

FIGURE 20. TYPICAL AGREEMENT BETWEEN WIRE THE REYNOLDS NUMBER COMPUTED FROM NUSSELT NUMBER MEASUREMENTS (RE(OX) AND THAT COMPUTED FROM THE VELOCITY, DENSITY AND STAGNATION VISIONITY (RERD). SOLID LINE REPRESENTS 100 % AGREEMENT.

$$\theta \equiv \frac{T(o) - T_\infty}{T_\infty} \tag{10}$$

were initially plotted versus the nondimensional distance x/D. The resulting curves were then extrapolated to

$$w\left[u(0) = 0\right] = 1 \tag{11}$$

$$\theta\left[T(0) = T_o\right] = 1.8$$

as shown on Figure 21. The velocity variation puts the origin at x/D = 8 while the temperature variation puts the origin at x/D = 10. As a compromise, the virtual origin, x_o, was set at nine diameters behind the base.

6.3.2 WAKE DRAG

The available theoretical treatment of laminar compressible wakes[28,29] and the phenomenological treatment of the turbulent wake[4] recognizes that in their similar or self-preserving state these flows can be adequately described by such integral properties as their momentum defect or drag. In this way it is recognized that the geometry of the model employed here and the details of the flow about its base are "forgotten" by the wake and that the present results can be applied to other body geometries if their drags are known. The "virtual" body which created the wake thus has a drag which can be equated to the measured momentum defect

$$\text{Drag} = \frac{1}{2}\rho_\infty u_\infty^2 C_D A = 2\pi \int_0^\infty \rho u(u_\infty - u)\, r\,dr \tag{13}$$

This quantity should be independent of x and should serve to define an effective (or virtual) body diameter

$$\sqrt{C_D A} = \left[4\pi \int_0^\infty \frac{\rho u}{\rho_\infty u_\infty}\left(1 - \frac{u}{u_\infty}\right) r\,dr\right]^{1/2} \tag{14}$$

The concept of the virtual diameter, $\sqrt{C_D A}$, was tested by numerical integration, through the WEB-V program, of the experimental results according to Equation (14). The constancy of $\sqrt{C_D A}$ from station to station, predicted by the conservation of momentum, is approximately verified by Figure 22 and it forms an added check of the measurement itself. This virtual diameter is the logical normalizing factor of the proper axial coordinate which, when combined with the results of Paragraph 6.3.1, becomes

$$\bar{x} \equiv \frac{x - x_o}{\sqrt{C_D A}} \tag{15}$$

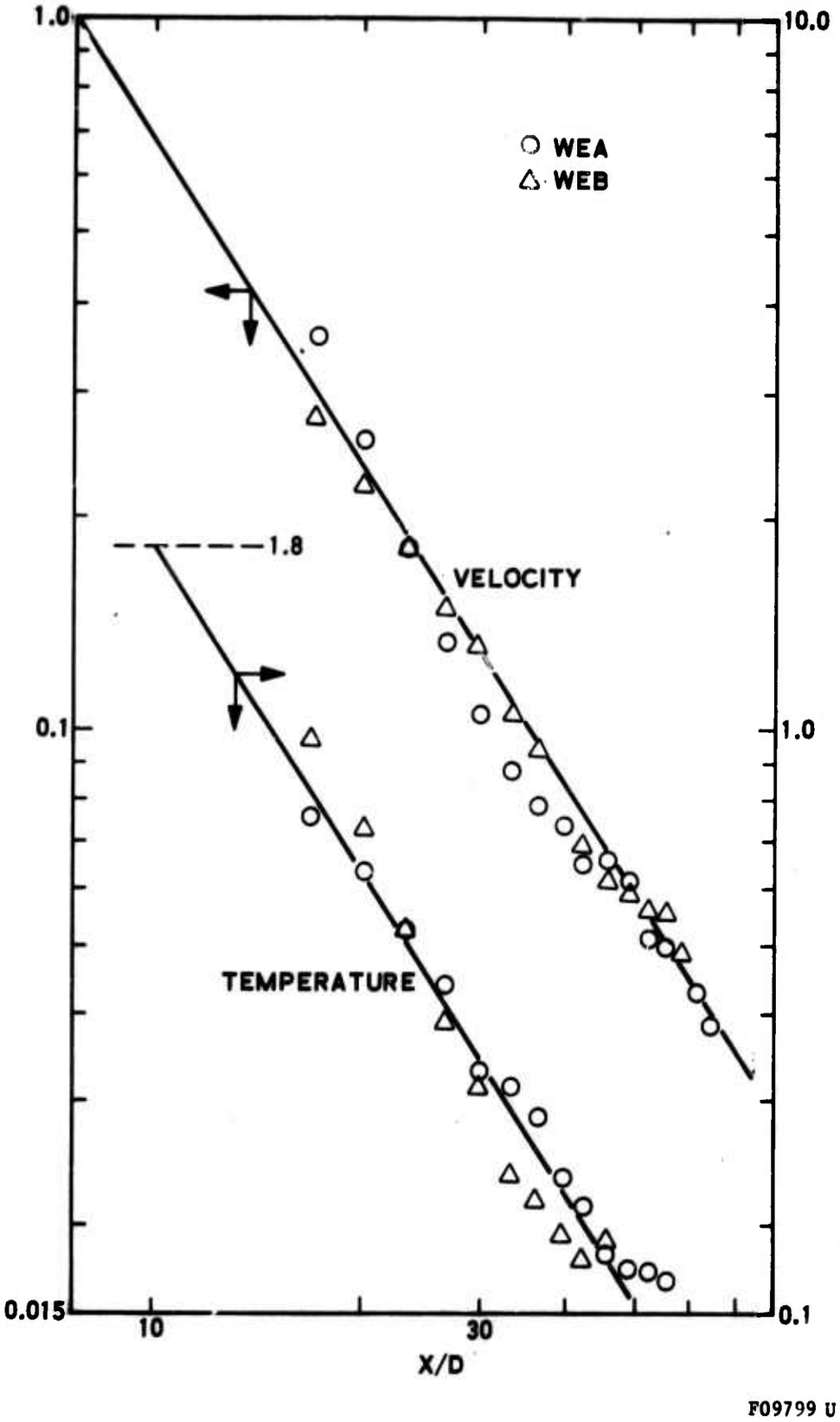

FIGURE 21. METHOD OF DETERMINATION OF WAKE VIRTUAL ORIGIN (X/D = 8 FOR THE VELOCITY, X/D = 10 FOR TEMPERATURE). ORDINATE IS PROPERLY NONDIMENSIONALIZED

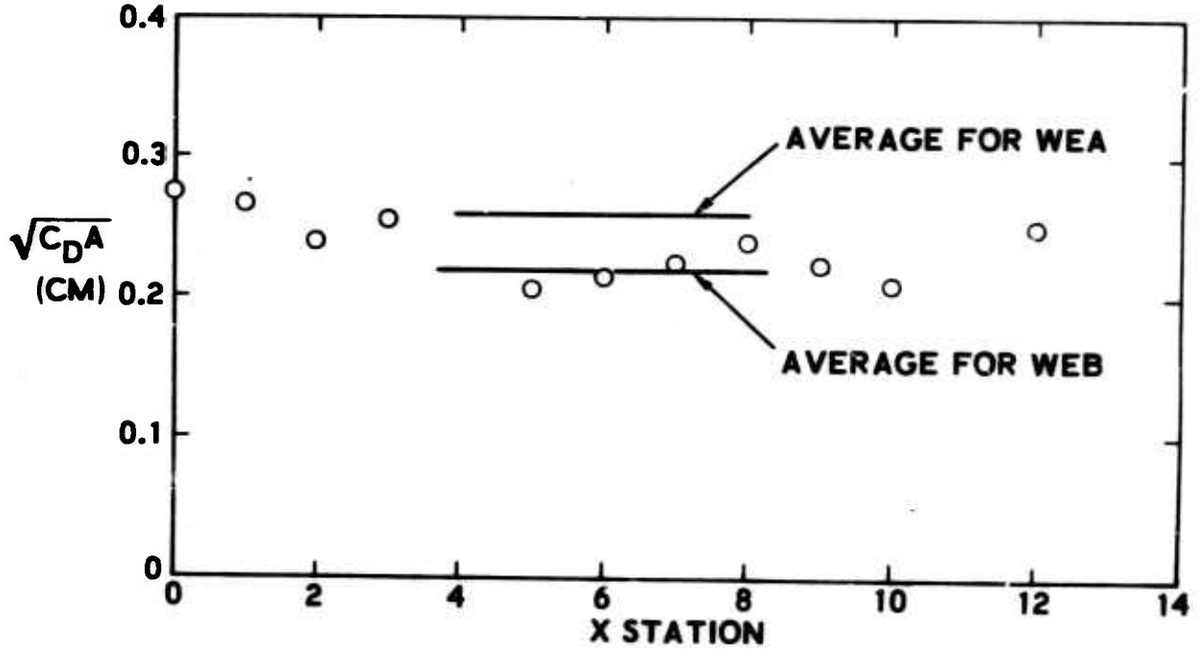

F09800 U

FIGURE 22. VARIATION OF THE WAKE EFFECTIVE OR VIRTUAL (DRAG) DIAMETER $\sqrt{C_D A}$ VERSUS AXIAL DISTANCE.

where the denominator has been averaged by the results of Figure 22. It is interesting to note that the virtual and model diameters are related by

$$\frac{\left(\sqrt{C_D A}\right)_{ave}}{D} = 0.70 \tag{16}$$

Alternately, if the area A in $(\sqrt{C_D A})_{ave}$ was to be that of the body itself ($A = \pi D^2/4$), then

$$C_D = 0.612 \tag{17}$$

6.3.3 PREDICTED FORM OF THE VELOCITY DISTRIBUTION

A self-preserving form of the wake of the following type is sought:

$$u = u_{\infty} - Uf(\eta') \qquad f \leq 1 \tag{18}$$

$$\rho = \rho_{\infty} - \rho' g(\eta') \qquad g \leq 1 \tag{19}$$

$$T = T_{\infty} - \textcircled{H} h(\eta') \qquad h \leq 1 \tag{20}$$

where the characteristic velocity, density, and temperature are defined by $U \equiv u_{\infty} - u$, $\rho' \equiv \rho_{\infty} - \rho$, $\textcircled{H} \equiv T(o) - T_{\infty}$, respectively and where

$$\eta' \equiv \frac{r}{L'} \tag{21}$$

with L' unknown. To find L' Equations (18) and (19) are inserted in the drag integral, Equation (13), resulting in

$$C_D A = 4\pi L'^2 w \int_0^{\infty} (1 - \rho' g - wf + \rho' w fg) f \eta' d\eta' \tag{22}$$

Since w, ρ', $\rho \ll 1$ in the self-preserving region the result is in the first approximation,

$$\frac{L'^2}{C_D A} = \frac{1}{4\pi wI} \tag{23}$$

where

$$I \equiv \int_0^{\infty} f \eta' d\eta' \tag{24}$$

is a pure number which is also unknown a priori. However, if similarity is obtained for η', it will also be obtained for

$$\eta = \frac{r}{L} = \frac{r}{L'}\frac{L'}{L} = \frac{\eta'}{\sqrt{I}} \tag{25}$$

where

$$L = \sqrt{I}\, L' = \left(\frac{C_D A}{4\pi w}\right)^{1/2} \tag{26}$$

The purpose of thus defining L is that it can be measured from the experiment directly and that, according to Equation (26), is exactly equal to (and can thus be identified with) the "traverse wake scale" as previously used by Tounsend.[4] The similarity parameter is thus r/L.

A similar result can be obtained if the Howarth-Dorodnitzyn radius

$$\bar{r}^2 = 2\int_0^\infty \frac{\rho}{\rho_\infty}\, r\,dr \tag{27}$$

is used with the drag integral, in which case the similarity variable is $\bar{r}/L$. This procedure, used by Lees and Hromas in their original calculations,[28] is somewhat dubious because it implies that turbulent and laminar flows transform in the same manner. In any event, the physical and transformed radii are equal to a good approximation for this experiment; therefore, $r \simeq \bar{r}$. It is concluded, from the previous discussion, that similarity can be searched for by plotting the quantity $f = (u_\infty - u)/(u_\infty - u(0))$ versus $\eta = r/L$ or $\bar{r}/L$.

Parenthetically, it should be noted that if the area A is taken to be that of the body cross section ($A = \pi D^2/4$) the following equation can be obtained from Equation (26):

$$\frac{L^2}{D^2} = \frac{C_D}{16w} \tag{27}$$

This equation is in complete agreement with Townsend[4] and Lees and Hromas.[28]

6.3.4 DEPENDENCE OF SCALE ON AXIAL DISTANCE

To complete the predicted behavior of the axial velocity it is necessary to postulate the dependence of U and L on the axial coordinate $\bar{x}$. At this juncture, the introduction of some sort of turbulent transport mechanism is inevitable. Insofar as the self-preserving behavior of the wake is concerned, Laufer's[29] suggestion that the concept of a turbulent Reynolds

number be tested against the results of this experiment as an extension of Townsend's formulation of low-speed turbulent transport will be adopted. Therefore

$$w = \frac{U}{u_\infty} = \frac{1}{\pi^{1/3}} \left(\frac{R_T}{6}\right)^{2/3} \frac{1}{\bar{x}^{2/3}} \tag{28}$$

Again, because of the constancy of the drag along the wake, the scale L becomes

$$\frac{L}{\sqrt{C_D A}} = \frac{1}{2} \left(\frac{\pi}{6} \frac{R_T}{\bar{x}}\right)^{-1/3} \tag{29}$$

These expressions, in which the virtual diameter $\sqrt{C_D A}$ is retained throughout, display the correct functional behavior with $\bar{x}$. The quantity R_T is the so-called turbulent Reynolds number defined by[4]

$$R_T = \frac{UL}{\bar{\nu}_T} \tag{30}$$

where $\bar{\nu}_T$ is the turbulent kinematic viscosity.* The R_T should be independent of both $\bar{x}$ and $\bar{r}$ if similarity in the far wake exists and if the correspondence between compressible and incompressible wakes is to remain.

A way to use the experiment to check the validity of the "universal" Reynolds number R_T is now evident. The slope of the curve $w = (u_\infty - u_o)/u_\infty$ versus $\bar{x}^{-2/3}$ should be a straight line for self-preservation, and the slope should be related to R_T through Equation (28); it would be especially interesting to see if R_T agrees numerically with the value of Townsend[4] or Hall and Hislop[30] ($R_T = 14$). Second, $\bar{\nu}_T$ can be formed directly from the linearized momentum equation

$$\bar{\nu}_T = \frac{\int_0^r \frac{\partial}{\partial x} (\rho u^2)\, r\,dr + \rho uvr}{\rho \left(r \frac{\partial u}{\partial r}\right)} \tag{31}$$

*In Townsend's notation, $U = u_o$ and $L = \ell_o$.

upon measuring $\rho(x,r)$ and $u(x,r)$. In any case, the measurement of $\overline{\nu}_T$ according to Equation (31) is, if feasible, the only hope of extracting $\overline{\nu}_T$ directly from the present work (or any work) without recourse to empiricisms and assumptions.

6.3.5 WAKE REYNOLDS NUMBER

In comparing wakes generated by different bodies at different speeds it is often convenient to describe the wake itself as a solid body whose motion is, in the self-preserving state, completely described by its integral properties and its local external flow conditions. Thus, there exists, as Townsend indicated, a meaningful Reynolds number

$$Re_w \equiv \frac{UL}{\nu_\infty} \tag{32}$$

which describes the motion of a body of characteristic dimension, L, moving with speed, U, through a medium of kinematic viscosity, ν_∞. For two-dimensional wakes this Reynolds number is constant along the wake,* but in the present case it should decrease as $\overline{x}^{-1/3}$; on this basis, Townsend expects that at far distances downstream the mean flow will become unable to transfer energy to the turbulence and a second self-preserving form of the wake flow (and its fluctuating component) will occur, referred to as the "final period."

6.3.6 PREDICTED FORM OF THE TEMPERATURE DISTRIBUTION

Conservation of energy can relate velocity and temperature by

$$C_p T_o = C_p T + \frac{u^2}{2} \quad . \tag{33}$$

For a completely isoenergetic wake (T_o = constant), a relation between U and $\textcircled{H}$ can be found immediately. For example, using h to denote enthalpy ($h = C_p T$)

$$\frac{\textcircled{H}}{h_\infty} \equiv \frac{h(0) - h_\infty}{h_\infty} \propto \frac{2(u_\infty - u(0))}{u_\infty \left(2 \frac{h_o}{u_\infty^2} - 1 \right)} \tag{34}$$

*See Reference 31, p 488.

because $u(0) \cong u_\infty$ far in the wake. Thus*

$$\frac{H}{h_\infty} = \frac{T(0) - T_\infty}{T_\infty} = (\gamma - 1) M_\infty^2 \frac{u_\infty - u(0)}{u_\infty} = (\gamma - 1) M_\infty^2 w \qquad (35)$$

By the same token, if at some portion of the wake it is desired to predict the distribution of the nondimensional temperature, $(T - T_\infty)/(T(0) - T_\infty)$, from a known distribution of $(u_\infty - u)/(u_\infty - u(0))$, the equation

$$\frac{T - T_\infty}{T(0) - T_\infty} = \frac{u_\infty - u}{u_\infty - u(0)} = f(\eta) \qquad (36)$$

can be formed because far in the wake $u \cong u_\infty \cong u(0)$. On the assumption of constant local total temperature, therefore, it looks as if the lateral spreading of temperature is the same as that of axial velocity and is also a unique function of η. This is contradictory to the experimental results as is the assumption of constant T_o (Figure 19). Even as rough a prediction as formulating here, therefore, should account for the variation of T_o as shown on Figure 19. The effect of the total temperature variation can be included by invoking the idea of a turbulent Prandtl number, σ_T. Then, in complete analogy with the far axisymmetric laminar compressible wake,[32,33] the following equation can be written

$$\frac{T(0) - T_\infty}{T_\infty} \sim \left(\frac{\sigma_T}{\frac{x}{}}\right)^{2/3} \qquad (37)$$

so that by combining Equations (35) and (37)

$$\frac{T(0) - T_\infty}{T_\infty} = (\gamma - 1) M_\infty^2 \sigma_T^{2/3} \left(\frac{u_\infty - u(0)}{u_\infty}\right) \qquad (38)$$

where σ_T is the so-called turbulent Prandtl number. Further, it can be reasonably expected that

$$\frac{T - T_\infty}{T(0) - T_\infty} = \left(\frac{u_\infty - u}{u_\infty - u(0)}\right)^{\sigma_T} \qquad (39)$$

---

*For variable total temperature across the wake, Equation (35) should contain a term proportional to T_o (see Reference 34, Equation (15)). Inspection of the present experimental results shows that this term is negligible in our case.

This relationship between the nondimensional wake temperature and axial velocity is a well-known empirical law which has been established for many varieties of free turbulent flows.[35] This law states that, because $\sigma_T < 1$ and $0 < (u_\infty - u)/(u_\infty - u(0)) < 1$, the "temperature wake" is thicker than the velocity wake, implying rather than explaining the complex processes of turbulent lateral transport. In the present experiment the turbulent Prandtl number can be found from the experimental data either by using Equation (38) and the data along the axis only, or by utilizing the radial distributions in conjunction with Equation (39).

6.3.7 PREDICTED FORM OF THE DENSITY DISTRIBUTION

Because the static pressure remains approximately constant along and across the wake, the distribution of density with axial and radial distance must be discussed. For the isobaric wake at hand, it may appear that the density follows precisely the same rules as the temperature in the sense that it is similarly distributed with r and $\bar{x}$. The fact that this is not so becomes evident by the following simple arguments. Consider first the density defect, $(\rho_\infty - \rho(0))/\rho_\infty$, corresponding to the temperature defect, $(T(0) - T_\infty)/T_\infty = \theta(\bar{x})$, Equation (38). Then, because $p = p(0) = p_\infty$,

$$\frac{\rho_\infty - \rho(0)}{\rho_\infty} = \frac{T(0) - T_\infty}{T_\infty}\frac{T_\infty}{T(0)} = \frac{\theta}{\theta + 1} \tag{40}$$

regardless of the form of θ; that is, regardless of whether the temperature variation has equilibrated to its self-preserving form or not. Now, θ can begin from large values ($\theta \leq 1$) near the body. In fact, at the effective origin of the wake ($T = T_o$) the density defect has the value 0.72. At the beginning, the defect should decrease slowly and would approach the $\bar{x}^{-2/3}$ dependence only much later, i.e., when $\theta << 1$. It is concluded, therefore, that the variation of the density along the wake axis approaches a self-preserving much later than either the velocity or the temperature.

By the same token, it should be considered that the temperature varies radially as indicated by Equation (39). Then, it turns out that

$$\frac{\rho_\infty - \rho}{\rho_\infty - \rho(0)} = \frac{\dfrac{T - T_\infty}{T(0) - T_\infty}}{\left(\dfrac{T - T_\infty}{T(0) - T_\infty}\right)\left(1 - \dfrac{T_\infty}{T(0)}\right) + \dfrac{T_\infty}{T(0)}} \tag{41}$$

which, unlike the velocity and temperature, is not a simple function of the variable $r/\bar{x}^{-1/3}$, except far in the wake where $T(0) \cong T_\infty$. Again, although self-preservation is eventually attained, it appears that the corresponding "relaxation" length for the density is forced to be longer than those of the other field variables.

6.4 RESULTS OF MEASUREMENTS

6.4.1 AXIAL VARIATION OF PROPERTIES

Figure 23 shows the variation of the velocity defect w, Equation (9), with the nondimensional distance $\bar{x}$ as given by Equation (15). It should be noted that the latter coordinate has been nondimensionalized by

$$C_D A = 0.0674$$

for experiment WEA and by

$$C_D A = 0.0464$$

for experiments WEB and WEC. Figure 23 shows essentially the results of the latter two experiments. In this figure, the variation $\bar{x}^{-1}$ and $\bar{x}^{-1/2}$ is also shown by representative slope along with the slope for $\bar{x}^{-2/3}$ and it is seen that, in spite of the existing scatter, the latter scaling seems to be appropriate for describing the asymptotic nature of the data. As expected, there exists a considerable length (a "relaxation length") or order of 40 virtual diameters before this somewhat precarious resemblance to the 2/3-power decay law is established, as given by Equation (28).

An identical situation exists for the ambient temperature defect along the wake, Figure 24, where the data have been representatively obtained from WEC. Because of the close connection of temperature and velocity, Equation (38), the same relaxation distance precedes the approach to equilibration as that for the velocity. The pertinent slopes are also shown for comparison.

A much slower approach to equilibration prevails for the density, Figure 25. Here, the data are scattered badly at large $\bar{x}$ and no statements about the 2/3-power decay can be made. It should be recalled that Equation (40) indicates that the density defect "lags" behind the temperature in an isobaric wake merely as a simple result of the form of the equation of state.

As a simple consequence of the shown variation of the velocity defect w, the transverse scale of the wake, $L/\sqrt{C_D A}$, varies as $\bar{x}^{1/3}$ in agreement with Equation (28); this is shown on Figure 26, which utilizes the results of WEB. Evidence of the relaxation distance is weaker in this representation. It is interesting that L does not become as large as the diameter, D, of the wake-producing model until some distance away from the most downstream position probed (see L = D line on Figure 26).

Another important consequence is the decrease of the wake Reynolds number, Re_w, which is shown on Figure 27 with data obtained from WEB. Scatter of the data does not allow for a precise determination of the inverse $\bar{x}^{1/3}$ dependence predicted by Equation (32), but the decrease with $\bar{x}$ is very

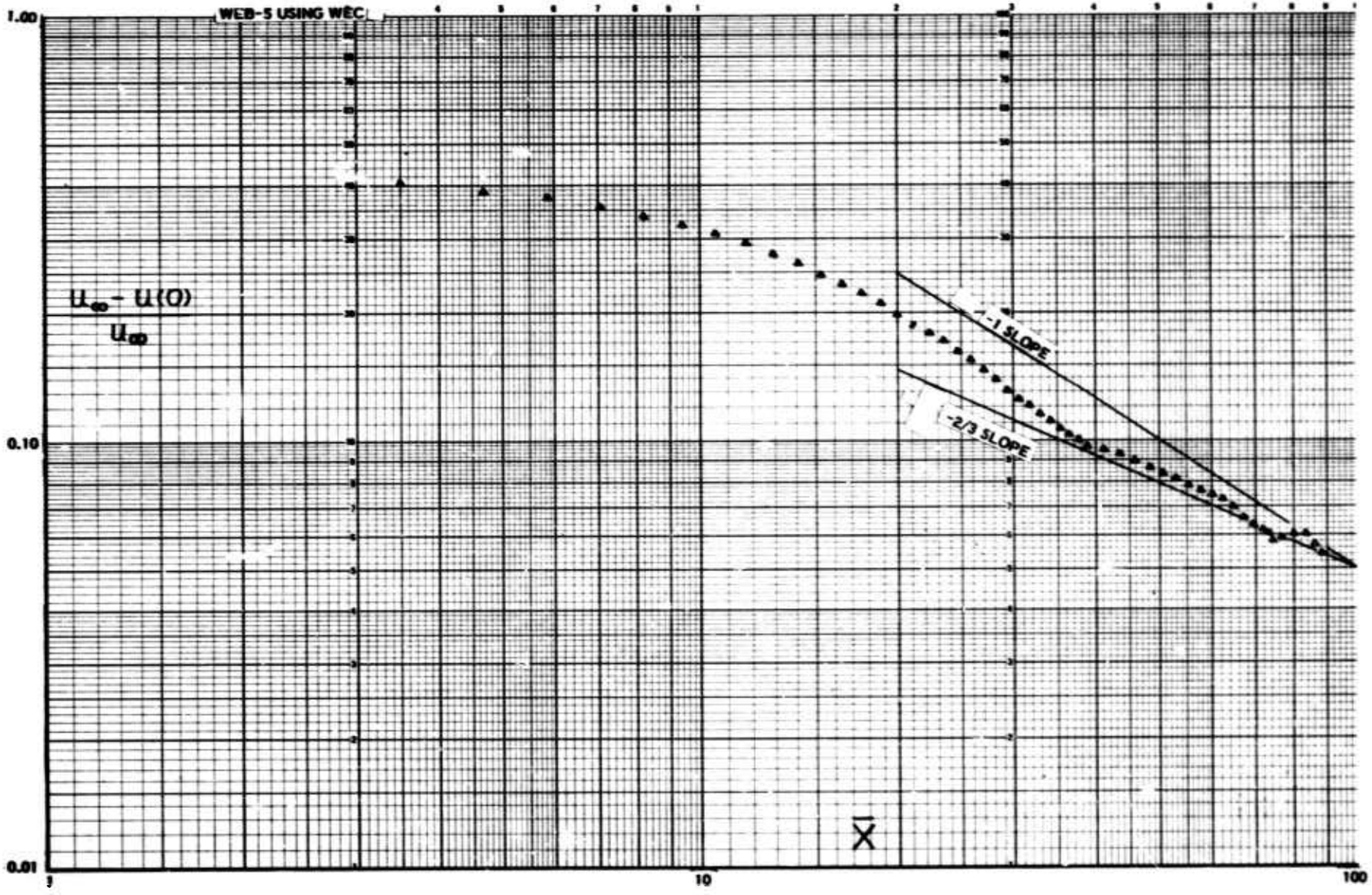

FIGURE 23. VARIATION OF AXIAL VELOCITY DEFECT WITH PROPER AXIAL COORDINATE.

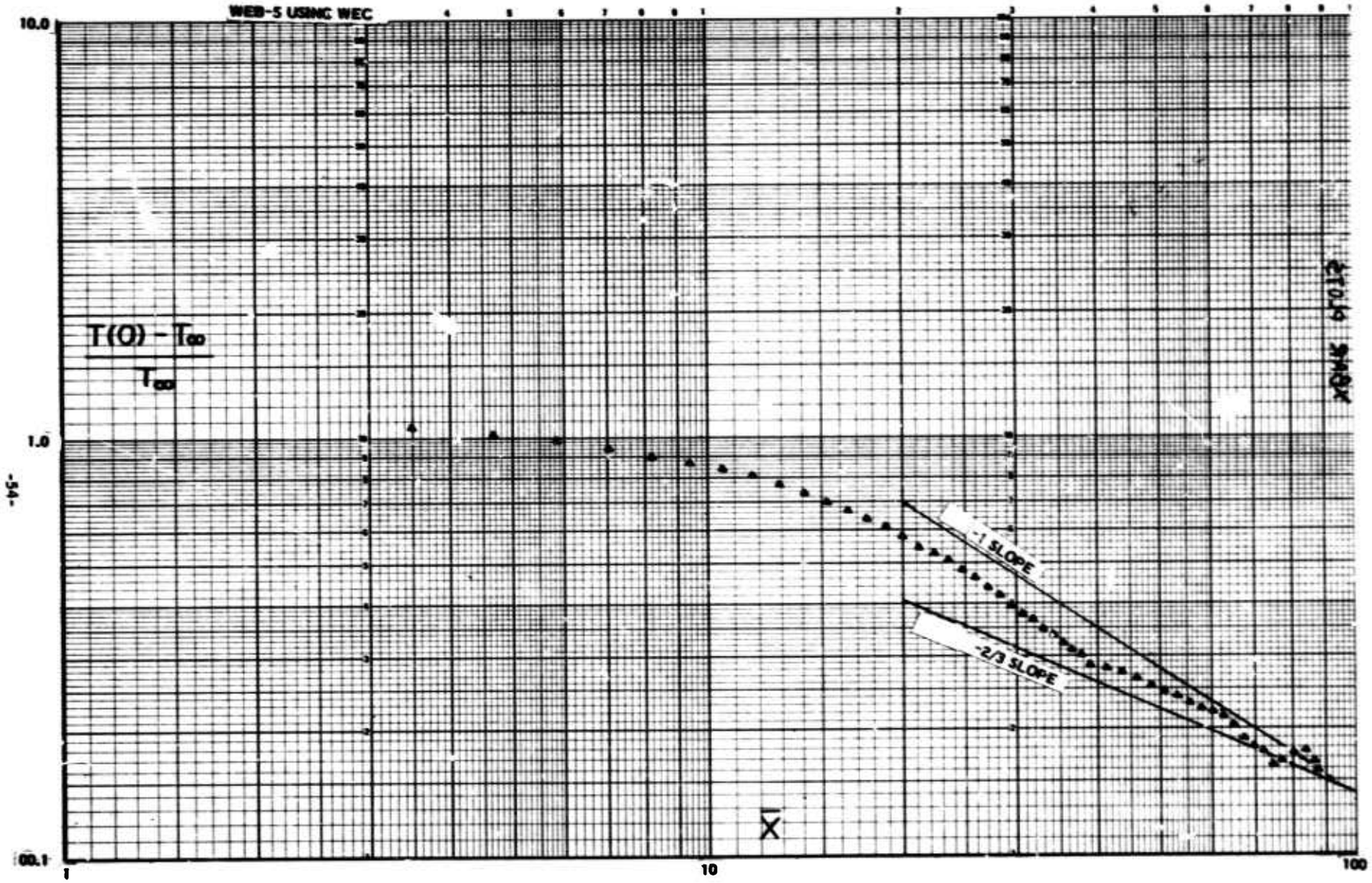

FIGURE 24. VARIATION OF WAKE TEMPERATURE DEFECT WITH PROPER AXIAL DISTANCE.

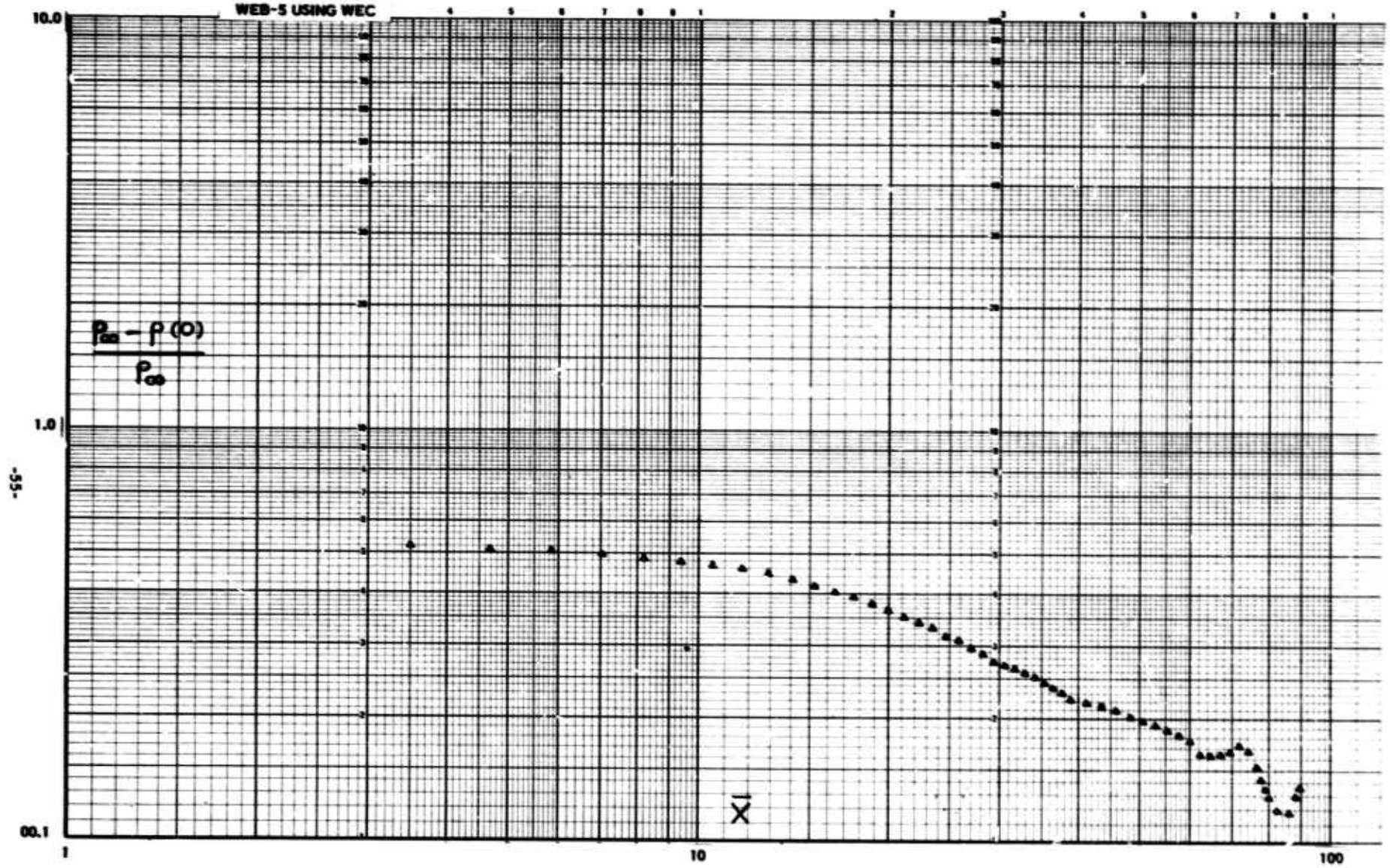

FIGURE 25. VARIATION OF WAKE DENSITY DEFECT WITH PROPER AXIAL DISTANCE.

FC9803 0

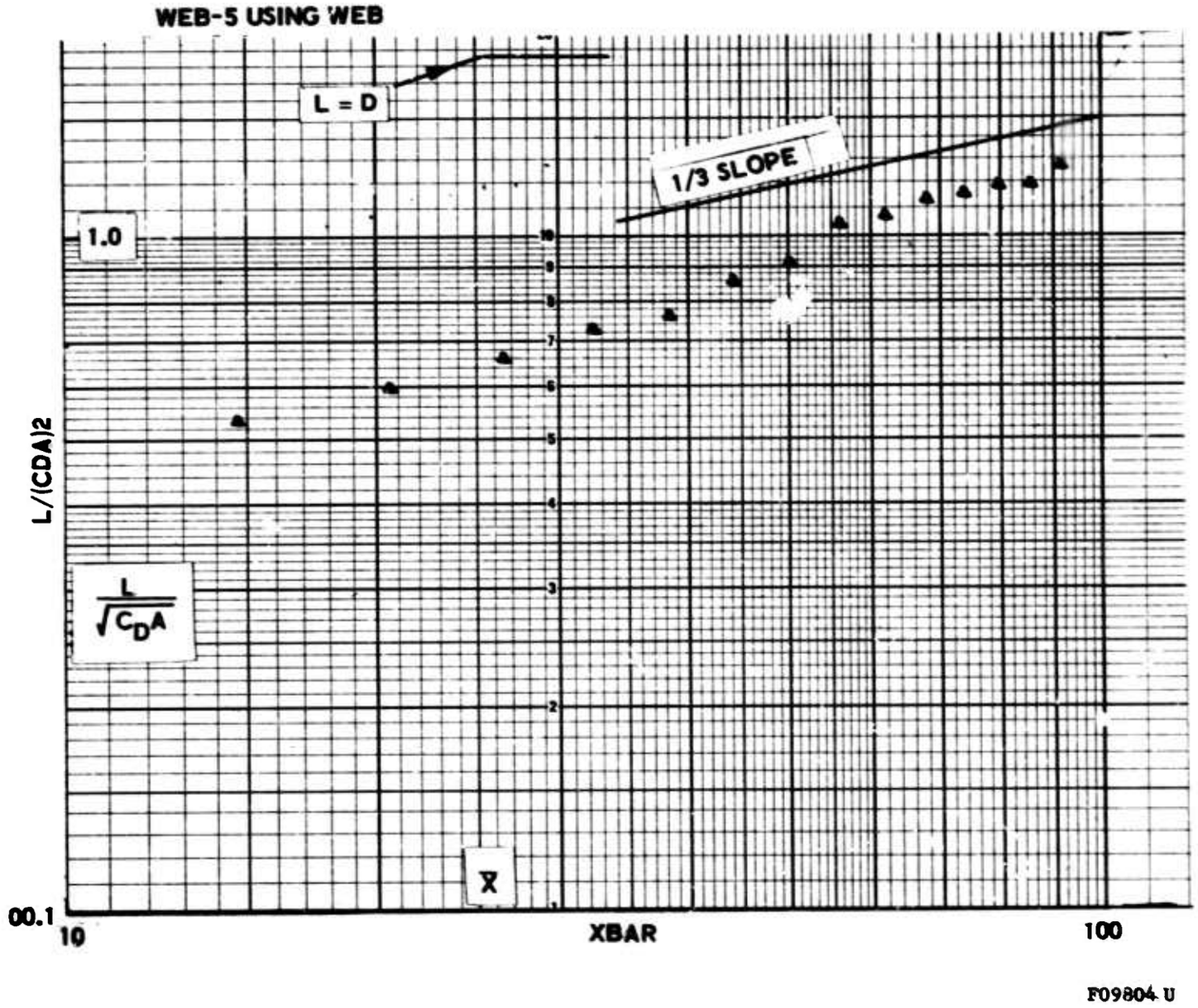

FIGURE 26. VARIATION OF TRANSVERSE WAKE SCALE WITH PROPER AXIAL DISTANCE. SCALE REMAINS SMALLER THAN MODEL DIAMETER FOR ENTIRE RANGE.

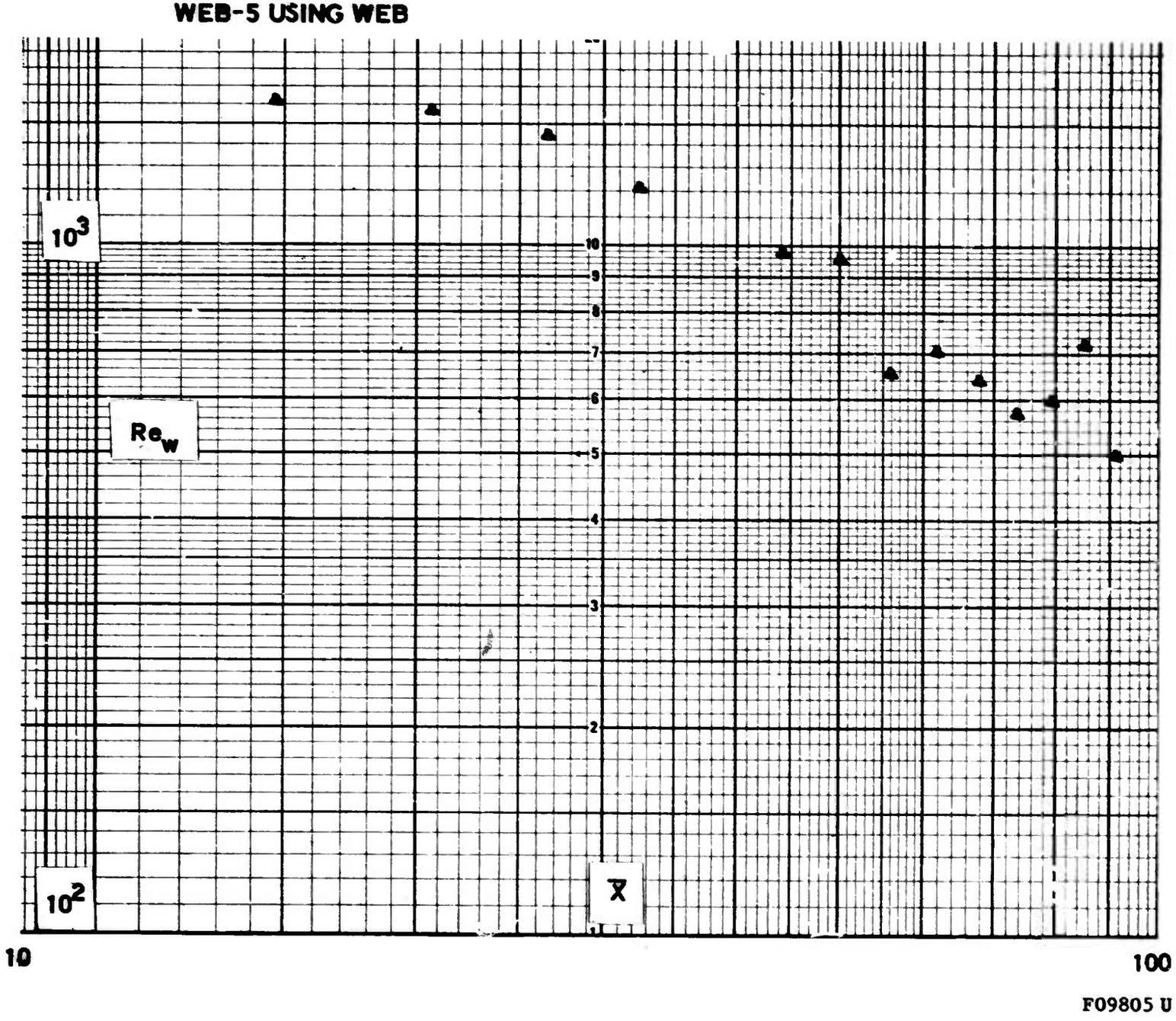

FIGURE 27. WAKE REYNOLDS NUMBER AS A FUNCTION OF PROPER AXIAL DISTANCE.

clear and, in fact, Re_w decreases from 1500 to approximately 500 over the range investigated in spite of the model Reynolds number of 21,000. Still, in view of the intense turbulence still extant at the end of the range, it is clear that Re_w would have to further decrease before Townsend's "final period" sets in.

6.4.2 RADIAL VARIATION OF PROPERTIES

The radial variation of the wake axial velocity, temperature, and density were originally collected and plotted versus the radius normalized with the so-called half-width radius, r*, where

$$r^* = r_{1/2} = \text{radius at } \frac{u_\infty - u}{u_\infty - u(0)} = \frac{1}{2}$$

This representation was convenient at the beginning and furthermore, was in keeping with low-speed tradition;[36] Figures 28, 29, and 30 show these results for experiment WEB. Unfortunately, this form of presentation is highly artificial in that it constrains the data to fulfill the three conditions

$$\frac{u_\infty - u}{u_\infty - u(0)} = 1 \text{ at } r/r^* = 0$$

$$= 0.5 \text{ at } r/r^* = 1$$

$$= 0 \text{ at } r/r^* = \infty$$

A less constrictive presentation is, as explained in a previous section, the use of the parameter

$$\eta = \frac{\bar{r}}{L} \simeq \frac{r}{L}$$

where $\bar{r}$ is the Howarth-Dorodnitzyn radius (Paragraph 6.3.3) and L is the transverse scale. It should be noted that only through the use of this variable does the wake scale, drag, and velocity defect fulfill the consistent relation of Equation (24). Figures 31, 32, and 33 show the radial distribution of properties as a function of η. There seems to be excellent correlation of all the experimental data, especially for the velocity and the temperature (Figures 31 and 32), except the first two or three x-stations (circles and squares). This slight disagreement is in keeping with the expectation of a finite relaxation distance for the self-preserving profiles to develop and it is, in fact, surprising that departure from perfect radial correlation is exhibited by such a small number of axial stations. The expected radial correlations are thus verified as it appears from the data, at an earlier development stage of the wake than obtained for the axial variations (see previous section). It was tentatively

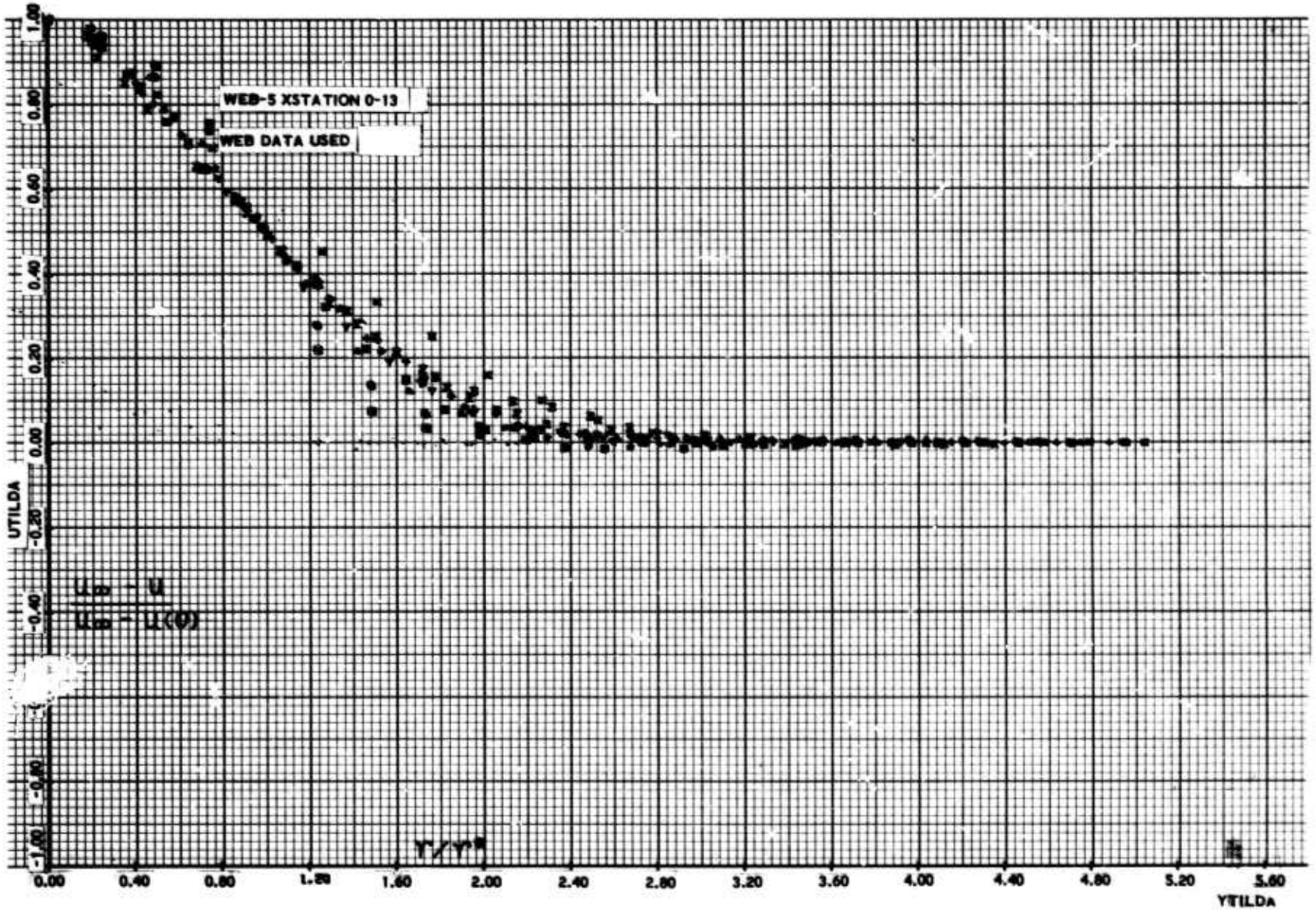

FIGURE 28. DISTRIBUTION OF AXIAL VELOCITY AS A FUNCTION OF THE WAKE HALF-RADIUS. (WEB DATA).

F09806 U

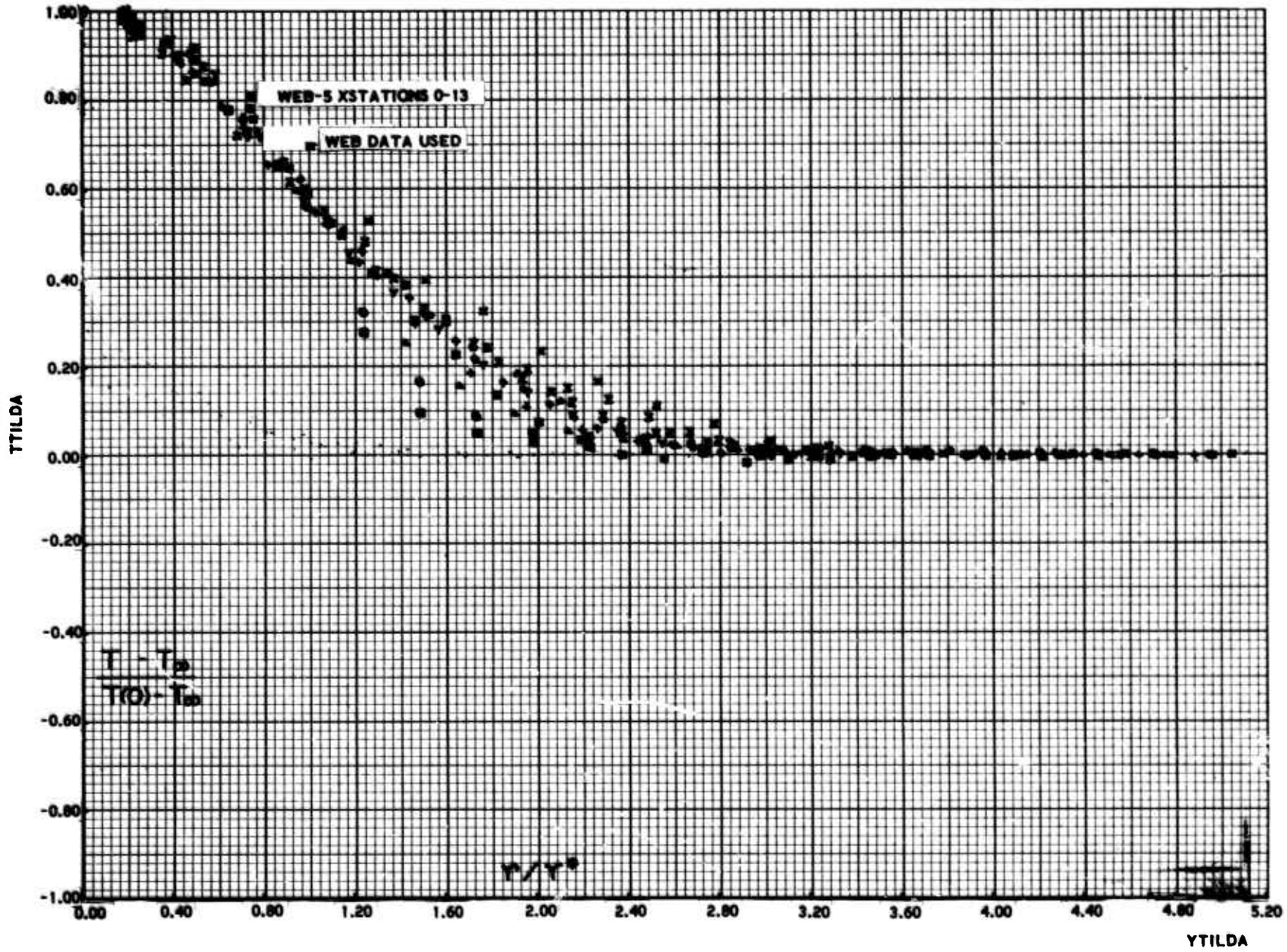

FIGURE 29. DISTRIBUTION OF TEMPERATURE AS A FUNCTION OF WAKE HALF-RADIUS (WEB DATA).

F09807 U

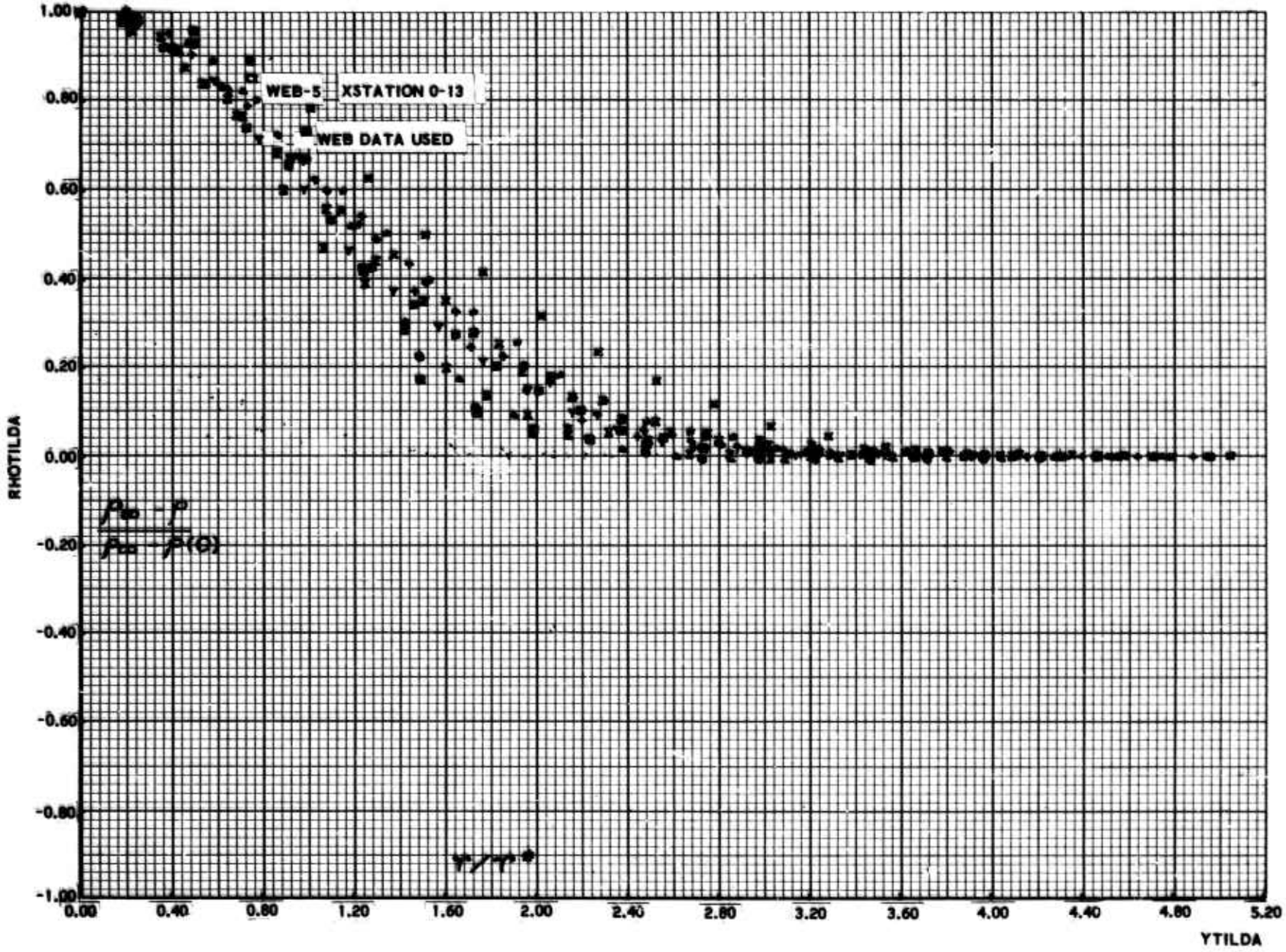

FIGURE 30. DISTRIBUTION OF DENSITY AS A FUNCTION OF WAKE HALF-RADIUS (WEB DATA).

F09808 U

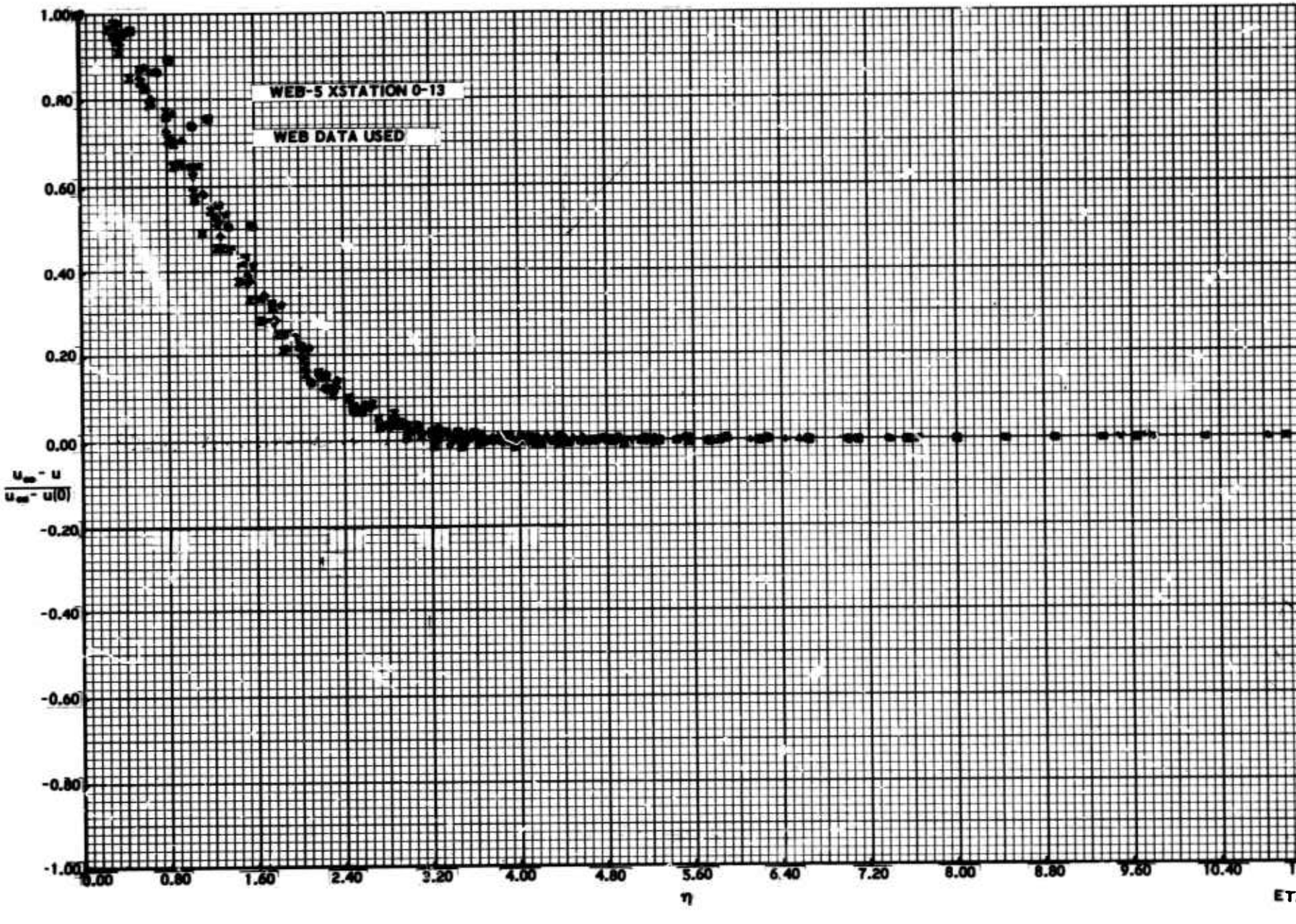

F09809 U

FIGURE 31. DISTRIBUTION OF AXIAL VELOCITY WITH HOWARTH-DORODNITZYN RADIUS (WEB DATA).

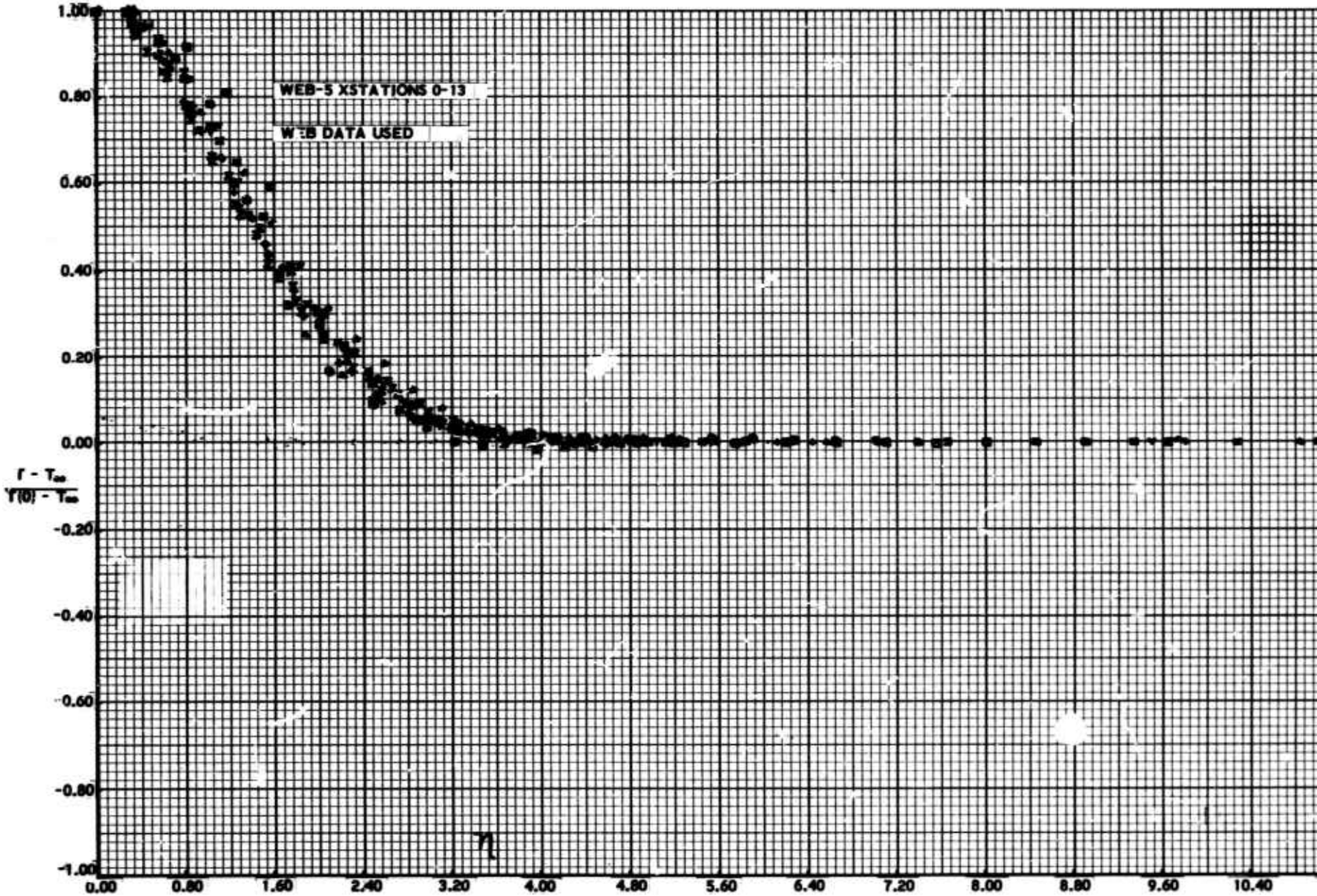

FIGURE 32. DISTRIBUTION OF TEMPERATURE WITH HOWARTH-DORODNITZYN RADIUS (WEB DATA).

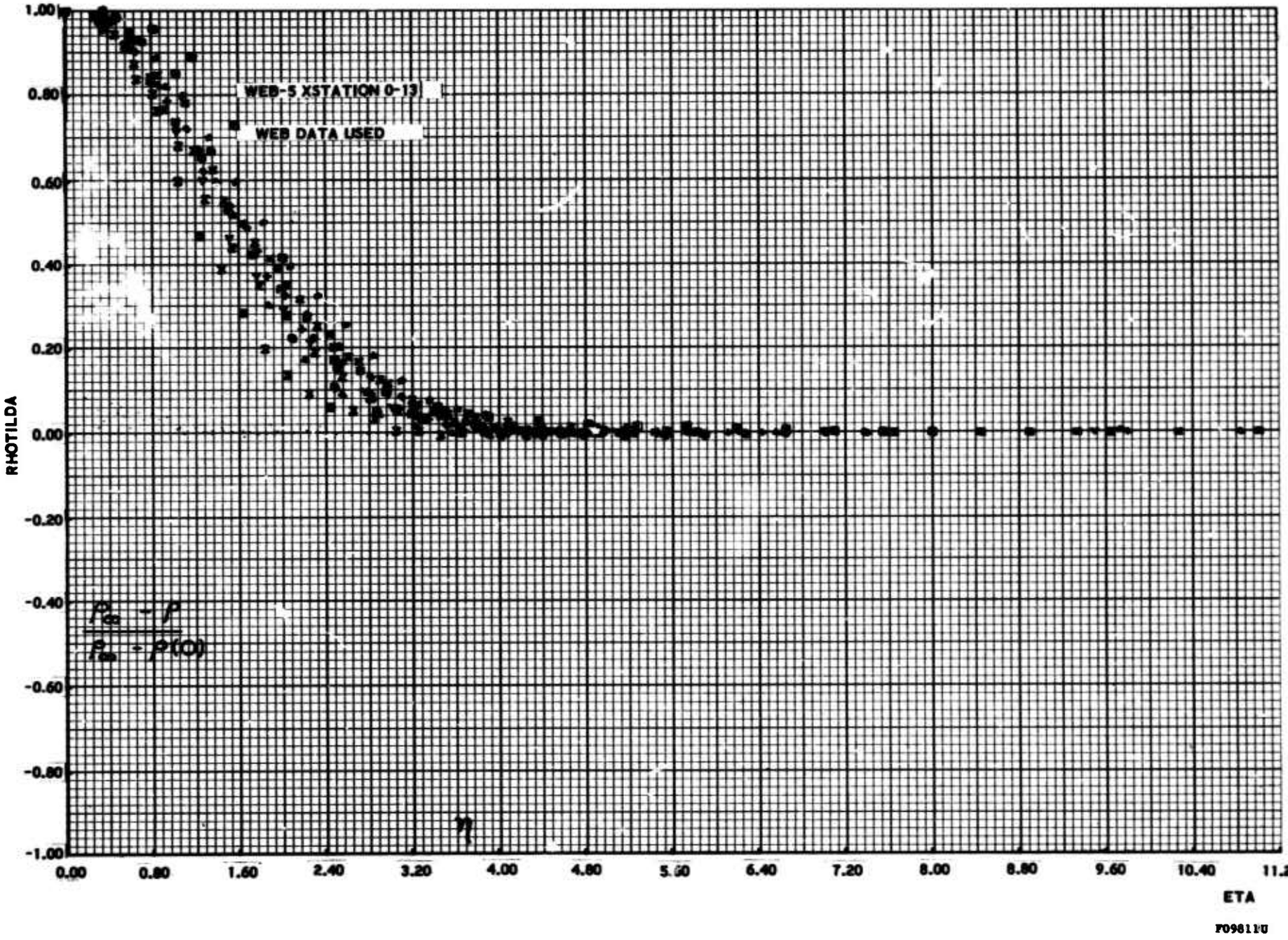

FIGURE 33. DISTRIBUTION OF DENSITY WITH HOWARTH- DORODNITZYN RADIUS (WEB DATA).

concluded that the transverse mixing mechanism is somewhat more dominant than the corresponding adjustments in the axial direction.

Comparison of the η-form of correlations with the half-width form favors the former as seen by comparing Figure 28 with Figure 31 and Figure 29 with Figure 32. This conclusion is the more gratifying because of the tortuous path necessary to compute η. This computation involves two numerical integrations of experimental data, the first to compute $\bar{r}$ from Equation (20) and the second to compute L from Equations (21) and (24).

A slightly different picture is presented by the density distribution of Figure 33. Here, correlation is indifferent at best, and probably quite incomplete. This is exactly what is expected from Equation (41). As with its axial variation, the radial density variation of density shows a much slower relaxation to a dynamically equilibrated (self-preserving) form.

Returning to the radial distributions of velocity and density, it is observed that the following analytical forms best correlate the data

$$\tilde{u} = e^{-0.43\,\eta^2} \tag{42}$$

$$\tilde{T} = e^{-0.34\,\eta^2} \tag{43}$$

The velocity distribution as shown is then wider, in the η sense, than that advanced by Townsend for the low-speed wake where 0.5 was used in place of 0.43.

6.4.3 TRANSPORT COEFFICIENTS

As indicated previously, an indirect evaluation of transport coefficients can be extracted from the data. Equation (28) was advanced by Townsend as the most rational description of the velocity decay along a low-speed wake. The present data were used to see if R_T was also constant for the compressible wake and, if so, what value it attained. Figure 34 shows the turbulent Reynolds number, R_T

$$R_T = \bar{x}\ \pi^{1/2}\ w^{3/2} \tag{44}$$

Here, it can be seen that in WEC the value of R_T underwent a relaxation period closely following that of w, featuring an initial rise and then a decay to a constant value. The sharp break in the curve at $\bar{x} = 40$ is, of course, fortuitous, and the points from WEB are plotted on the same figure to illustrate this fact. Eventually, however, both experiments give approximately the same asymptotic value of R_T amd the value obtained from WEC will be adopted here:

$$R_T \simeq 12.8 \tag{45}$$

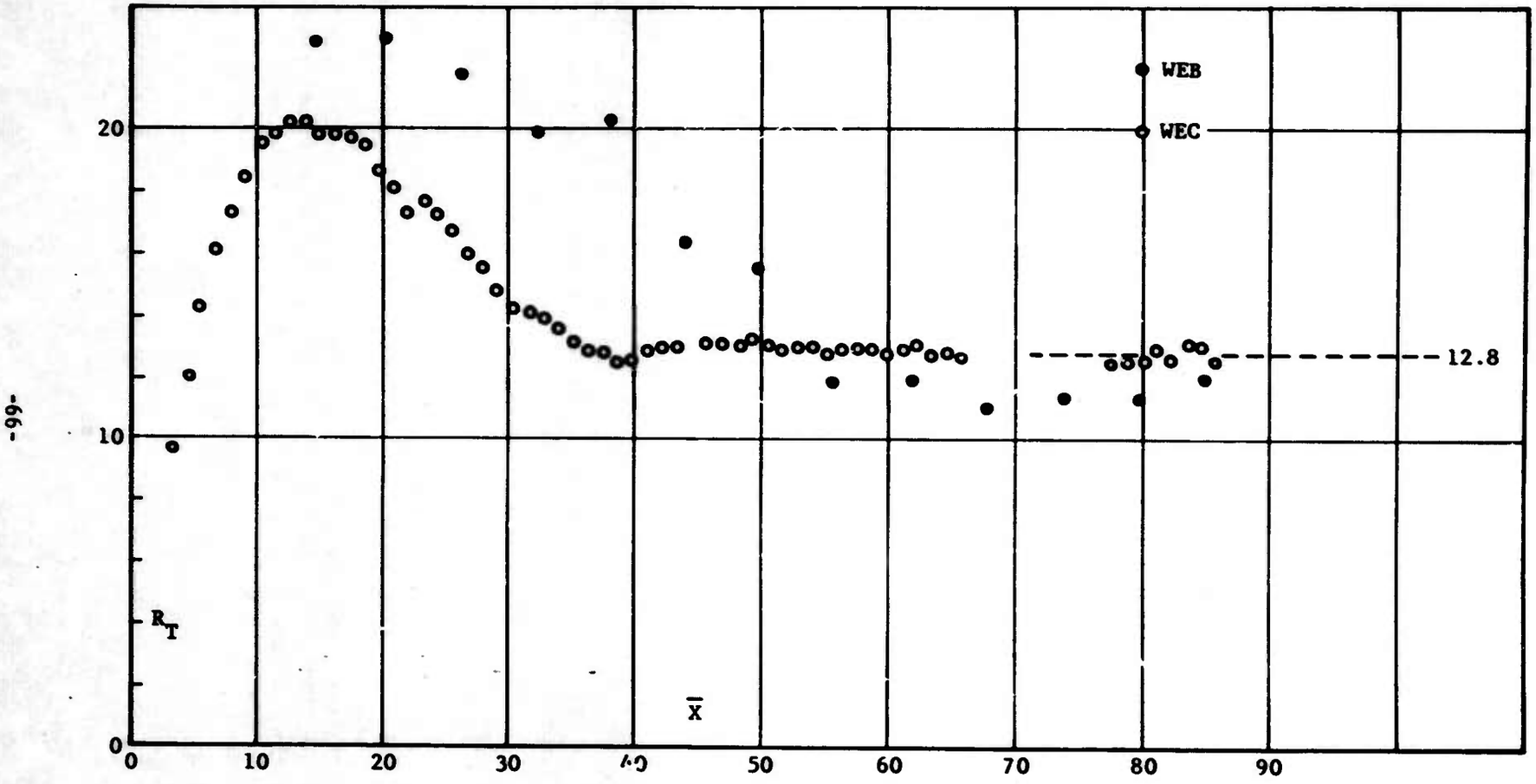

FIGURE 34. TURBULENT REYNOLDS NUMBER COMPUTED INDIRECTLY FROM THE DECAY OF THE AXIAL VELOCITY DEFECTS. RESULTS FROM TWO DIFFERENT EXPERIMENTS ARE SHOWN

It is interesting that this value is very similar to that obtained for two-dimensional wakes by Townsend[4] ($R_T = 12.5$), although it is below the value, $R_T = 14.1$, found by Hall and Hislop.[30] The latter, however, measured only up to 17 diameters behind the body, whereas Figure 34 shows that at least twice that distance is taken up by the relaxation process. This implies that the better analogy of the present results is Townsend's value of 12.5, which enhances the universality of this parameter by making it independent of compressibility and geometry.

A similar computation can be made for the turbulent Prandtl number. This can be first computed by using the data from, and the aid of, Equation (38)

$$\sigma_T^{2/3} = \left[\frac{\theta}{(\gamma - 1)\, M_\infty^2\, W}\right] \tag{46}$$

with the results shown on Figure 35. Here, the relaxation process is more gradual, but a value of

$$\sigma_T^{2/3} = 0.845 \tag{47}$$

$$\sigma_T = 0.78 \tag{48}$$

can be adopted. Next, from Equations (39), (42), and (43)

$$\sigma_T = \frac{\log \tilde{T}}{\log \tilde{u}} = 0.79 \tag{49}$$

Therefore, there is good agreement between these two independent although indirect, measurements of σ_T. As an added check of the curve-fitting process by which Equations (42) and (43) were found, the ratio $\log \tilde{T}/\log \tilde{u}$ was formed by the WEB-5 computer program and the relation, Equation (49), was again verified. It should be noted that this measurement of σ_T is close to that found by Corrsin[37] in the axisymmetric heated jet ($\sigma_T = 0.72$). Again, it can be concluded that, as with the turbulent Reynolds number, the applicability of nondimensional transport properties in turbulent flows may be wider than hitherto thought.

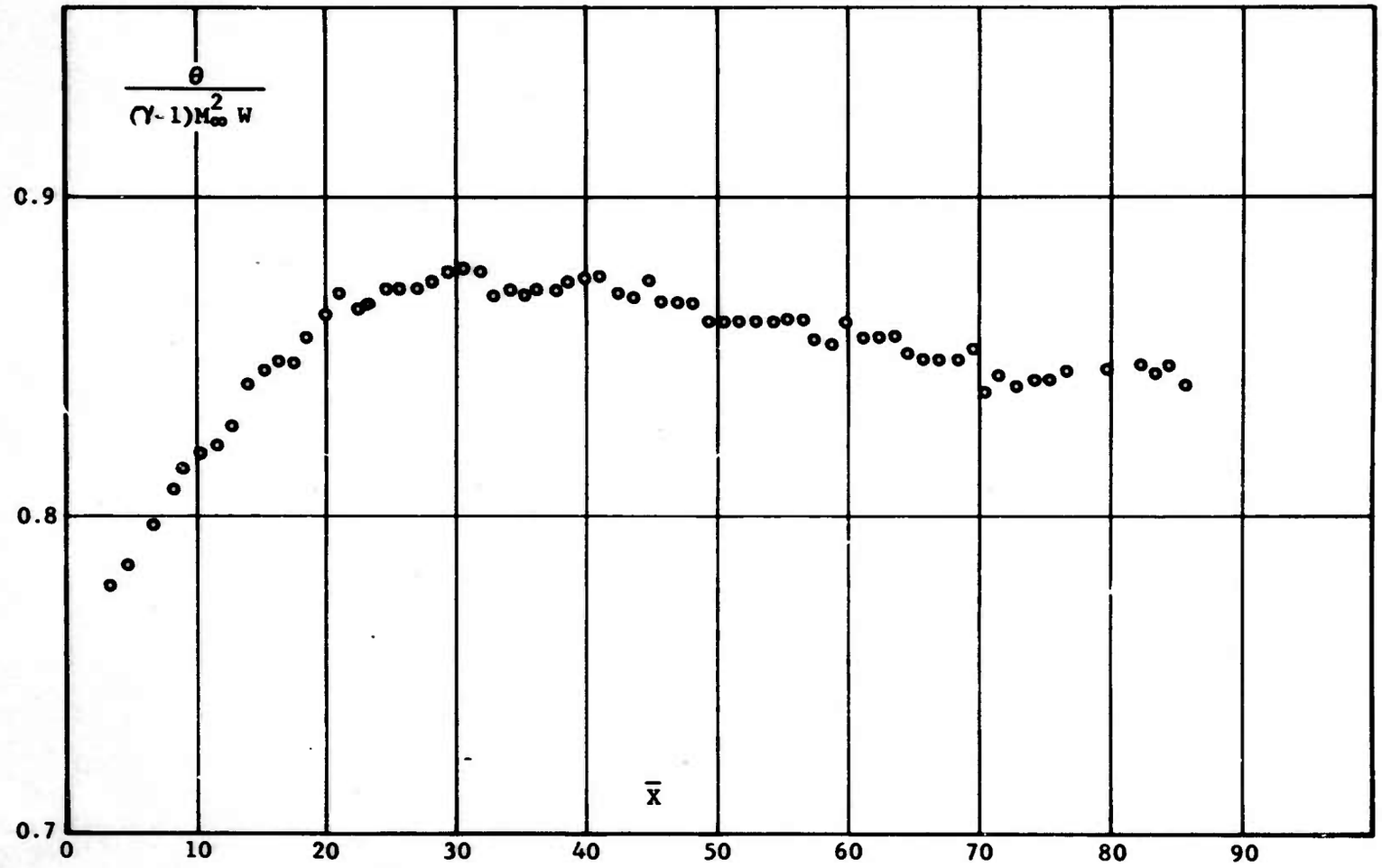

FIGURE 35. INDIRECT COMPUTATION OF THE TURBULENT PRANDTL NUMBER FROM THE RATIO OF THE MEASURED AXIAL VELOCITY AND TEMPERATURE DEFECTS

SECTION 7

SUMMARY

The findings of the study can be collected and presented as follows:

$$w(\bar{x}) = \frac{1}{\pi 1/3}\left(\frac{R_T}{6}\right)^{2/3}\frac{1}{\bar{x}^{2/3}}\ ;\ R_T = 12.8$$

$$L = \left[\frac{C_D A}{4\pi w}\right]^{1/2}$$

$$\frac{u_\infty - u}{u_\infty - u(0)} = e^{-0.43\eta^2}\ ;\ \eta = \frac{r}{L}$$

$$\theta \equiv \frac{T(0) - T_\infty}{T_\infty} = (\gamma-1)\, M_\infty^2\, \sigma_T{}^{2/3} w$$

$$\frac{T - T_\infty}{T(0) - T_\infty} = \left(\frac{u_\infty - u}{u_\infty - u(0)}\right)^{\sigma_T}\ ;\ \sigma_T = 0.785$$

$$\frac{\rho_\infty - \rho(0)}{\rho_\infty} = \frac{\theta}{\theta + 1}$$

$$\frac{\rho_\infty - \rho}{\rho_\infty - \rho(0)} = \frac{T - T_\infty}{T(0) - T_\infty}\left[\left(\frac{T - T_\infty}{T(0) - T_\infty}\right)\left(1 - \frac{T_\infty}{T(0)}\right) + \frac{T_\infty}{T(0)}\right]^{-1}$$

The experimental results presented in this report describe the wake flow as seen in a mean or average sense by an observer fixed relative to the model and wind tunnel. As indicated by the plots shown of the radial distribution of properties, the latter decrease smoothly toward the external flow field. By contrast, a long history of free-turbulence studies frequently documents the existence of a sharp "front" or boundary separating the turbulent fluid from the external undisturbed flow. The question arises, therefore, whether this turbulent front escaped detection in the measurements reported here and, if so, how this affects the validity and use of the data.

An affirmative answer to the first question has already been given.* At the same time, the validity of the present data is completely determined by its interpretation and use. Care has been taken throughout this report to put weight on the word "mean" so that the description applies to a sufficiently long time average at a certain geometrical point in the wake. If these data were then to be used for the prediction of mean properties, their use would, therefore, be legitimate. It is equally legitimate, in fact, to include in this mean-average aspect concepts of gradient transport and to derive the apparent transport coefficients as was done in previous sections. There is no basic distinction, of course, between such a flow and a laminar flow other than numerical points such as growth rates, etc.

The mean-average aspect is naturally unsuited to the guest of the random-stationary characteristics of wakes. By this, we mean the aspect presented by an "instant observation" such as photographic or radar picture of exposure time much shorter than that of the mean of turbulent motion. The main feature of this aspect is the intermittency of the wake front. The mean-flow field of the random-stationary aspect can be obtained immediately by measuring the intermittency factor and applying it to the data presented in this report. Different radial property distributions and transport coefficients than shown herein, will then be obtained, both reflecting the existence and the effect of the wake boundary. It is from this random-stationary aspect that a more basic picture of lateral transport along the lines proposed by Townsend[4] and elaborated by Meyer and Divoky[38] will arise.

*The study of the turbulent front will be reported in Part II.

SECTION 8

CONCLUSIONS

The following conclusions can be drawn from and about the wake-flow experiments used in this work:

(1) The wake temperature and axial velocity defects decay in a manner approaching the inverse 2/3-decay low characteristic of the imcompressible axisymmetric wake. This is preceded by a relaxation distance of at least 40 virtual-wake diameters and probably longer.

(2) Best correlation of the radial distribution of the temperature and axial velocity is obtained for a radial coordinate consisting of the Howarth-Dorodnitzyn radius divided by the transverse velocity scale (η-form). However, the role of the Howarth-Dorodnitzyn radius is somewhat dubious on theoretical grounds and by the fact that it is nearly equal, in this experiment, to the physical radius.

(3) The transverse scale as defined is inversely proportional to the velocity defect and thus increases asymptotically as the 1/3-power of distance. The wake Reynolds number similarly decreases from approximately 1500 to approximately 500 in the region investigated.

(4) The similar (self-preserving) radial distributions of the velocity and temperature are well described by Gaussian distributions of the type $e^{-k\eta^2}$, where k is 0.43 for the velocity and 0.34 for the temperature.

(5) The turbulent Reynolds number, R_T, indirectly computed from the velocity defect decay, appears to attain, after a relaxation distance of approximately 40 virtual diameters, a value of 12.8, very much in agreement with Townsend's value of 12.5 for the low-speed wake.

(6) A value of the effective turbulent Prandtl number lower than unity accounts for differences between the decay of the velocity defect and that of the temperature, as well as for the larger transverse temperature scale. The value of the Prandtl number found by this method is 0.785.

(7) Similarity in the radial distribution of density is not achieved. This is exactly as anticipated from the structure of the equation of state.

SECTION 9

ACKNOWLEDGEMENTS

The author wishes to acknowledge with gratitude the assistance of Mr. Lee Von Seggern with the instrumentation and the assistance of Dr. John Laufer, University of Southern California, for stimulating discussions and his many suggestions.

SECTION 10

REFERENCES

1. Feldman, S., "Trails of Axisymmetric Hypersonic Blunt Bodies Flying Through the Atmosphere," Journal of Aeronautical Science, Vol. 28, pp 433-448, 1961.

2. Lees, L., "Hypersonic Wakes and Trails," AIAA Journal, Vol 2, pp 417-428, 1964.

3. Lykoudis, P. S., "A Review of Hypersonic Wake Studies," AIAA Journal, Vol. 4, No. 4, pp 577-590, 1966.

4. Townsend, A. A., The Structure of Turbulent Shear Flow, Cambridge University Press, 1956.

5. McCarthy, J. F., Jr., "Hypersonic Wakes," GALCIT Hypersonic Research Project Memo No. 67, July 1962.

6. Kingsland, L., Jr., "Experimental Study of Helium and Argon Diffusion in the Wake of a Circular Cylinder at M = 5.8," GALCIT Hypersonic Research Project Memo No. 60, June 1961.

7. Mohlenhoff, W., "Experimental Study of Helium Diffusion in the Wake of a Circular Cylinder at M = 5.8," GALCIT Hypersonic Research Project Memo No. 54, May 1960.

8. Zakkay, V. and Fox, H., Experimental and Analytical Consideration of Turbulent Heterogeneous Mixing in the Wake, New York University Report NYU AA-66-54, April 1965.

9. Ragsdale, W. C. and Darling, J. A., "An Experimental Study of the Turbulent Wake Behind a Cone at M = 5," Proceedings of the 1966 Heat Transfer and Fluid Mechanics Institute, Stanford University Press, p 12, 1966.

10. Demetriades, A. and Bauer, A. B., Supersonic Wind Tunnel Experiments With Axisymmetric Wakes, AIAA Paper 66-453, Los Angeles, California, 27 June 1966.

11. Demetriades, A. and Von Seggern, L., Design, Performance and Operation of the Mach 3 Wind Tunnel, Aeronutronic, Division of Philco-Ford Corporation, Publication No. U-3390, November 1965.

12. Martellucci, A., Trucco, H., and Agnone, A., "Measurements of the Turbulent Near Wake of a Cone at Mach 6," AIAA Journal, Vol. 4, pp 385-391, 1966.

13. Vas, I. E., Murman, E. M., and Bogdonoff, S. M., Preliminary Studies of Support-Free Sphere Wakes at M = 16 in Helium, Gas Dynamics Laboratory Memo No. 4, Princeton University, October 1964.

14. Behrens, W., Flow Field and Stability of the Far Wake Behind Cylinders at Hypersonic Speeds, AIAA Paper 67-32, New York, New York, January 1967.

15. Bogdonoff, S. M., Private Communication, 1966.

16. Richmond, R. L., Experimental Investigation of Thick, Axially Symmetric Boundary Layers on Cylinders at Subsonic and Hypersonic Speeds, GALCIT Hypersonic Research Project Memo No. 39, June 1957.

17. Badrinarayanan, M. A., "An Experimental Investigation of Base Flow at Supersonic Speeds," Journal of Royal Aeronautical Society, No. 65, pp 475-482, 1961.

18.. Bauer, A. B., Private Communication, 1965.

19. Goldstein, S., Proceedings of Royal Society of London, Vol. 155A, p 570, 1936.

20. Matthews, M. L., An Experimental Investigation of Viscous Effects on Static and Impact Pressure Probes in Hypersonic Flow, GALCIT Hypersonic Research Project Memo No. 44, June 1958.

21. Behrens, W., "Viscous Interaction Effects on a Static Pressure Probe at M = 6," AIAA Journal, Vol. 1, No. 12, p 2864, December 1963.

22. Dewey, C. J., Jr., Hot-Wire Measurements in Low Reynolds Number Hypersonic Flows, GALCIT Hypersonic Research Project Memo No. 63, 15 September 1961. See also ARS Journal, No. 31, pp 1709-1718, 1961.

23. Herzog, R. T., Nitrogen Injection Into the Base Region of a Hypersonic Wake, GALCIT Hypersonic Research Project Memo No. 71, 15 August 1964.

24. Spangenberg, W. G., "Heat Loss Characteristics of Hot-Wire Anemometers at Various Densities in Transonic and Supersonic Flow," NACA TN 3381, May 1955.

25. Morkoving, M. V., "Fluctuations and Hot-Wire Anemometry in Compressible Flows," AGARDograph 24, 1956.

26. NBS-NACA Tables of Thermal Properties of Gases, NBS July 1949.

27. Ames Research Staff, "Equations, Tables and Charts for Compressible Flow," NACA Report 1135, 1953.

28. Lees, L. and Hromas, L., "Turbulent Diffusion in the Wake of a Blunt-Nose Body at Hypersonic Speeds," Journal of Aeronautical Science, Vol. 24, No. 8, p 976, August 1962.

29. Laufer, J., "The Fluctuating Field and Energy Spectrum of a Hypersonic Wake," excerpts from NESCO Report SN 219-2, Pasadena, California, 1964.

30. Hall, A. A. and Hislop, G. S., "Velocity and Temperature Distributions in the Turbulent Wake Behind a Heated Body of Revolution," Proceedings of Cambridge Philosophical Society, Vol. 34, pp 345-350, 1938.

31. Schlichting, H., Boundary Layer Theory, McGraw-Hill Book Company, Inc., 1955, Chapter XXIII.

32. Kubota, T., Laminar Wake With Streamwise Pressure Gradient, GALCIT Hypersonic Research Project 1M 9, 1962.

33. Gold, H., "Laminar Wake With Arbitrary Initial Profiles," AIAA Journal, p 949, May 1964.

34. McCarthy, J. F., Jr. and Kubota, T., "A Study of Wakes Behind a Circular Cylinder," AIAA Journal, Vol. 2, No. 4, p 629, April 1964.

35. Lin, C. C. (Editor), "Turbulent Flows and Heat Transfer," High-Speed Aerodynamics and Jet Propulsion, Vol. V, Chapter 5, Princeton University Press, 1959.

36. Cooper, R. D. and Lutzky, M., "Exploratory Investigation of the Turbulent Wakes Behind Blunt Bodies," David Taylor Model Basin Report 963, 1955.

37. Corrsin, S. and Uberoi, M. S., Further Experiments on the Flow and Heat Transfer in a Heated Turbulent Jet, NACA TR 998, Washington, D.C., 1950.

38. Meyer, E. and Divony, D., "Correlation of Intermittency With Preferential Transport of Heat and Chemical Species in Turbulent Shear Flows," AIAA Journal, Vol 4, No. 11, p 1995, 1966.

APPENDIX A

SIMPLIFICATION OF THE HOT-WIRE TECHNIQUE IN STEADY FLOW MEASUREMENTS

The hot-wire anemometer is by now an almost indispensable tool for the measurement of steady-state properties in supersonic and hypersonic flows. In recent demonstrations of its usage it has helped map wake flow fields produced in research wind tunnels. In such flows, however, the hot-wire technique is encumbered by significant end-loss corrections which can be accounted for only by additional measurements (e.g., support temperature measurements) and computer programs necessary to manipulate the iterations arising from the end losses. Such encumberances decrease the usefulness of the anemometer. The work described herein presents a variation of the hot-wire technique wherein end-effect corrections are unnecessary.

A.1 BACKGROUND

The work of Laufer, McLellan, and Dewey has shown that the $M \geq 2$ and zero overheat, the infinite-wire Nusselt number is a unique function of the Reynolds number based on, say, the free-stream density and velocity and the stagnation viscosity. In principle, this curve can be used for any wire of known material, length, diameter, temperature-resistance slope, and support temperature to give the unit Reynolds number of the flow without need for any additional wire calibration. Actually, insofar as the Reynolds number is concerned, the role of the support temperature usually is secondary to those end-effect corrections originally proposed by Kovasznay and Tornmarck, which are controlled by the aspect ratio and the measured Nusselt number.

A method alternative to using this "universal" curve for infinite wires is to calibrate each wire individually in a known flow ("flow-calibration") and use the resulting Nu-Re curve uncorrected for end effects in the wake

measurement. This procedure is safe provided that the aspect ratio does not change in this process (such a change is unlikely in the type of experiment described below), that the Reynolds (or Nusselt) number range covered in the flow-calibration includes the particular Reynolds number(s) in the wake, and that the end-loss corrections depend only on the local flow properties; this was also the case in the present experiment. This method would then utilize the physical but not the numerical features of the universal correlation (such as the Mach number, Reynolds number, and overheat dependence) without need of lengthy iterations and additional measurements.

A similar argument can be advanced for the measurement of the wire recovery factor, which can be also measured as a function of the stream Reynolds number if a region of known flow conditions is available. In this context Dewey demonstrated that a correction factor analogous to that used for the Nusselt number (and including the aspect ratio and the measured Nusselt number) is necessary to obtain the proper recovery factor. Here, the support temperature is of significance; Herzog resorted to the measurement of just this temperature in his hot-wire tranverses through the wake. The reason is that, like Dewey, he could neither predict nor control his wire support temperature because of the conditions peculiar to his experiment. These included (a) a wake flow highly nonuniform in local T_o and (b) needle supports held at an angle of attack with the nonuniform wake flow such that the support temperature was not controlled by the local T_o at the point occupied by the hot-wire. As a result of this difficulty, the continuous monitoring of the support temperature was necessary.

A.2 TECHNIQUE

Our experiments concern the mapping of the flow field in an axisymmetric wake of a very slender adiabatic body. For laminar boundary-layer at separation, the expansion-recompression events in our near wake have been found to be extremely mild so that the flow external to the viscous wake (for many diameters downstream) is at free-stream condition, i.e., there is no "inviscid wake." Thus, when the wire is moved to a short distance out of the wake its Nusselt number versus Reynolds number calibration can be effected there by changing the tunnel P_o as usual; also, its recovery factor is calibrated in the same way at the same time (both at that location and inside the wake the Mach number has been found to be higher than 2). The wire can then be lowered into the wake and its Nusselt number measured at any desired location. The free-stream calibration can then be used to yield the Reynolds number and recovery factor. Note that our hot-wire probes are constructed with the needle supports at zero angle of attack; also, our unheated flow and low Mach number (which is 3, compared to Herzog's 6) result to a T_o-defect in the wake much smaller than Herzog's (order of a few degrees C at most). Therefore, there is little chance that the wire support temperature is affected by a flow field other than that at or downstream of the wire, and even if it were, it would encounter

a flow field of about the same T_o (within about 1 percent) as the flow field at the wire location. In other words, the wire aspect ratio and Reynolds number determined uniquely our end correction to good accuracy.

The following three tests were devised to test this reasoning:

(1) Wire traverses (at zero overheat) through the wake should show no asymmetries of the type Herzog attributed to nonuniform support heating.

(2) Wires of same diameter but different aspect ratios should, when flow-calibrated in the free stream, measure the same Reynolds number in the wake without need for end corrections.

(3) Wires of same aspect ratio but different diameter should, when flow-calibrated in the free stream, measure the same (unit) Reynolds number in the wake without need for end corrections.

If tests (2) and (3) were successful, then the unit Reynolds number so measured in the wake would be the same as would be measured by using the universal correlation method of Dewey and Herzog.

A.3 TEST 1

Several traverses were made through the turbulent axisymmetric wake at the following conditions:

M_∞ = 3.0

T_o = 70°F

P_o = from 400 mm Hg to 730 mm Hg

x/D = from 20 to 60

Reynolds number (based on model diameter) = 16,000 to 30,000

The results were:

(1) The total temperature defect in the wake was of order of a few degrees C at most (of order of 1°C at the higher x/D).

(2) There was no noticeable asymmetry or hysteresis of the "cold" wire resistance profile of the wake, even for traverse speeds of order of one body diameter per 7 sec.

From this test one concludes that the anomalies observed by Herzog are absent in our experiment.

A.4 TEST 2

Three Pt 10-percent Rh wires of different aspect ratios were used as follows:

Wire No.	Diameter (in.)	ℓ/d
9-21/1	0.0001	193.6
9-21/2	0.0001	257
9-21/3	0.0001	139.4

The procedure for each wire was as follows:

(1) The wire was mounted, examined under the microscope and annealed.

(2) It was then subjected to about one hour of supersonic flow in the tunnel and to several starts and stops of the flow.

(3) Next, the wire was over-calibrated, i.e., its 0°C resistance and its resistance-temperature variation was determined.

(4) The wire was next remounted in the wind tunnel and positioned at $x/D = 45.8$ and at $r/D = 4.5$ off the wake axis. Previous pitot-static measurements at this point gave the Mach number there as 3.00, which is identical to that obtained in the free stream. The wire was then flow-calibrated by changing the tunnel stagnation pressure P_o. The Nusselt number was computed from

$$Nu_{o_m} = \left(\frac{\alpha_r R_r}{\pi \ell}\right) \frac{1}{k_o} \frac{R_{a_{wm}}}{\left(dR/di^2\right)_{i=0}}$$

where $\alpha_r R_r$ is the resistance-temperature slope (from Step (c)) and k_o is the thermal conductivity at the recorded stagnation temperature. The Nu_{o_m} - Re_o and η-Re_o calibrations were thus obtained.

(5) The wire was then lowered to the wake axis, (x/D = 45.8, r/D = 0), the P_o set to 500 mm Hg abs, and the Nusselt number measured, first by using k_o from the stagnation temperature of the tunnel.* This zeroth approximation $Nu_{\delta_m}^{(o)}$ is used to find the corresponding $Re_\delta^{(o)}$ from the calibration of the wire as obtained from (d) and the latter is used to obtain $\eta_m^{(o)}$ from which $T_o^{(o)}$ and $k_\delta^{(1)}$ are computed. With this new value of the k_o one then computes $Nu_{\delta_m}^{(1)}$, $Re^{(1)}$, and $T_\delta^{(1)}$. For out particular experiments $Re^{(o)}$ was within 1 percent of $Re_\delta^{(1)}$ which greatly decreases the need for further approximations and perhaps for the iteration itself.

(6) The wire was finally recalibrated in the oven: all wires showed no change in the resistance-temperature slope $\alpha_r R_r$ and R (T = 0°C) changes amounting to no more than a few tenths of 1 percent.

The measured unit Reynolds number Re_o' on the wake axis (at x/D = 45.8, P_o = 500 mm) is shown below:

Wire No.	ℓ/d	Re_o' (per in.)
9-21/1	193.6	0.421×10^5
9-21/2	257	0.418
9-21/3	139.4	0.426

We see that the spread in the measured values of Re_o' is 1.9 percent which is not far from the accuracy of the measurement. We conclude that this Reynolds number obtains independently of the wire aspect ratio and is thus the true unit Reynolds number on the wake axis.

*The k_o can also be approximated first by using Ta_{w_m}.

A.5 TEST 3

An identical procedure was followed with a second set of three Pt 10 percent Rh wires of approximately equal aspect ratios but different diameters (i.e., different Re_o ranges). The results were as follow:

Wire No.	d (in.)	ℓ/d	Re'_o (per in.)
9-28/3	0.00005	186	0.422×10^5
9-21/1	0.0001	193.6	0.421
9-24/2	0.00014	186.5	0.426

Again, we note the excellent agreement among the measured Re'_o values and, also, the agreement with those of the previous test.

A.6 DISCUSSION AND CONCLUSIONS

The tests performed confirm that under certain circumstances the hot-wire anemometer requires no end-loss corrections and no recourse to the "universal" Nu_o - Re_o correlation.

It should be remembered that the observed scatter of our Re'_o values is actually much smaller than the scatter of experimental points through which the universal correlation was drawn (that scatter is of order of 5 percent) by Dewey.

It should also be made clear that end-loss corrections require certain idealized assumptions. For example, the entire length of the wire is supposed to be wetted by a uniform flow, an assumption which is incorrect near the support tips, especially when using the wire for fluctuation measurements where a large amount of wire slack may be necessary. A direct flow calibration of each individual wire is therefore an improvement in technique.

A.5 TEST 3

An identical procedure was followed with a second set of three Pt 10 percent Rh wires of approximately equal aspect ratios but different diameters (i.e., different Re_o ranges). The results were as follow:

Wire No.	d (in.)	ℓ/d	Re'_o (per in.)
9-28/3	0.00005	186	0.422×10^5
9-21/1	0.0001	193.6	0.421
9-24/2	0.00014	186.5	0.426

Again, we note the excellent agreement among the measured Re'_o values and, also, the agreement with those of the previous test.

A.6 DISCUSSION AND CONCLUSIONS

The tests performed confirm that under certain circumstances the hot-wire anemometer requires no end-loss corrections and no recourse to the "universal" Nu_o - Re_c correlation.

It should be remembered that the observed scatter of our Re'_o values is actually much smaller than the scatter of experimental points through which the universal correlation was drawn (that scatter is of order of 5 percent) by Dewey.

It should also be made clear that end-loss corrections require certain idealized assumptions. For example, the entire length of the wire is supposed to be wetted by a uniform flow, an assumption which is incorrect near the support tips, especially when using the wire for fluctuation measurements where a large amount of wire slack may be necessary. A direct flow calibration of each individual wire is therefore an improvement in technique.

APPENDIX B

THE WEA AND WEB-I COMPUTER PROGRAMS

The purpose of the WEA and WEB-I programs was to reduce the raw data of the average (mean) measurements in the axisymmetric compressible turbulent wake. Inputs to this program were the pitot pressure, static pressure, (five) hot-wire voltages, and their corresponding currents at each point in the wake. The program output gave the following relevant data: Mach number M (MACH NO.), wire Reynolds number Re_o (REO(1)), total temperature T_o (TO(1) DEGK), temperature T (TDEGK), axial velocity u (UCMSEC-1), density ρ (RHO CGS), the three nondimensional forms of velocity $\tilde{u}$ (UTILDA), density (RHOTILDA), temperature $\overline{T}$ (TTILDA), and the nondimensional r/r^* radius YTILDA; also, at each x-station it gave the velocity, density, and temperature differences $u_\infty - u(0)$ (DELTAU), $\rho_\infty - \rho(0)$ (DELTA RHO) and $T(0) - T_\infty$ (DELTA T) respectively, and the half-radius r^* (YSTAR). Other computationally helpful quantities were also outputed.

There is no basic difference between these two programs. WEA corresponds to the WEA experiment in which a 0.0001-inch diameter hot-wire was used, whereas a 0.00005-inch wire was used for WEB. Certain conversion formulas were thus changed from one program to the other, and the wire Reynolds numbers of WEA are naturally twice those of WEB-I.

At each point of the wake, a pitot pressure P_T, a static pressure, p, and five wire resistance values (produced by each of five different currents) are available. The pitot and static pressures supply the local Mach number. From the slope of the wire resistance versus current-squared curve one can obtain, as also observed by Dewey, the adiabatic wire temperature T_{aw} and the zeroth approximation $Nu^{(0)}$ to the Nusselt number. For the latter the thermal conductivity of the fluid is initially evaluated at T_{aw}. From $Nu^{(0)}$ and the flow calibration curve Re_o versus Nu_o the zeroth approximation $Re_o^{(0)}$

to the local Reynolds number is obtained, while the recovery factor $\eta^{(0)}$ is used along with T_{aw} to obtain the zeroth approximation $T_o^{(0)}$ to the local stagnation temperature, which in turn supplies an improved value of the thermal conductivity and thence $Nu_o^{(1)}$. This is finally used to compute the Reynolds number $Re_o^{(1)}$, recovery factor $\eta^{(1)}$, and local stagnation temperature $T_o^{(1)}$. Experience has shown that this iteration could be truncated at this point without loss of accuracy. The combination of static pressure, p, temperature, $T_o^{(1)}$, and Mach number then results immediately in the velocity, u, static temperature, T, and density ρ. In principle, any combination of the four measured properties (P_T, p, T_o, and Re_o) could be used to deduce the flow field. Of these the Reynolds number, being determined from the slope of a curve, is perhaps the least reliable and was thus given the role of a redundant check on the measurement. The above operations are also shown graphically in the computational procedure for this program, shown on Figure B-1.

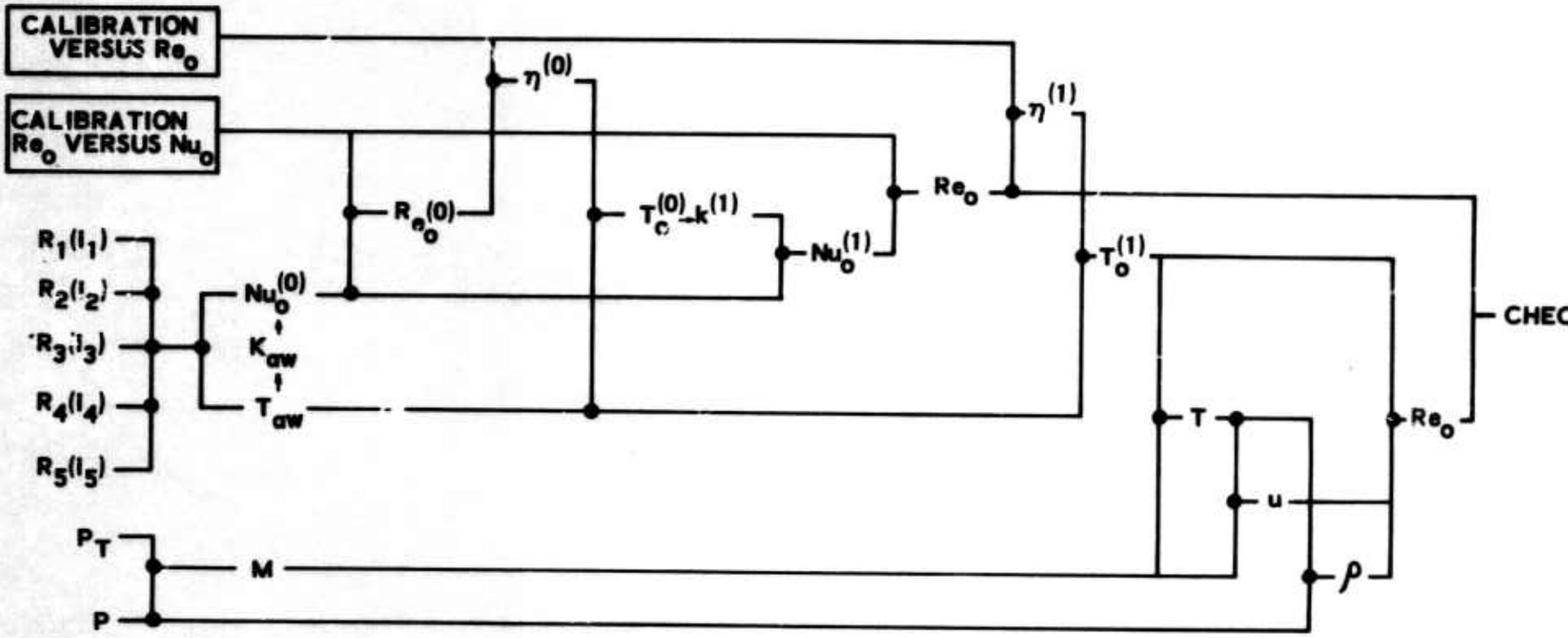

FIGURE B-1 THE WEA - WEB-I COMPUTER PROGRAM.

APPENDIX C

THE WEC COMPUTER PROGRAM

The objective of this experiment was to reduce the raw data of WEC (Wake Experiment C). The input of this program were (a) a curve of static pressure versus axial distance x beginning from x = 1.70 inches (X/D = 10.90) and ending at X = 9.10 inches (X/D = 58.33), on the wake axis; (b) a similar curve of pitot pressure, (c) a static pressure curve similar to (a) but taken off axis (y = 0, z = 0.400 inch); and (d) a pitot pressure curve similar to (c). Outputs were given at x positions (XSUB); spaced 0.10 inch apart; included X/D, the differences in velocity, density, and temperature across the wake $u_\infty - u(0)$ (DELTA U), $T(0) - T_\infty$ (DELTA T) and $\rho_\infty - \rho^{(0)}$ (DELTA RHO), respectively, the velocity, density, and temperature defects w (UDEFECT), $(\rho_\infty - \rho(0))/\rho_\infty$ (RHODEFECT), and θ (TDEFECT), respectively; and, finally, the on-axis and off-axis values of the velocity, density, temperature, and Mach number.

Because of reasonable assumption of the local total temperature (T_o = 300°K) was made, this program was particularly simple. The Mach number given by the Rayleigh formula was combined with T_o to give the temperature, and the density and velocity were then computed directly.

Figure C-1 shows the computational procedure for this program.

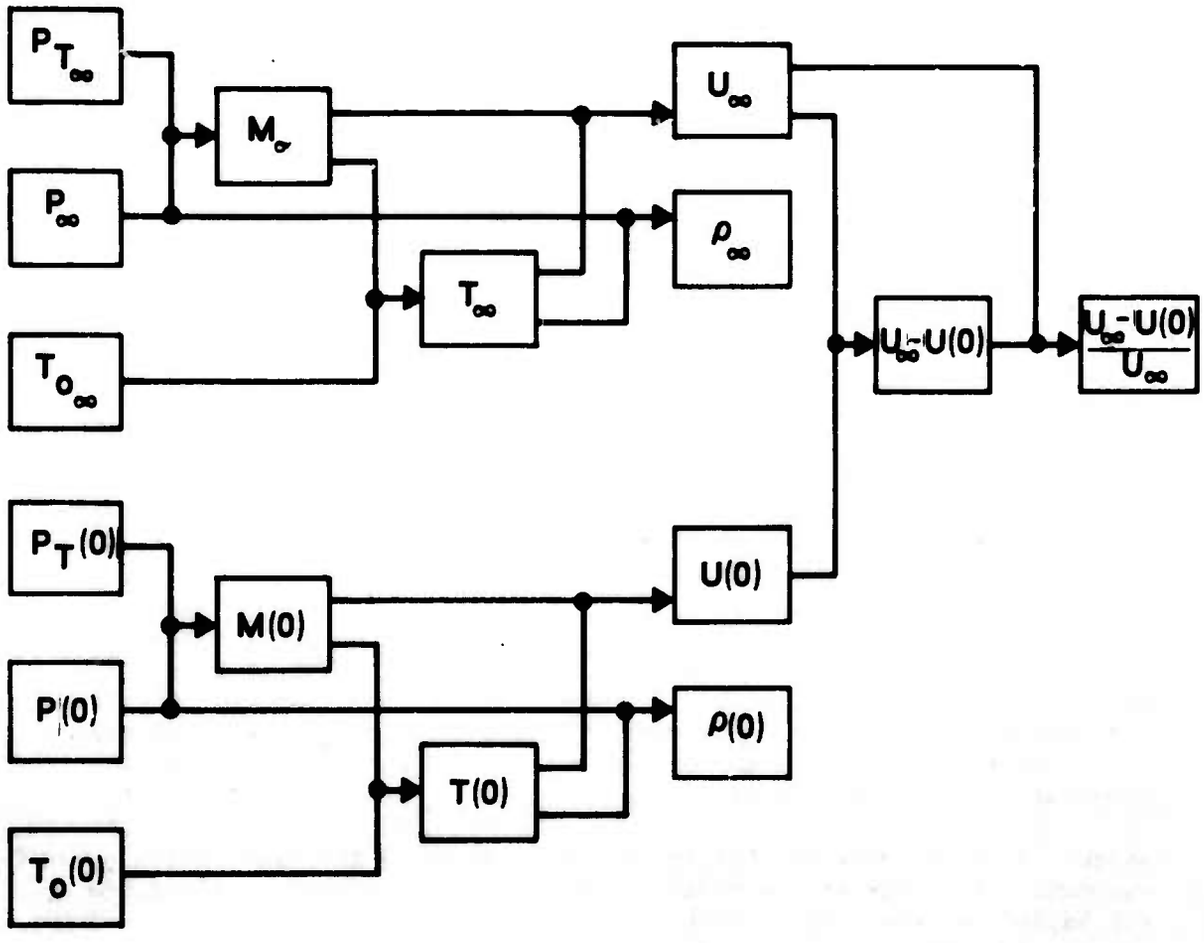

F09838 U

FIGURE C-1. THE WEC COMPUTER PROGRAM, SHOWING ONLY THE COMPUTATIONS FOR THE AXIS VALUES (0).

APPENDIX D

THE WEB-V COMPUTER PROGRAM

The purpose of this program was to further manipulate the experimental data into parameters more meaningful than those supplied by WEA, WEB, and WEC; it drew all its inputs from the outputs of the latter three programs. In its original conception, WEB-V also aimed at computing transport coefficients for the turbulent fluid; as explained below, this procedure failed, however, and will be modified in a future program.

At each x-station, this program supplied: the velocity, temperature, and desnity defects w (UNDEFECT), θ (TDEFECT), and $(\rho_\infty - \rho(0))/\rho_\infty$ (RHODEFECT), respectively; the quantity X/D and the proper axial coordinate $\bar{x}$ (XBAR); the Howarth-Dorodnitzyn half-radius $\bar{r}^*$ (RBARTILDA); the transverse scale L and its nondimensional form $L/\sqrt{C_DA}$ (L/CDA2); the local wake drag C_DA (CDA); the wake Reynolds number Re_w (REWAKE); and the turbulent kinematic viscosity ν_T on the axis. Further, at each x the following properties were outputed at each radius: the Howarth-Dorodnitzyn radius $\bar{r}$ (RBAR), nondimensional radius η (ETA), the redundant Reynolds number Re_o (RERD) and the product of turbulent Reynolds number, and turbulent kinematic viscosity $Re_T\ \nu_T$ (RTNU).

The redundant Reynolds number was computed on the basis of the local total temperature and the Sutherland formula; the local drag coefficient was computed by integrating properties measured along the radius. The average drag at each station was computed by accounting for all x-stations, and the proper axial coordinate $\bar{x}$ was computed by accounting for the virtual origin; the Howarth-Dorodnitzyn radius r is given by

$$\bar{r}^2 = 2 \int_o^\infty \frac{\rho}{\rho_\alpha}\, r\, dr$$

The proper radial coordinate is

$$\eta \equiv \frac{\bar{r}}{L}$$

where L is the lateral ("transverse") wake scale, the nondimensional form of which is given by

$$L^2 = \frac{C_D A}{4\pi w}$$

where w is the velocity defect. Finally, the product of turbulent Reynolds number and turbulent kinematic viscosity was computed by the formula shown in the text.

As mentioned above, a large part of this program was devoted to computing the kinematic viscosity directly from the boundary-layer approximation of the axisymmetric momentum equation in which the turbulent transport terms were lumped into a single viscosity parameter. As shown in the text, this involves the computation of the radial velocity from the data, as well as first and second velocity derivatives. Such a computation results, after a multitude of steps, in a "propagation" of errors which tends to distort the results grossly. Although the raw data were in analog form, only an extreme reduction of experimental inaccuracy and supreme control of the digitization and computation processes could make this technique work. At this writing, the only promising alternative is the use of a "smoothing" process introduced at some critical step in the computation.

The computational procedure for WEB-V is shown on Figure D-1.

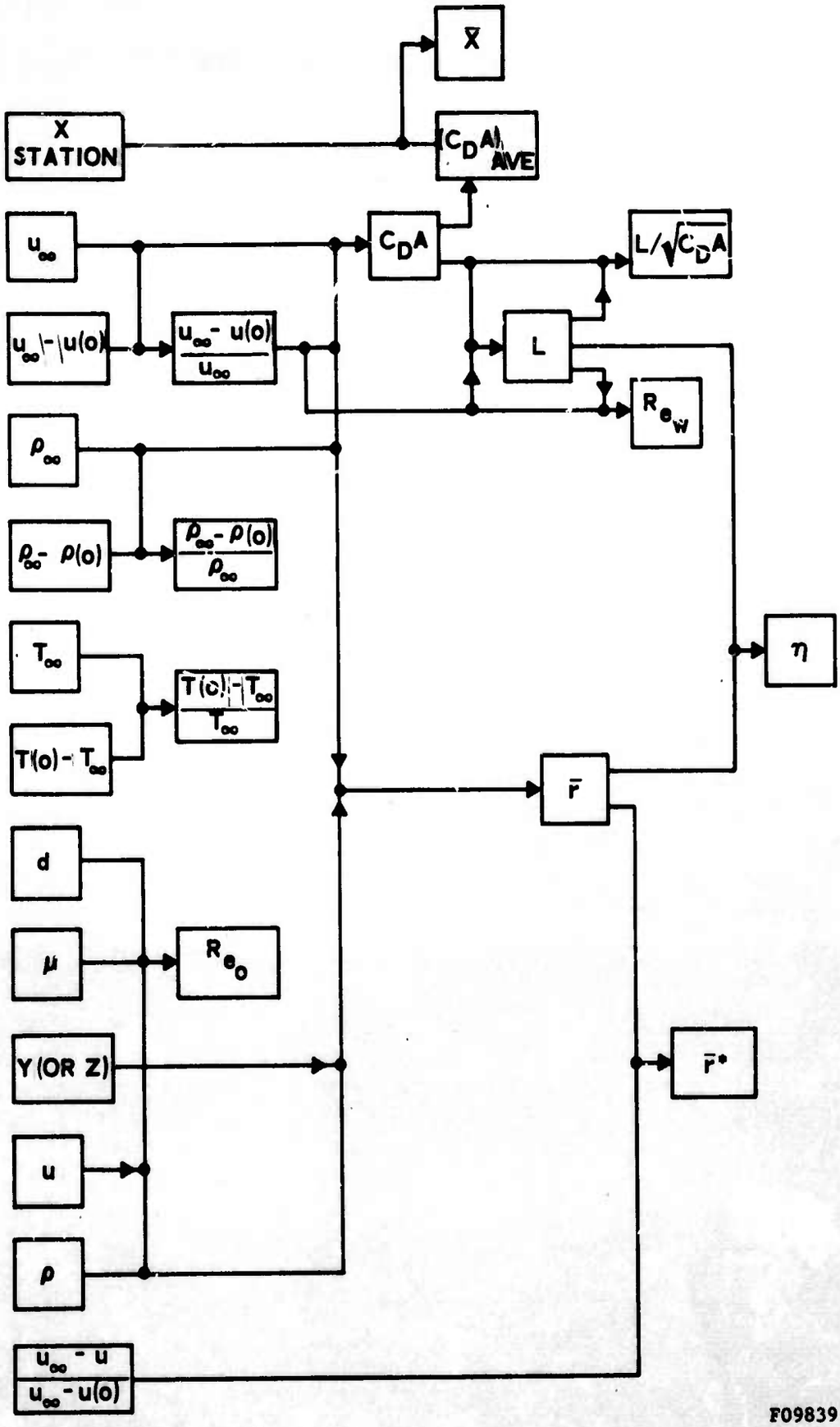

F09839 U

FIGURE D-1. THE WEB-V COMPUTER PROGRAM